Universitat Politècnica de Catalunya

Doctoral dissertation

Biomedical Engineering program

Development of Methodologies for Estimating the Dose to the Eye Lens in Interventional Radiology. Operational Implications of the Eye Lens new Dose Limit

Author:
Sara Principi

Supervisor:
Dr. Mercè Ginjaume

UNIVERSITAT POLITÈCNICA DE CATALUNYA
BARCELONATECH
Institut de Tècniques Energètiques

UNIVERSITAT POLITÈCNICA DE CATALUNYA BARCELONATECH

Development of methodologies for estimating the dose to the eye lens in interventional radiology : operational implications of the eye lens new dose limits

Sara Principi

The truth is, most of us discover where we are headed when we arrive.

Bill Watterson

Acknowledgements

This thesis has been developed with the financial support from the Consejo de Seguridad Nuclear and the Cátedra Argos, to whom I would like to acknowledge my gratitude.

I am deeply thankful to my supervisor, Mercè Ginjaume, for the unconditional support at any time. She has been an essential guide during this work and she is an example of perseverance, hard work and efficiency.

I would like to thank all the people met at INTE for making the workplace a very comfortable environment. I want to express my gratitude for the encouragement received from my colleagues during the last months of the writing of this thesis, especially from Dani and Maria. Many people pass through this Institute. Among all, I will remember with special affection the moments spent at the very beginning with Marta and Consuelo, mentors and friends.

Barcelona will always be special to me and it is also because of the people I have met here. Gaia, Themis, Emma, thanks for being my family during these years. You have been more than friends to me. Joan, thank you for so many things.

I am very grateful to all the people I met in Paris. It has been a profoundly rewarding experience. From IRSN, a special thanks goes to Jad for his help and support and to Anthony for the laughs during the coffee breaks. I was astonished by the greatness of the people I met at the Colegio de España. They make me think, laugh and grow. Among all, I want to mention Silvia. You gave me so much in such a short time.

I will never thank enough my lifelong friends. Francesca and Monica, we know how rare and special our link is. It doesn't matter the place or time, there will always be Us.

Finally, I am immensely proud of my family. Lori, you are at once the humblest and smartest person I know. This thesis is dedicated to my parents and to my brother, examples of genuineness and candor.

Summary

Recent epidemiological evidences on very late opacities or cataract manifestation have led to a review of the actual limit for the eye lens (150 mSv/year) for workers exposed to ionizing radiation. ICRP 118 recommends reducing the limit to 20 mSv per year. This drastic change in the dose limit has been incorporated into the revised European and International Basic Safety Standards (European Commission 2013, International Atomic Energy Agency 2014) and it should be implemented in national legislation of member states in 2018. Up to now, eye lens dose is not routinely measured and there are no general international recommendations regarding procedures on how correctly estimate the dose to the eye lens. The present work provides proposals regarding metrological, dosimetric and radiation protection needs associated to the new limit. At first, a calibration procedure and an easy-to-use dosemeter for the eye lens have been set-up to accurately measure eye lens doses in terms of $H_{\mathrm{p}}(3)$ for photon radiation fields. Secondly, a measurement campaign on phantom was performed in order to test several dosimetric systems and to analyze the influence of the position of the eye lens dosemeter. The best position for an accurate assessment of the eye lens dose is to locate the dosemeter as close as possible to the most exposed eye. Measurements at four Spanish hospitals in real clinical conditions were performed in order to evaluate whether the risk of exceeding the new recommended eye lens dose limit of 20 mSv per year is of real concern. 24 physicians and 12 nurses were monitored. Results show that approximately 40% of the monitored physicians and 25% of monitored nurses would exceed the new limit. The relation between the eye lens equivalent dose $H_{\mathrm{p}}(3)$ and other quantities, easier to measure such as $H_{\mathrm{p}}(0.07)$ with an unprotected whole body dosemeter situated at the chest or the KAP registered in the X-ray console have been investigated. Results highlight that the relation between $H_{\mathrm{p}}(3)$ and $H_{\mathrm{p}}(10)$ or $H_{\mathrm{p}}(0.07)$ measured on the chest or collar with an unprotected whole body dosemeter is more reproducible than the relationship between $H_{\mathrm{p}}(3)$ and KAP, in particular in the case of nurses. Large uncertainties are associated to the estimation of $H_{\mathrm{p}}(3)$ through other quantities (such as KAP or whole body doses). The relationship is dependent on the type of procedure, position of the monitored person and use of protection means. Thus, this methodology is only recommended to monitor the staff exposed to eye lens doses below 6 mSv or in order to identify which individuals are likely to require regular eye lens monitoring. The recommended correction factor is $H_{\mathrm{p}}(3) = 0.8 \cdot H_{\mathrm{p}}(0.07)_{thorax}$. For individuals at risk, the use of a dedicated eye lens dosemeter is strongly recommended. Monte Carlo simulations were carried out in order to analyse the influence of several parameters on eye lens equivalent dose and to provide recommendations on eye lens dose reduction and on the effectiveness of the protective glasses. This thesis proposes simple precautions to reduce the dose, such as the positioning of the monitors away from the X-rays. A rotation of the head of 30° or 45° away from the tube is shown to reduce eye lens dose by approximately 50%, in particular at distances of 20 *cm* and 40 *cm* from the X-ray source. Furthermore, a correction factor of 0.3 for wraparound-style lead glasses and a more conservative value of 0.5 for any design of glasses is recommended. This correction should be applied when an eye lens dosemeter is used on an unprotected region close to the eye, as the measurement of the eye lens equivalent dose does not take into account the protection provided by the glasses. This proposal is in agreement with previously published work and with the recommendations from ISO in 2015. Finally, this thesis highlights the need of training to improve the use of the protection systems, in particular the ceiling suspended screen during clinical practice.

Resumen

Evidencias epidemiológicas sobre la manifestación precoz de cataratas u opacidades han comportado la revisión del límite anual de dosis equivalente al cristalino (150 mSv /año) para los trabajadores expuestos a la radiación ionizante. ICRP 118 recomienda reducir dicho límite a 20 mSv por año, promediado en un período de 5 años. Este cambio drástico en el límite de dosis se ha incorporado en las Normas básicas de protección radiológica europeas (Comisión Europea, 2014) e internacionales (IAEA, 2013) y deberán ser transpuestas a la legislación nacional de los Estados miembros en 2018. Actualmente, no se lleva a cabo el control dosimétrico de la dosis al cristalino y no se dispone de recomendaciones internacionales consensuadas sobre cómo llevar a cabo dicho control. Esta tesis presenta diversas propuestas para cubrir las nuevas necesidades metrológicas, dosimétricas y de protección radiológica en el ámbito de la cardiología y radiología intervencionista, asociadas al nuevo cambio legislativo. Se ha desarrollado y puesto a punto un procedimiento para la calibración de dosímetros personales de cristalino en unidades de $H_{\mathrm{p}}(3)$. También se ha caracterizado el dosímetro de cristalino UPC-ELD de acuerdo con la norma IEC 32687 (2012) para campos de radiación fotónica. Dicho dosímetro se ha utilizado en una campaña de medidas en maniquí antropomórfico para la validación de diversos sistemas dosimétricos y para analizar la influencia de la posición del dosímetro para la estimación de la medida de la dosis equivalente en cristalino. Se concluye que la posición óptima del dosímetro de cristalino es sobre la oreja, en el lado correspondiente al ojo más expuesto, habitualmente el izquierdo. Se efectuaron mediciones en cuatro hospitales españoles utilizando el dosmetro UPC-ELD. Participaron 24 facultativos y 12 enfermeras. Los resultados muestran que aproximadamente el 40% de los médicos y el 25% de las enfermeras superarían el nuevo límite. Paralelamente se ha investigado la relación entre $H_{\mathrm{p}}(3)$ y otras magnitudes como $H_{\mathrm{p}}(0.07)$ determinado con un dosímetro de cuerpo entero situado a nivel de tórax encima del delantal plomado o el KAP registrado en la consola de rayos X. Los resultados ponen de manifiesto que la relación entre $H_{\mathrm{p}}(3)$ y $H_{\mathrm{p}}(10)$ o $H_{\mathrm{p}}(0.07)$, medidas en el tórax, es más reproducible que la relación entre $H_{\mathrm{p}}(3)$ y KAP, en particular en el caso de las enfermeras. La determinación indirecta de la dosis en cristalino presenta importantes incertidumbres puesto que la relación entre las distintas magnitudes depende del tipo de procedimiento, de la posición de la persona y del uso de los sistemas de protección. Por ello, esta metodología sólo se recomienda para la vigilancia individual, si es muy poco probable que la dosis equivalente anual en el cristalino supere 6 mSv, o bien si el objetivo consiste en identificar los puestos de trabajo que pueden requerir un control dosimétrico sistemático. El factor de corrección recomendado para estimar $H_{\mathrm{p}}(3)$ es: $H_{\mathrm{p}}(3) = 0.8 \cdot H_{\mathrm{p}}(0.07)_{thorax}$. Cuando no es improbable superar 6 mSv, se recomienda el uso de un dosímetro específico para el cristalino. Mediante simulaciones Monte Carlo se analiza la influencia de varios parámetros en la dosis equivalente en cristalino y se determina la atenuación de distintos tipos de gafas protectoras. En base a los resultados de las simulaciones se propone situar los monitores alejados del haz de rayos X y girar la cabeza de 30° a 45° en dirección opuesta al tubo de rayos X. Dicha posición reduce la dosis en cristalino aproximadamente el 50%, en particular a distancias de 20 *cm* y 40 *cm* de la fuente de rayos X. Además, se ha determinado un factor de corrección igual a 0.3 para las gafas de plomo de estilo envolvente y un valor más conservador de 0.5 para otros diseños menos ajustados. Por último, esta tesis subraya la necesidad de mejorar la formación sobre el correcto uso de los sistemas de protección, en particular del blindaje de techo.

Contents

Part I

Introduction

Chapter 1

Basis and impact of the new eye lens dose limit

The lens of the eye has long been known to be a radiosensitive tissue (ICRP, 2007; UNSCEAR, 2011). Radiation exposure can cause opacities or cataracts, producing a loss of eye lens function. When opacities occur, the light is scattered inside the eye and cannot normally pass and focus on the retina. Therefore, vision is reduced and the image is perceived to be blurred. Up to now, radiation cataractogenesis is considered to be a deterministic event (ICRP, 2000, 1991), and thus, opacities or cataracts may occur when a threshold dose is exceeded. The threshold dose is defined as the dose resulting in a 1% incidence of specified tissue or organ reactions.

In 2007, the International Commission of Radiological Protection, ICRP, (ICRP, 2007) approved the revised Recommendations for a System of Radiological Protection which formally replaced the previous Recommendations issued in 1991 such as Publication 60 (ICRP, 1991). The new recommendations maintained the major concepts of the previous ones, but updated some of the data and developed additional guidance on the control of exposure from radiation sources. In particular, ICRP retained estimates of thresholds for tissue effects in the adult human lens from ICRP 1984, Publication 41 (ICRP, 1984), and the equivalent dose limit for the eye given in Publication 60 (ICRP, 1991). However, they also recognized that further information was needed and that revised judgements may be required as regards these data. In these documents, thresholds of 2-10 Gy for acute dose and 8 Gy for chronic exposure were set for visually disabling cataracts, while the threshold doses for induction of detectable opacities were 0.5-2.0 Gy and 5 Gy was applied for acute and protracted exposures.

Nevertheless, new recommendations were proposed in ICRP 118 (ICRP, 2012) based on several epidemiological studies on specific groups of workers, especially on astronauts (Chylack et al., 2009), interventional cardiology and radiology (IC/IR) workers (Vano et al., 2010; Junk et al., 2004), radiological technologists (Chodick et al., 2008), atomic bomb survivors (Neriishi et al., 2007) and Chernobyl accident liquidators (Worgul et al., 2007). Most of these studies presented very late manifestation of radio-induced opacities, and results suggested that the threshold dose for loss of eye lens functionality may be lower than previously considered in ICRP publications (ICRP, 2007, 1991). These human epidemiological studies, as well as work with experimental radiation cataracts in animals (Worgul et al., 2002; Kleiman et al., 2007), suggest that cataracts may occur following exposure to significantly lower doses of ionising radiation than assumed previously. For cataracts in the eye lens induced by acute exposure, recent studies, where formal estimates of threshold dose were made after long follow-up periods, indicate values of approximately 0.5 Gy with 90-95% confidence intervals including zero-dose. For chronic exposure over several to many years, again much of the evidence refers to minor lens opacities. ICRP 118 considered the threshold in absorbed dose for the lens of the eye to be 0.5 Gy based on these observations and it recommended reducing the equivalent dose limit for the lens of the eye for workers from 150 mSv per year to 20 mSv per year, averaged over a period of 5 years, with no single year exceeding 50 mSv (ICRP, 2012). This drastic change in dose limit was incorporated into the revised European and International Basic Safety Standards (EURATOM, 2014; IAEA, 2013). The Directive 2013/59 EURATOM is to be implemented in national legislation of member states in 2018. This reduction of the occupational dose limit to 20 $\mathrm{mSv{\cdot}y^{-1}}$ will have important implications for IC/IR workers, who represent the targeted population of this study.

Several studies have been devoted to medical workers (Vano et al., 2010; Sim et al., 2010; Rehani et al., 2011; Duran et al., 2011; Bouffler et al., 2012; Ciraj-Bjelac et al., 2012) and all of them suggested an

increased risk of late adverse radiation effects, such as eye lens opacities, for this group of workers. In Vano study (Vano et al., 2010), the risk of radiation cataracts after occupational exposure in interventional cardiology personnel was evaluated. Slit-lamp examinations were performed both in interventional cardiologists and a control group. Radiation exposure was estimated by using experimental data from catheterization laboratories and data collected from questionnaires. 38% of interventional cardiologists and 21% of exposed personnel, among nurses and technicians, had radiation-associated posterior lens changes typically associated with ionizing radiation exposure, compared with 12% from the unexposed population (control group). Median values of lens doses were estimated at 6.0 Sv for cardiologists and 1.5 Sv for associated medical personnel. These epidemiological studies and the consequent recommendation by the ICRP to decrease the exposure limit for workers have emphasized the role of radiation protection within the IC/IR framework and in eye lens dosimetry. An important difficulty is the fact that eye lens dose is not routinely measured and there is no general international consensus regarding the best procedure to correctly estimate the dose to the eye lens in practice. Before the eye lens dose limit reduction, whole body monitoring was considered as being a reliable way to ensure that the dose limit to the eye lens was not exceeded, but this is not always ensured with the new limit. As expected, implementation of the limit reduction in European legislation implies a greater focus on individual supervisory control and emphasis on the role of protection tools on occupational exposure at some workplaces. Consequently, optimization of calibration procedures and measurement techniques for this specific tissue (eye lens) is needed. Furthermore, an urgent need to educate radiation exposed professionals is suggested, in order to reduce the likelihood of radio-induced cataracts.

This work will be focused on radiation protection within the field of medicine. The focus will especially be on interventional cardiologists (IC) and radiologists (IR) who are among those groups who receive the highest doses to the eyes. The procedures performed in IC/IR require the physician to stand close to the patient, who represents the main source of scattered radiation. In fact, a photon source is focused on the patient to follow the path of the catheter inside the blood vessels. The photon radiation is then scattered by the patient itself to the operator. Furthermore, the number of IC/IR procedures has increased rapidly in the past few years because of the rapid development of imaging technology and advances in digital imaging. Consequently, staff should be considered at risk of having cataracts when the cumulative dose to the eye is considered throughout a number of working years (Vano et al., 2008).

Several studies have highlighted the need to perform eye lens dose monitoring. One of the largest studies conducted so far on this subject was carried out within the framework of the ORAMED (Optimization of RAdiation Protection for MEDical staff) project, funded by the European Union between 2008 and 2011(Vanhavere et al., 2012). The dose to the eye was measured through passive dosemeters located close to both the left and right eye. Annual doses were estimated from eye lens dose measurements and annual workload for each operator under study. For the operator with the highest workload, the estimated annual eye lens dose was 49.3 mSv. This value largely exceeds the recommended new dose limit. Furthermore, it was found that 45% of monitored operators in interventional cardiology and radiology had annual doses above $3/10^{th}$ of the new annual dose limit of 20 mSv and 24% even exceeded it. These results highlight the need to perform systematic monitoring of the eye lens dose for these workers.

In most countries, whole body doses $H_{\mathrm{p}}(10)$ and $H_{\mathrm{p}}(0.07)$ are regularly measured in IC/IR with passive whole body dosemeters located under the lead apron. However, in some hospitals it is common practice to clip an additional dosemeter outside the lead apron and this is often used as an estimate of the dose to the eyes (Carinou et al., 2014). A lack of standardized methods for eye lens dosimetry has led to the need to define guidelines and provide international recommendations for calibration and measurements of the eye lens dose. Additionally, the awareness of a major risk of eye lens opacities has led to the need to establish measures to ensure the protection of exposed workers by optimizing the radiation protection tools in IC/IR.

This thesis addresses the major issues of concern in relation to occupational exposure of the eye lens in IC/IR by:

1. Defining the most appropriate operational quantity for eye lens monitoring
2. Designing a suitable eye lens dosemeter
3. Establishing a proper eye lens calibration procedure
4. Proposing a procedure for eye lens dose monitoring to be implemented in routine practice

These topics will be treated in greater detail in the following chapters.

Chapter 2

Dose quantities

Radiation protection aims at preventing biological deterministic effects and at limiting stochastic effects to values that may be considered acceptable for professionally exposed personnel and the public. In practice, to ensure compliance with the basic principles of radiation protection so that individuals are not exposed to unacceptable radiation risks, received dose is subject to limits established by law. National and international authorities are responsible for defining these dose limits for people exposed to ionizing radiation. These regulations are based on the recommendations of the International Commission of Radiological Protection (ICRP) and the International Commission of Radiologic Units and Measurements (ICRU). Figure 2.1 summarizes the relation between dose quantities of interest in radiation protection for external dosimetry.

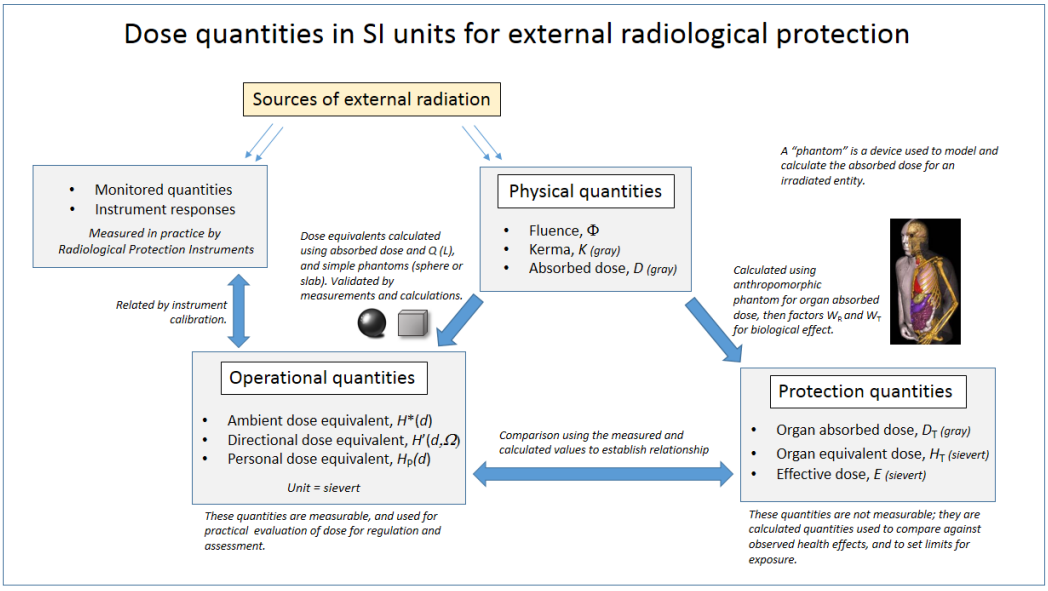

Figure 2.1: Relation between physical, operational and protection quantities for external dosimetry based on ICRU 57 (ICRU, 1998) (adapted from Mattson and Soderberg: "Dose Quantities and Units for Radiation", Chapter 2 of "Radiation protection in nuclear medicine" Springer Verlag 2013)

ICRP and ICRU have both defined two types of dose quantities for radiation protection applications: protection quantities and operational quantities. Protection quantities defined in ICRP 103 (ICRP, 2007) are the equivalent dose in an organ or tissue, H_T, and the effective dose, E. The equivalent dose, H_T, is defined by:

$$H_T = \sum_R w_R D_{TR} \tag{2.1}$$

where D_{TR} is the average absorbed dose in the volume of a specified organ or tissue T, w_R is the radiation weighting factor for radiation R. The sum is performed over all types of radiation involved. The unit of H_T is J·kg^{-1} and has the special name of sievert ($Sv = J \cdot kg^{-1}$).

The effective dose is defined by a weighted sum of tissue equivalent doses as:

$$E = \sum_T w_T H_T \tag{2.2}$$

where H_T is the equivalent dose in tissue or organ T and w_T is the tissue weighting factor for tissue T. The w_T values are chosen to represent the contributions of individual organs and tissues to overall radiation detriment from stochastic effects. The unit of E is sievert.

H_T and E are defined to ensure that the occurrence of adverse stochastic effects is kept below an acceptable level as well as to prevent tissue reactions. Limits of these quantities are established in national legislation following ICRP recommendations. Table 2.1 shows the dose limits applicable at present in Spain and those that will be implemented from 2018 for occupational exposure. The first limits are derived from ICRP 60, while the new limits correspond to ICRP 103 and 118 recommendations (ICRP, 1991, 2007, 2012).

Dose quantity	Limit in 2017 (RD783, 2001)	Limit after February 2018 (Implementation Directive 2013/59)
E	100 mSv in a consecutive five-year period subject to a maximum E of 50 mSv in any single year.	20 mSv in any single year. In special situations, a higher E up to 50 mSv may be authorised.
H_{lens}	150 mSv/year	20 mSv per year, averaged over 5 years, with no single year exceeding 50 mSv.
H_{skin}	500 mSv/year This limit shall apply to the dose averaged over 1 cm^2.	500 mSv/year This limit shall apply to the dose averaged over 1 cm^2.
$H_{extremities}$	500 mSv/year	500 mSv/year

Table 2.1: Comparison of dose limits for occupational exposure between 2016 and after the implementation of the 2013/59 Directive EURATOM (EURATOM, 2014)

Protection quantities, as they are defined, are not measurable in practice. Therefore, operational quantities are used for the assessment of effective dose or mean equivalent dose in tissues or organs. These quantities aim to provide a conservative estimate for the value of the protection quantities related to an exposure. Operational quantities for area and individual monitoring of external exposure were introduced by ICRU in 1992 (ICRU, 1992). These quantities are related to physical quantities (see Figure 2.1) that can be reproduced in radiation metrology laboratories through conversion coefficients and the definition of appropriate phantoms. The joint ICRP and ICRU publication (ICRP, 1996; ICRU, 1998) includes a complete set of conversion coefficients to calculate the operational quantities from fluence and air kerma.

Within the framework of this thesis we are mainly interested in the operational quantity for individual monitoring of external exposure, which is the personal dose equivalent, $H_p(d)$. $H_p(d)$ is the dose equivalent in ICRU (soft) tissue at a depth d below a specified point of the human body. This position is normally taken to be where the individual dosemeter is worn. To monitor skin dose a depth d of $0.07mm$ is recommended, while $10mm$ is used for organ dose monitoring. Notations of these quantities are respectively $H_p(0.07)$ and $H_p(10)$. $H_p(10)$ is used for the assessment of effective dose, and is usually measured with a whole body dosemeter, worn on the anterior part of the chest. For the assessment of skin and extremities (hands and feet) dose, $H_p(0.07)$ is chosen. For the lens of the eye, a depth d of $3mm$ was proposed (ICRU, 1988, 1992), as the lens is covered by about $3mm$ of soft tissue. Although $H_p(3)$ is recommended for eye lens monitoring, it is rarely measured in practice up to now. At a first stage, there were proposals of employing $H_p(0.07)$ for eye lens dose monitoring. ICRP 103 (ICRP, 2007) states that in practice $H_p(0.07)$ can be used when $H_p(3)$ measurements are not available. Also Behrens' work (Behrens and Dietze, 2010) suggests that the use of a dosemeter calibrated in terms of $H_p(0.07)$ on a slab phantom is appropriate in radiation fields where most of the dose comes from photons. Several studies were initially carried out using skin dose $H_p(0.07)$ for eye lens dose monitoring (Vanhavere et al., 2012; Domienik et al., 2012). However, nowadays, it is generally agreed that the use of the dedicated operational quantity $H_p(3)$ for eye lens dose monitoring is optimum. However, possible ways of obtaining

$H_{\mathrm{p}}(3)$ values still create debates within the radiation protection scientific community. $H_{\mathrm{p}}(3)$ can be assessed either directly or indirectly. Both methods have been used so far, and they will be detailed in the following chapter.

Chapter 3

Possible approaches to eye dose assessment

The IAEA TecDoc No. 1731 'Implications for occupational radiation protection of the new dose limit for the lens of the eye' provides advice to ensure appropriate individual monitoring of the eye lens (IAEA, 2013). Likewise, in 2015, the International Standard, ISO-15382, 'Radiological protection Procedures for monitoring the dose to the lens of the eye, the skin and the extremities', provides guidance on how and when monitoring of the eye lens should be done, for all the different types of workplace fields (ISO, 2015).

Both documents state that the most accurate method for monitoring the equivalent dose to the lens of the eye, H_{lens}, is to measure the personal dose equivalent at 3 mm depth, $H_p(3)$, with a dosemeter worn as close as possible to the eye and calibrated on a phantom that is representative of the head. Nevertheless, they also recognize that this procedure may be difficult to implement in practice and thus they indicate that other methods may also be used such as evaluating $H_p(3)$ through $H_p(10)$ or $H_p(0.07)$ both measured with dosemeters worn on the trunk or using other quantities such as the dose area product (DAP) or kerma area product (KAP)[1]. In particular, in the case of photon radiation fields, recommendations are given on the appropriate position of the dosemeter and quantity to be used in order to accurately assess the eye lens dose, depending on the energy and the direction of the radiation field, the geometry and the use of protection means. The IAEA Tecdoc (IAEA, 2013) states that, when protective equipment such as the ceiling shield is employed, the monitoring near the eyes is necessary. However, dosemeters calibrated in terms of $H_p(0.07)$ may be used. If the mean energy field is above 40 keV and the radiation is coming mainly from the front or the person is moving in the radiation field, also $H_p(10)$ quantity may be employed. Furthermore, when homogeneous radiation fields are present, the eye lens monitoring with dosemeters worn on the trunk may be performed. However, there is still a lack of international ISO and IEC standards related to the calibration procedures of eye lens dosemeters, for a proper radiation protection policy for the eye lens dose monitoring and for the assessment of the performance criteria of active personal dosemeters and area monitors.

3.1 Direct measurement of eye lens dose: suitable eye lens dosemeters

In order to ensure appropriate individual monitoring, the eye lens dosemeters should comply with internationally agreed-upon performance requirements. These requirements should be stated in standards of the International Electrotechnical Commission (IEC) and the International Organization for Standardization (ISO). At present, only IEC 62387 (IEC, 2012) provides performance requirements for passive photon dosemeters to measure $H_p(3)$. The dosemeters used for monitoring the eye lens are generally based on passive techniques and are made of thermoluminscent materials.

Ideally, the dosemeters should be designed to be type-tested and calibrated in terms of $H_p(3)$. However, previous works, such as Behrens (Behrens et al., 2012), demonstrated that dosemeters calibrated in terms of $H_p(0.07)$ and placed on the head may deliver the correct estimation of the H_{lens} for photon irradiation. Few passive dosemeters are available for the measurement of $H_p(3)$. One of the first prototypes designed as a passive eye lens dosemeter was proposed within the framework of the

[1] Within the framework of this thesis the term KAP will be preferably used throughout. The two quantities are indistinctly used in interventional radiology and although the concept is not the same, the numerical value is.

ORAMED project. It is based on a LiF:Mg,Cu,P thermoluminescent detector placed in a hemispherical specifically designed holder to measure $H_p(3)$ (Bilski et al., 2011). This dosemeter is now produced by Radcard (Krakow,Poland,http://www.radcard.pl/) and distributed by RadPro International GmbH, https://www.radpro-int.com/, under the trade name EYE-D^{TM}. It should be located as close as possible to the most exposed eye lens. A head band can be provided to hold the dosemeter.

Since 2012 several other designs have been proposed. In 2014, the first intercomparison exercise for eye lens dosimetry was organized by EURADOS at a European level (Clairand et al., 2016). In this exercise, 20 services participated from 15 European countries with 12 different types of dosemeters. For active dosemeters, currently no international standard is available for the quantity $H_p(3)$. The use of active personal dosemeters has been recommended for operational monitoring of medical staff in IC/IR (Struelens et al., 2011). However, electronic devices can be used for eye lens dose assessment if they are optimized in terms of $H_p(3)$ with respect to energy and angular dependence, or if the quantity they are optimized for provides an adequate estimate of the dose to the eye lens. Very few active dosemeters specific for eye lens dose assessment are manufactured. However, whole body active personal dosemeters have been used for the evaluation of the eye lens doses in some specific studies (Sanchez et al., 2014; Vano et al., 2015). The advantage with respect to passive dosimetry is that active dosemeters provide a real-time estimation of the dose. On the other hand, the main limitations to their application in this field are their size and cost. In this case, small semi-conductor detectors clipped onto spectacles would be a suitable approach to eye lens dose measurements for active dosimetry when lead glasses are worn (Antic et al., 2013).

3.2 Assessment of eye lens dose from other quantities

The use of a specific personal dosemeter for the assessment of eye lens dose introduces several challenges. Firstly, the eye lens dosemeter should be properly calibrated in terms of $H_p(3)$. Secondly, it is an extra dosemeter for the practitioners that should be worn as close as possible to the region of the eye. This might be neither practical nor comfortable. This has led to alternative issues being investigated in the past few years from several studies. Two main approaches have been analyzed:

- Assessment of eye lens dose from routinely measured whole body doses
- Assessment of eye lens dose from kerma-area product (KAP) values.

Whole body quantities are not defined for the estimate of eye lens dose, but there is the possibility to obtain $H_p(3)$ through dosemeters calibrated in terms of $H_p(10)$ and $H_p(0.07)$, by applying proper correction factors. In 2000, ICRP publication 85 (ICRP, 2000) recommended wearing an additional dosemeter at collar level and above the thyroid protective collar in order to have an indication of eye dose. Indeed, the use of a second whole body dosemeter on an unprotected part of the body, is a well-established procedure recommended by ICRP for interventional procedures and it consists of the use of two passive dosemeters, one below the lead apron at the level of the chest and another on the protective apron at a collar or chest level. The aim is to use a combination of the measurements from the two dosemeters to assess the effective dose. Several studies then investigated the relation between eye lens dose and dose at the collar. One of the most renowned studies is Clerinx et al. work which suggested the application of a factor of 0.75 to convert the dose reading $H_p(0.07)$ from a dosemeter worn on an unprotected part of the collar to eye lens dose (Clerinx et al., 2008). The calculations were performed through Monte Carlo simulation. This correction factor has been put forth again by Martin in his review on dose indicator values (KAP or $H_p(0.07)$) that could be used to predict doses to the eye lens (Martin, 2011). However the estimate of eye lens dose provided by a collar dosemeter depends on multiple factors related to the specific irradiation configuration, such as the position of the tube and of the operator and the use of protection tools. These issues were highlighted by an extensive measurement campaign on phantoms, performed within the European study ELDO to estimate correction factors to eye lens dose from whole body doses measured above the protection lead collar or apron (Farah et al., 2013). Several projections and access routes for mono-tube and biplane-systems were considered. No shielding was used during the tests. The estimation of the eye lens dose from dosemeters worn on the collar, chest or waist was studied. It was shown that $H_p(3)$ measured at the left eye correlates best with $H_p(10)$ measured on the left side of the collar, above the protective wear. The collar represents the wearing position closest to the eyes, so that the thyroid dosemeter is exposed to a similarly scattered X-ray field to the eye lens dosemeter. The suggested correction factor to obtain $H_p(3)_{lefteye}$ from $H_p(10)_{leftcollar}$ was 3.36. This factor differs considerably from data found in the literature. Carinou et al.'s review (Carinou et al., 2015) collects the main published results on the relation between whole body doses and eye lens dose and it underlined the fact that the relation between these quantities is strictly situation-dependent.

In most of the cases the doses measured in the thyroid and chest region are higher than the eye lens doses, but this does not represent a general rule. Correction factors varying from 0.44 to 1.45 have been gathered for interventional cardiology procedures only. Data on the distributions of ratio of eye lens and thyroid dose from 17 studies reviewed from 1991 to 2011 by Martin (Martin, 2011) show that correction factor vary from 0.24 to 1.25, with mean value of 0.63. Attention should be focused on the fact that studies performed on phantoms or with Monte Carlo simulation do not take into account the protection provided by protective tools in the room, which are usually used in clinical practice. Although the use of correction factors and doses measured by whole body dosemeters worn on the collar or chest represents a tempting strategy for the assessment of the eye lens dose, care should be taken and, probably, no general rules can be drawn in order to have a standard procedure of estimating eye lens dose through whole body dosemeters. Further studies should be undertaken to reduce the uncertainty of the dose estimate (keeping in mind the fact that the main objective is to determine whether or not dose limits are reached).

Since staff exposure is mainly associated with radiation scattered by the patient, the use of KAP values and a proper correction factor as a first estimate of $H_p(3)$ has been proposed (Vano et al., 2009). KAP is automatically recorded during interventional procedures, as it is required by present regulation and is considered to be a reliable quantity for the assessment of patient doses during fluoroscopic procedures. In Antic et al.'s study (Antic et al., 2013), ocular lens doses were measured with an active personal dosemeter calibrated in terms of $H_p(3)$. Estimated mean $H_p(3)$ per unit KAP for first operator, second operator or nurse and radiographer were 0.94 μSv Gy^{-1}cm^{-2}, 0.34 μSv Gy^{-1}cm^{-2} and 0.16 μSv Gy^{-1}cm^{-2}, respectively. This study highlights the fact that information on location of the staff within the room should be provided in order to apply the proper correction factor. Martin's review showed correction factors from 0.29 to 1.9 μSv Gy^{-1}cm^{-2}, with mean and median values of 0.79 and 0.43 (and third quartile of 1.0) (Martin, 2011). At first, he proposed to use the maximum KAP-to-eye lens dose correction factor of 1.9, to ensure the worst case to be assessed, but in order to avoid too conservative results, he suggested that the use of the third quartile value of 1.0 μSv Gy^{-1}cm^{-2} would be more appropriate. This value is in agreement with mean $H_p(3)$/KAP of 0.94 for first operator from Antic's work and with 1.0 μSv Gy^{-1}cm^{-2} obtained during the ORAMED campaign for deriving eye lens dose estimate from DAP (Vanhavere et al., 2011). However, the correlation between eye lens dose and KAP is of concern. The most important factor contributing to the variation of these correction factors is the use of shields.

The advantage of these two indirect methods to estimate $H_p(3)$ is that they are based on dose quantities which can be more easily measured and recorded than having to wear a specific additional dosemeter close to the eyes. The main limitation is that the relation depends on too many parameters of influence (Carinou et al., 2011; Donadille et al., 2011). Therefore, the use of correction factors to derive $H_p(3)$ leads to a degradation of the accuracy of the eye lens dose estimate with respect to the direct measurement of $H_p(3)$. Thus, in our opinion, as it is also pointed out by most authors (ISO, 2015), the indirect evaluation of $H_p(3)$ can be proposed for guidance in risk assessment in order to identify those individuals who may exceed the 20 mSv limit and for planning an initial protocol for dose monitoring, but this method cannot be applied to all routine cases. In many epidemiological studies on eye lens exposure, dosimetric measurements are poor or inexistent, thus improving our knowledge about the relation between the different dose quantities is of interest for retrospective dosimetry.

3.3 Radiation protection tools in interventional cardiology and radiology

IEC 61331 specifies the protective devices to be used against diagnostic medical X-rays (IEC, 2014). The lead apron must be worn by all the people present in the room where X-rays are used. The level of protection provided by the apron depends on the voltage applied to the tube: the larger the patient, the higher the kV set by the fluoroscopy machine. Higher voltages mean greater penetration of the X-ray beam. In order to protect the operator from backscattered radiation, the higher the lead thickness the better. On the other hand, the weight of the apron is of concern. For this reason, lead aprons with thicknesses equal to 0.5 mmPb at the front reach a good compromise between protection and comfort (ICRP, 2010). Apart from body protection, radiological protection for the eyes is essential for IC/IR physicians (ICRP, 2013). This protection is provided by the ceiling suspended screen. This shield should be located between the operator and the radiation sources (the primary and the scattered) and should provide protection to the upper part of the body, including the head, if well-positioned. However, sometimes, the use of this shield is not practical and it interferes with the operator's ability to perform the procedure (ICRP, 2013). In these cases, lead glasses should be worn. Several studies have shown that the effectiveness of lead glasses can be largely reduced, when they do not fit the operator's head

properly, and scattered radiation passes through the lens of the glasses and the operator's head. For highest effectiveness, the protective eyewear should have side protection or a wraparound design. Even in this case, radiation to the eyes is reduced by only a factor of two or three (Moore et al., 1980; Thornton et al., 2010; Koukorava et al., 2014).

The use of protection introduces some difficulties when evaluating the eye lens dose. When the dose is directly measured by an eye lens dosemeter, if lead glasses are used, the positioning of the dosemeter is of concern, as it can be located on an unprotected part in order to avoid discomfort. In this case a correction factor should be applied to take into account the protection provided by the glasses (ISO, 2015). Otherwise, the eye lens dosemeter may be located under the protection. If eye lens dose is assessed by means of other quantities, such as whole body quantities, the fact that whole body dosemeters may be exposed to a different radiation field than to the head, as they may be protected by room protection tools, should be taken into account. In fact, eye lens dose may be underestimated in this case.

Chapter 4

Calibration procedure for eye lens dosemeters

Although, there is common agreement on using $H_{\mathrm{p}}(3)$ as the operational quantity for eye lens dosimetry, no calibration phantom and no conversion coefficients $h_{\mathrm{p}K}(3)$ have been officially decided upon and published in the ISO standards for the calibration of personal dosemeters. Behrens and Hupe state that in photon radiation fields, especially X-ray fields, both quantities $H_{\mathrm{p}}(0.07)$ and $H_{\mathrm{p}}(3)$ are suitable for monitoring exposure of the eye lens if the dosemeters are calibrated on the ISO slab phantom (ISO, 1999) for simulating the backscattering properties of the head (Behrens and Hupe, 2015). However, the urgency in defining a more rigorous method for calibration and measurement of eye lens dose has raised attention in order to find a more suitable phantom for eye lens dosimetry.

Within the ORAMED project, this topic was discussed in depth, and a new phantom was proposed. In fact, a dosemeter calibrated in terms of $H_{\mathrm{p}}(3)$ requires a proper calibration phantom that is able to reproduce the characteristics of the part of the body where the dosemeter should be worn (the head in the case of eye lens dosimetry). A cylindrical phantom of ICRU tissue, with height and diameter of 20 cm was defined (Gualdrini et al., 2011). Data show that a reasonable approximation of the backscattered properties of the head is ensured with the proposed cylindrical phantom. For calibration purposes, a practical phantom with the same outer dimension as the ICRU cylindrical phantom but with PMMA walls 0.5-mm-thick and filled with water was proposed. In 2015 Behrens and Hupe (Behrens and Hupe, 2015) conducted a study comparing the angular response of an EYE-D dosemeter by irradiating it on a slab, a cylinder and on a human-like Alderson phantom. It turned out that the response for the three phantoms is nearly equal for angles of radiation incidence up to 45° and deviates only at larger angles of incidence. For calibration purposes, usually performed at 0° radiation incidence, the use of both the slab and the cylinder phantoms provide equivalent results. However, it was shown that for large angles of incidence the responses on the cylinder and the Alderson phantoms are quite similar, whereas the response on the slab significantly deviates from that of the Alderson phantom. Conversion coefficients $h_{\mathrm{p}K}(3)$ are needed to establish the equivalent dose $H_{\mathrm{p}}(3)$ from the measurement of air kerma with a reference instrument. Up to now, international organizations have not proposed specific conversion coefficients for the eye lens, but some sets of $h_{\mathrm{p}K}(3)$ can be found in the literature. Grosswendth (Grosswendt, 1990) calculated $h_{\mathrm{p}K}(3)$ for monoenergetic beams and for several angles of impinging radiation on the phantom surface. Calculations were performed on several phantoms, but not for the phantom recently recommended by ORAMED. Daures et al (Daures et al., 2011) and Gualdrini et al. (Gualdrini et al., 2013) determined the air kerma to $H_{\mathrm{p}}(3)$ conversion coefficients by Monte Carlo simulation for monoenergetic photons from 10 keV to 10 MeV in the suggested cylindrical phantom. Penelope (Salvat et al., 2006) and MCNP (Pelowitz, 2005) codes were used and the results compared. The simulations were carried out both in kerma approximation mode and transporting electrons. The geometry simulated consisted of the proposed ICRU cylindrical phantom and a sensitive volume centered at a depth of $3mm$ inside the phantom. The results of the two papers showed very good agreement, with a statistical uncertainty of approximately 0.06% for kerma approximation mode. The uncertainty increases to 0.4% when the transport of electrons is considered. It is shown that the kerma approximation is appropriate for energies up to 1 MeV. The ORAMED study also included a short set of conversion coefficients calculated on the cylindrical phantom with Monte Carlo simulation for a few RQR (IEC, 2005) and N (ISO, 1996) series (Vanhavere et al., 2012).

Behrens (Behrens, 2011, 2012a) calculated $H_{\mathrm{p}}(3)$ conversion coefficients for ISO 4037-1 photon spectra (ISO, 1996) using conversion coefficients from mono-energetic beams by using interpolation techniques.

Coefficients were calculated both for a square and a cylindrical phantom. This set of conversion coefficients was included as informative data in IEC Standard 62387 (IEC, 2012). Table 4.1 summarizes the $h_{\mathrm{p}K}(3)$ found in the literature for non-mono energetic spectra.

	$h_{\mathrm{p}K}(d)_{slab}$			$h_{\mathrm{p}K}(3)_{cylinder}$
	d = $0.07mm$	d = $10mm$	d = $3mm$	d = $3mm$
N (ISO 4037-1)	ISO 4037-3	ISO 4037-3	Behrens (2011) IEC (2012)	Behrens (2012a)
RQR (IEC 61267)	None	None	None	few RQR- Daures et al. (2011)

Table 4.1: $h_{\mathrm{p}K}(3)$ available in the literature for non-mono energetic spectra

Part II

Aims

Chapter 5

Aims and outlines

Part I of this thesis highlights the main challenges derived from the new eye lens dose limit, in particular in the case of interventional radiologists and cardiologists. The main scope of this work is to contribute to having better knowledge on the assessment of eye lens monitoring for medical staff. The study includes both experimental dose measurements and Monte Carlo simulation of different scenarios of interest in order to improve our understanding of the potential risk of eye lens exposure during interventional procedures. The project has been developed at the Institut de Tècniques Energètiques of the Universitat Politècnica de Catalunya in collaboration with the Hospital Clínico San Carlos of Madrid and with partial funding support of the Consejo de Seguridad Nuclear, the Spanish Nuclear regulator. Within this framework, this thesis provides answers regarding:

1. Metrological needs: new conversion factors are calculated and a calibration procedure for eye lens dosemeters has been set up.
2. Dosimetric needs: an eye lens dosemeter is characterized to be able to accurately measure eye lens doses for photon radiation.
3. Radiation protection needs: this is the main objective of the study and it includes the following features:
    - Measurement campaigns in phantoms were first planned to help in the design of the survey in hospitals. The aims were to test several dosimetric systems and to analyze the influence of the position of the eye lens dosemeter.
    - Measurements were then organized at several hospitals. This part aimed at identifying workers that will require eye lens dose monitoring and estimate annual eye lens doses.
    - Simulation calculations were carried out to analyze the influence of several parameters on eye lens dose to study the effectiveness of the protection systems available in operating rooms for eye lens dose reduction, to compare different techniques for the assessment of eye lens dose, to identify and if possible overcome the difficulties of adequately measuring eye lens dose.

The results of the study will become a calibration procedure of eye lens doses at the Calibration and Dosimetry Laboratory of the INTE-UPC, which will be available for authorized personal dosimetry services. It will also inform of the eye lens dose levels and will aim to set up a procedure to identify potentially high lens exposure practices. In addition, it will provide a practical and sufficiently accurate solution for the regular monitoring of the eye lens in these workers as well as a procedure to estimate eye-lens doses by other parameters when monitoring is not needed. Finally, last but not least, it will provide information on the effectiveness of several radiation protection means, in order to reduce worker dose.

Part III gathers the main methods used for the development of the thesis. On one hand, for the experimental determination of the doses, an accurate dosimetry protocol needs to be defined. INTE-UPC is provided with both thermoluminescent and calibration laboratories for external dosimetry. This institute has great experience in this field and is the reason why thermoluminescent detectors were employed during this project. On the other hand, the Monte Carlo method yields very accurate dose calculations and provide a valid method of dose calculation for dosimetry purposes. However, experimental measurements are still fundamental for the benchmarking of Monte Carlo results, and the large demand in computing time is still currently prohibitive for routine use of Monte Carlo in clinics. Multiple tools are also necessary for handling and analysis of the data, such as SPSS and Matlab. It

is followed by Part IV which includes specific chapters corresponding to the results of the main studied topics. Most of these studies have been presented in international or national scientific meetings and published in peer-review journals. They are included in Appendix A. Part V presents a general discussion on the results and proposes answers to the identified needs. Finally, Part VI summarizes the main conclusions.

Part III

Methods

Chapter 6

Operational thermoluminescent dosimetry

Thermoluminescent (TL) detectors are largely employed in operational dosimetry and TL dosimetry represents the most frequent type of personnel radiation exposure monitoring. TL detectors are suitable for measurements in interventional cardiology and radiology. Some of the advantages of these detectors are their small size, the possibility of re-use and affordable cost. The first part of this chapter will be devoted to the characterization and calibration of thermoluminscent dosemeters (TLDs). The second part will describe the eye lens dosemeter developed by the UPC within the framework of this study.

6.1 Definition of a thermoluminescent dosimetric system

Thermoluminescent means emitting light when heated. A TL detector is a crystal which has the capability of emitting visible light when it heats up after being exposed to ionizing radiation. The amount of light emitted is dependent upon the absorbed radiation energy. Materials exhibiting thermoluminescence in response to ionizing radiation include lithium fluoride (LiF). The main characteristic of this material is the presence of one or more impurities inside the crystal which produce trap states for energetic electrons. In fact, as the radiation interacts with the crystal, electrons are freed and jump to higher energy states, leaving holes of positive charge. The electrons travel through the solid in the conduction band and may be trapped due to the impurities in the crystal. When the TL material is heated, the electrons drop back to their ground state, releasing a photon of energy equal to the energy difference between the trap state and the ground state. This extra energy is released in the form of light. The light intensity can be measured and related to the amount of energy initially absorbed during exposure.

A thermoluminescent dosimetric system consists of several parts:

- The detector, sometimes also called dosemeter, i.e. the LiF:Mg,Cu,P crystal.
- A TL holder, where the TL detector will be located. The whole system of holder and detector is the TL dosemeter (TLD).
- A TL reader consisting of a heating element, a photomultiplier tube and an electronic network. The reader heats the exposed detectors and provides the signal stored in the detector in terms of electric charge (Coulomb). The INTE-UPC dosimetry laboratory is provided with the HARSHAW-BICRON 5500 reader.
- Ovens used for thermal treatments of the dosemeters (annealing procedures). These treatments are necessary both in the preliminary stage of characterization of the batch, and before each measurement to restore the initial stage of the dosemeter after usage.
- Appropriate algorithms to convert the TL signal (response provided by the reader) to dose values.

6.1.1 Thermoluminescent detector

In this work, dose measurements in photon radiation fields were performed using TLDs containing LiF crystals, doped with magnesium, copper and phosphor (LiF:Mg,Cu,P). The LiF: Mg, Cu, P material was chosen due to its high sensitivity and flat response with energy. Furthermore, as it is an approximately tissue-equivalent material, it responds in a similar way as human tissue would respond.

LiF:Mg,Cu,P TL detectors manufactured by Conqueror Electronics Technology Co. Ltd.(Beijing. China, http://www.cet-cns.com/index.htm) under the trade name TLD-2000C were used. They are circular pellets of 4.5mm diameter and are 0.8mm thick, with a density of 2.65 g/cm^3.

6.1.2 TLD holder

To obtain a good measurement of the operational quantity of interest, the design of the TLD includes the definition of a casing or holder for the thermoluminescent detectors. The holder contains one or more filters of specified thickness and material, depending on the operational quantity $H_{\mathrm{p}}(d)$ to be measured. These filters can be used to differentiate between skin and organ doses, in the case of whole body dosimetry.

Two types of TLD holders are used in this study for eye lens dose monitoring. On one hand, the EYE-D dosemeter described in Part I was employed. Although this dosemeter provided an accurate measurement of $H_{\mathrm{p}}(3)$, it had some limitations. It has to be located close to the eye, on an operator head band or on the lateral eyepiece of the operator's glasses. Some operators, however, did not wear a head band or glasses and thus could not wear it or in other cases found it cumbersome.

The need to find a compromise between placing the eye lens dosemeter (ELD) as near as possible to the most exposed eye and at the same time avoiding discomfort of the worker, have led us to considering defining a simple casing. The ELD designed at the INTE laboratories consists of two TL detectors sealed in small plastic bags of opaque polyethylene, with density thickness of 11 $mgcm^{-2}$ (Figure 6.1). Henceforth, this ELD would be referred to as the UPC-ELD. The UPC-ELD dosemeter has been optimized to respond in terms of $H_{\mathrm{p}}(3)$.

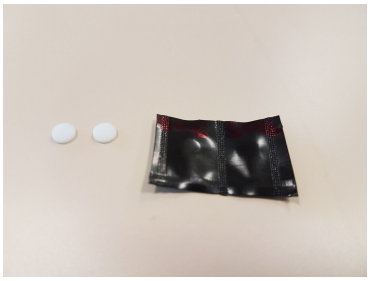

Figure 6.1: The TL detectors and the UPC-ELD

In addition, for whole body dosimetry, the standard badge of the Universitat Politecnica de Catalunya (UPC) personal dosimetry service was used. This service has been accredited by the Spanish Accreditation body (ENAC) according to ISO 17025. The UPC whole body dosemeter (UPC-WBD) contains two detectors for $H_{\mathrm{p}}(0.07)$ and two for $H_{\mathrm{p}}(10)$, located in the upper and lower part of the dosemeter, respectively, and the holder material is made of PVC. The same pellets employed in the UPC-ELD dosemeter were used as detectors for the UPC-WBD.

6.1.3 HARSHAW-BICRON 5500 reader

The Harshaw-Bicron 5500 reader includes a nitrogen heating system to heat the dosemeter. The emitted luminescence is then amplified by a photomultiplier tube (PMT). The PMT consists of two electrodes, a photocathode and an anode, in a vacuum tube, in the absence of external light. The photocathode generates electrons as a result of impinging light and the electric signal is amplified by the photomultiplier and collected at the anode. The reading process of TLDs proceeds as follows at the INTE laboratory (Ginjaume et al., 1999)

1. The dosemeters are placed in a reading wheel inside the HARSHAW-BICRON 5500 reader (Figure 6.2). The reading wheels accommodate up to 50 TL chips.

2. They are submitted to a preheating cycle for 10 seconds at 160°C. The light emission that occurs during this phase is not taken into account for the output signal.

3. Data acquisition then starts for 26.6s. TLDs are heated at 4°C/s until the temperature reaches 250°C. In Figure 6.3 the profile of the temperature cycle during data acquisition is shown in red. The blue curve represents the plot of the light intensity emitted by the TLD; this curve is called the glow-curve.

Figure 6.2: HARSHAW reader and wheel at the start of the reading process

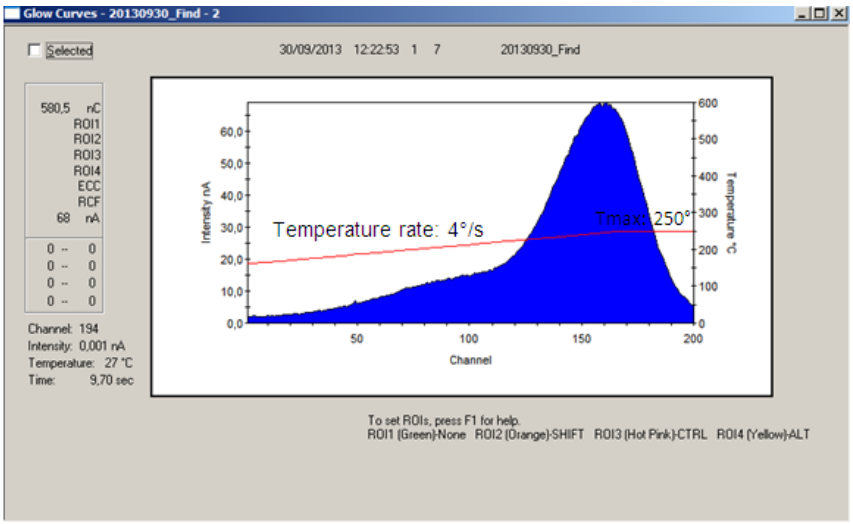

Figure 6.3: Signal from a TL detector

The time-temperature profile, the PMT noise range, the reference light range and the gain are handled by the user, on a separate computer, through the operational software Thermo Scientific^{TM} WinREMS^{TM}. A cooler for the PMT is needed to maintain gain stability and low noise within the PMT itself. To ensure the entire light signal derives from the TLDs (and not from external light sources), a photodiode is included in the system and measures the light within the tube when it is not reading: if the light signal exceeds the PMT noise limits, set by the user at $90pC$, the reader stops and the user may decide to continue the reading or repeat it. The reference light is a parameter used to verify the stability of the system and is usually given by a light emission diode. These two parameters are measured periodically by the system. The user sets their frequency; in general, every 10 readings. Finally, the gain of the PMT is determined by the voltage applied to the PMT itself and determines the amplification of the electric signal inside the tube. For low dose irradiation, a high gain is needed. A PMT can produce an amplification of the signal by a factor of 10^6 or more. In all performed readings the gain was set to high. To guarantee the reliability of the system, both sensitivity and quality controls are necessary. The typical cycle time reading per detector is 40 seconds.

6.1.4 PTW-THELDO oven

At the INTE-UPC dosimetry laboratory a PTW-THELDO oven is available. The user controls the oven thanks to a program interface called THELDO. During the heating cycle, the hot air stream is circulated by a built-in fan to ensure equal temperature distribution throughout the oven volume. The oven is used to perform annealing of the LiF:Mg,Cu,P detectors, which consists of submitting them to a well-defined

heating cycle. The annealing treatment at the INTE laboratory for LiF:Mg,Cu,P is set to a temperature of 240° for 10 minutes, as suggested by the manufacturer. This heating cycle is used in the initial characterization of the batch and prior to each irradiation.

The characterization of the batch starts with several annealing cycles: the treatment at 240° for 10 minutes is repeated 3 times. The aim is to reduce the possibility of variations in dosemeter performance during its usage, overall in terms of sensitivity. The process of annealing must be as reproducible and homogeneous as possible to guarantee all the detectors are submitted to the same treatment.

After the three annealing cycles, in order to ensure the batch homogeneity, the whole batch has to be irradiated using a calibrated gamma source, under the appropriate electron equilibrium conditions. The gamma source used was a Cs-137 source. Electronic equilibrium is ensured by locating the dosemeters in a plastic holder during irradiation. After irradiation, the detectors are read. The detectors which do not comply with tolerance limits, set at 10% of the mean response of the whole batch, were rejected.

TLDs may be re-used after a controlled heating treatment. An annealing cycle of 240° for 10 minutes is carried out prior to the irradiation of the detectors to completely erase all the information stored from any previous exposure to radiation. The aim of this annealing cycle is to recombine all electron-hole pairs and restore the original condition of the TLDs.

6.2 Read-out of dosemeters and determination of the dose for personal monitoring

After a designated monitoring period during which the dosemeters have been exposed to radiation, the TLDs are collected and read with the TLD reader. To correctly assign a specific reading to the person exposed to radiation and wearing that particular TLD, each detector was identified by a number. Background TLDs during the monitoring period have to be kept for each measurement. Once the TLDs exposed to the radiation are read, the background signal is subtracted from the measured TLD signals. However, the output from the reader is not immediately usable for radiation protection purposes. A personal dosimetry service, as in the case of the INTE facility, must provide results in terms of personal dose equivalent $H_{\mathrm{p}}(d)$. $H_{\mathrm{p}}(d)$ is defined as the product between the reading L of a single TLD in terms of electric charge and the calibration factor N_{cal}. The calibration factor is determined in reference conditions. In addition, other factors have to be taken into account, as shown in (6.1).

$$H_{\mathrm{p}}(d) = (L_i f_i - < B >) N_{cal} \frac{\varepsilon_{cal}}{\varepsilon_t} \tag{6.1}$$

L_i represents the reading for a dosemeter i at time t. The individual calibration factor, f_i, is a term that takes into account the response of a single dosemeter with respect to the whole batch (see subsection 6.2.1). $< B >$ is the background, obtained as the average value of readings from multiple dosemeters not exposed to the radiation field under investigation. N_{cal} is the energy calibration factor and ε is the efficiency of the system at the moment of the energy calibration (ε_{cal}) and at time t of measurement (ε_t). The ratio of efficiencies takes into account the stability of the response in time of the whole batch with respect to the response obtained when the energy calibration was performed.

6.2.1 Individual calibration factors and efficiency

To determine the response of a single detector with respect to the whole set, individual calibration factors f_i were calculated for each TLD. The individual calibration factors are determined by irradiating all detectors with a Cs-137 source, at a value of air kerma of 3 mGy. After irradiation, the chips were read and the f_i factors, for each chip, were calculated as $f_i =< M > /M_i$. M_i is the reading of detector i and $< M >$ is the mean of all M_i readings. This process was carried out 6 times from mid-2013 to early-2016, in order to control the stability of the batch.

As stated previously, the parameter used to quantify the stability of the whole batch through time is the ratio of the efficiencies ε_t and ε_{cal}. The efficiency ε_{cal} is calculated as $\varepsilon_t =< M_t > /D$, where D is the given dose of 3 mGy and $< M_t >$ is the mean value of the batch read at time t. The differences in ratios between the first calibration and the following 5 calibrations are within 1%, thus no correction factors for the efficiencies were introduced during this thesis.

6.2.2 Energy calibration factors: energy beam selection

As previously mentioned, the reader output L_i is given in terms of electric charge (Coulomb), consequently it is necessary to estimate an energy calibration factor N_{cal} to convert the unit of charge to the $H_p(d)$dose unit (Sievert). As the name itself indicates, energy calibration factors are energy dependent. Therefore, some energy beams have been selected for calibration. The main radiation qualities of interest for occupational monitoring are the X-ray narrow (N) series defined in ISO 4037-1 (ISO, 1996). The INTE calibration laboratory is accredited by the Spanish National Accreditation Authority to reproduce N qualities. However, since ISO narrow radiation spectra are slightly distant from the energy domain used in IC/IR, additional less filtered radiation beams which can better approximate the field conditions for IC/IR procedures were also considered in this study. RQR qualities defined in IEC 61267 IEC (2005) were also used for energy calibration. Nowadays, it is a common practice to use these radiation qualities for calibration purposes in radiology workplaces. N_{cal} values were calculated for radiation qualities: RQR5, RQR6, RQR7, RQR8, RQR9, N60, N80, N100, N120. The characteristics of these beams are presented in Table 6.1: radiation quality code, tube voltage, mean energy, first and second value layer and the added filtration used in the laboratory to reproduce the reference qualities.

Radiation quality	Tube voltage (kV)	$< E >$ (keV)	HVL	Added filtration (mm)		
				Al	Cu	Sn
N60	60	48	1st- 0.239 mmCu 2nd- 0.269 mmCu	4	0.6	
N80	80	65	1st- 0.591 mmCu 2nd- 0.640 mmCu	4	2	
N100	100	83	1st- 1.118 mmCu 2nd- 1.187 mmCu	4	5	
N120	120	100	1st- 1.714 mmCu 2nd- 1.782 mmCu	4	5	1
RQR5	70	38	1st- 2.41 mmAl 2nd- 3.45 mmAl	2.5		
RQR6	80	41	1st- 3.03 mmAl 2nd- 4.38 mmAl	3		
RQR7	90	44	1st- 3.42 mmAl 2nd- 5.06 mmAl	3		
RQR8	100	48	1st- 3.83 mmAl 2nd- 5.73 mmAl	3		
RQR9	120	56	1st- 5.0 mmAl 2nd- 7.30 mmAl	3.5		

Table 6.1: Characteristics of beam qualities chosen for eye lens dose calibration

6.2.3 Calibration phantom

As mentioned in the introduction, the need for calibrating eye lens dosemeters is very recent, thus ISO 4037-3 (ISO, 1999) does not define any phantom for this purpose. For eye lens dosimetry, the head-shaped phantom recommended within the ORAMED project (Figure 6.4) would simulate the human head and the relative backscattered radiation behavior better than the slab phantom. Because of the lack of a recommended phantom in the standards, and taking into account the recent recommendation in the scientific literature (Gualdrini et al., 2011), (Behrens, 2012b), this cylindrical water filled phantom with PMMA walls was acquired by the INTE laboratories to carry out the present study. This phantom was also chosen for the two EURADOS eye lens intercomparisons (Clairand et al., 2016).

6.3 Characterization of the dosimetry system according to IEC 62387:2012

600 TLD-2000C were acquired by the INTE. 300 pellets were used for calibration and measurement purposes. The remaining TLDs were used to verify that the whole set complies with the IEC 62387 (IEC, 2012) international standard. IEC 62387 specifies the performance requirements of a dosimetry system, including the detectors, the holder and additional equipment, and the corresponding methods to check that these requirements are met.

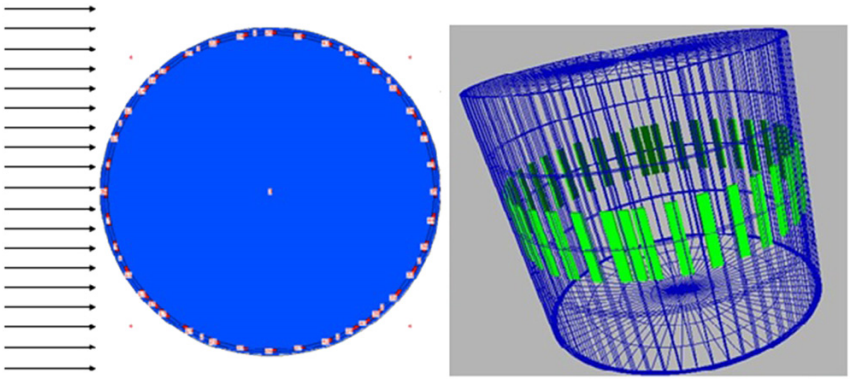

Figure 6.4: Monte Carlo model of the head phantom for eye lens dose calibration (Gualdrini et al., 2011)

According to IEC 62387, the dosimetry system has to comply with several radiation performance requirements, namely repeatability (coefficient of variation), linearity, overload characteristics and reusability, the variation of the relative response due to a change of radiation energy and angle of incidence and over-response to the case of radiation incidence from the side (IEC, 2012). Secondly, other tests are required to check the environmental performance of the dosemeters: the stability of the response with respect to ambient temperature and relative humidity, both for the dosemeter and the reader, the relative response of the dosemeter due to a change in light exposure, dose build-up, fading, self-irradiation, response to natural radiation, the stability of the reader with respect to a change in light exposure and primary power supply. Furthermore, electromagnetic compatibility (low EM disturbances) and mechanical performance (the dosemeter should be able to withstand drops from a height of 1.0 meter) requirements of the dosimetry system are needed. The requirements are fulfilled when the results are within the tolerance limits established by the IEC.

The eye lens dosemeter described in section 6.1 was developed for this thesis. Complete characterization of the dosemeter following the IEC 62387 standard for photon radiation was performed by C. Cagua in her Master's thesis (Cagua and Ginjaume, 2016). Details are beyond the scope of this work and are not provided.

Chapter 7

Monte Carlo calculation for dosimetric purposes

Measurements in real clinical settings present high variability because they depend on numerous parameters. A method broadly used to investigate the influence of individual parameters in personal monitoring is Monte Carlo (MC) simulation of radiation transport. The information provided by MC data helps to understand the results obtained from measurements, where the influence of a single parameter cannot be determined because of high variability of several factors.

7.1 MC simulation: basic concepts

Radiation interactions are stochastic events and so is the transport process, therefore multiple random variables are involved, such as the position, energy and direction of the particles. A random variable is characterized by a probability distribution function (PDF) that is determined by interaction models (differential cross sections). Once the PDFs are known, a random track of a particle (history) can be generated by numerical sampling of random variables, according to their PDF.

The statistical sampling process is based on the selection of random numbers. When a history of a certain particle is generated, a number between 0 and 1 is selected randomly (random-number generator) to determine what kind of interaction (if any) takes place, based on the physics and probabilities governing the processes (i.e. their PDF), to determine the outcome of the particles life at each step. The number of histories necessary to adequately describe a phenomenon is usually quite large: if it is large enough, the average over the simulated histories provides reliable quantitative information of the simulated process.

7.2 Use of PENELOPE and MCNPX

In this work the main general-purpose Monte Carlo codes used are PENELOPE and MCNPX. PENELOPE stands for PENetration and Energy Loss of Positrons and Electrons in matter (Salvat et al., 2006). It was developed at the Universitat de Barcelona and it is freely distributed by the OECD-NEA Data Bank (Paris). It simulates all kinds of interactions, except nuclear reactions, in the energy range from 50 eV to 1 GeV. The general-purpose main program for PENELOPE is called PENEasy and it has been employed for the development of this thesis (Sempau et al., 2011). It provides the user with a set of source models, tallies and variance reduction techniques that are called from a modular code. PENEasy, like PENELOPE, is both free and open software. MCNPX stands for Monte Carlo N-Particle eXtended and is a general-purpose Monte Carlo code developed at Los Alamos (Pelowitz, 2005). MCNPX can be used for neutron, photon, electron, or coupled neutron/photon/electron transport. Energy ranges are from 10^{-11} to 20 MeV for neutrons with data up to 150 MeV for some nuclides, 1 keV to 1 GeV for electrons, and 1 keV to 100 GeV for photons. In MCNPX, similarly to PENELOPE/PENEasy, a txt input file interfaces the user to the Fortran program in which MCNPX is coded. MCNPX is neither an open source program nor is it free.

Similar features can be given for both codes. The user creates an input file that is subsequently read by the MC codes. The input file contains information about:

a) The geometry specification: the three dimensional geometry is defined by cells of specific materials, bounded by quadratic surfaces defined by the user

b) The description of the source: position, type and energy of the particle, ...

c) The type of output (or tallies) desired

d) Any variance reduction techniques used to improve the efficiency of the calculation.

The MCNPX code allows the performance of a MC simulation to be improved by using parallel computing to speed up the calculation. Therefore, in this thesis, its use was preferred when complex geometries were modeled. MCNPX simulations were performed for the sensitivity analysis of parameters of influence in eye lens doses. In this case a realistic clinical scenario was modeled. The simplified IC/IR scenario defined within the framework of the European projects ORAMED (Vanhavere et al., 2011) and ELDO (Koukorava et al., 2014) was adopted. In these simulations, both the patient and the operator, who stands on the right of the patient, were represented by two modified anthropomorphic ORNL-MIRD phantoms (Snyder et al., 1978), as shown in Figure 7.1. The patient is in the supine position. Quadratic surfaces are employed to define all the bodies. Three materials have been used for human tissue: bone, soft tissue and air for the lungs. Very thin tally volumes of $4 \cdot 10^{-3} mm$ thickness were introduced at a depth of 3 mm in the soft tissue of the eye to calculate the personal dose equivalent $H_{\mathrm{p}}(3)$. An hemispherical tally volume of soft tissue and volume of 0.16 cm_3 was defined close to the left eye, at the left lateral position, which realistically represents the position where the dosemeter can be used for the measurement of the dose to the left eye. The code implemented during the ELDO project was used as a basis and modified according to the requirements of this thesis. $H_{\mathrm{p}}(d)$ was calculated by energy deposition tally F6. F6 gives the energy deposited averaged over a cell, in MeV/g. SD cards are used together with the tallies to specify the mass of the tally volumes. The photon p MODE ($F6:p$) was used, namely secondary particles were not included on the MODE card, as electrons generated during photon collisions, are not tracked and their energies are deposited locally at the point of the interaction (the so-called kerma approximation). This approximation is suitable for the selected beams as they are low energetic. In a cell where most of the electrons lose all of their energy before exiting from the cell itself represent a good approximation and is the case for this study. Otherwise, if these generated electrons can carry significant energy into the neighboring cells, the use of the $F6:p$ tally for this cell can result in a large overestimation of the deposited energy (kerma is larger than absorbed dose at high energy).

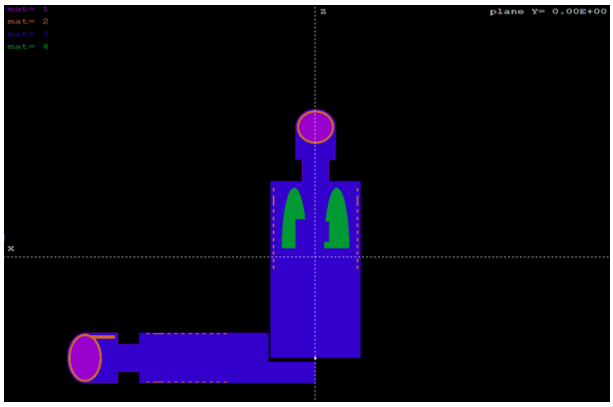

Figure 7.1: IC/IR scenario implemented in MCNPX. Section at plane x=50

The PENELOPE code was used during the preliminary phase. To easily describe a process, an example of how PENELOPE works is given henceforth. When a history is generated, after the first event occurs the particle may be, for instance, scattered. The angle of scattering is then selected randomly from the physics of the scattering distribution (PDF). A secondary particle may be generated and followed (or not) for later analysis. When the particle reaches a certain energy threshold, the particle history is complete. These energy thresholds, called absorption energies (Eabs), are defined by the user. When the particle reaches an energy below Eabs, its interactions are no longer simulated and it is absorbed in the material. Simulations with PENELOPE were used for calibration purposes for the calculation of conversion coefficients $h_{\mathrm{p}K}(d)$. The aim was to have results as reliable as possible. Therefore, all secondary particles generated by a history are tracked. For this reason, Eabs are set at the value of 1 keV, which represents the minimum resolution of the energy beam. On the other hand, following secondary particles slows down the simulation. If a high precision of the simulation is not required, the local absorption of the secondary particles (if any) generated from primary photons can be applied by increasing the Eabs for electrons and positrons to the maximum value of the beam energy spectrum. The quantities of interest requested by the user are tallied. The requested PENELOPE output was the energy deposited in the detection material. This quantity was then divided by the mass of the scoring volume to obtain the absorbed dose.

All interaction events in a photon history are simulated in chronological succession, until the photon reaches an energy lower than Eabs and it is absorbed locally. As regards electron and positron tracks, the simulation is performed by means of a mixed algorithm. Hard collisions are simulated in detail and controlled by several parameters defined by the user: C1, C2, Wcc, Wcr. C1 and C2 control the electron step length between consecutive hard elastic events (in perfectly elastic collisions there is no loss of kinetic energy). C1 is the average angular deflection per step, C2 is the maximum average fractional energy loss per step, Wcc and Wcr are the cut-off energy loss for hard inelastic collisions and for hard bremsstrahlung emission, respectively. The simulation gets faster for large values of these parameters (with $0 \leq$C1,C2≤ 0.2). However, to ensure accuracy, these values should be small. Collision by collision electron/positron simulation is achieved by setting C1, C2, Wcc equal to zero. In the case of the simulations in this thesis, for C1 and C2 parameters a value of 0.02 is adequate and recommended and is then used for calculation of conversion coefficients. Wcc, and Wcr are set to 1% and 0.1% of the mean energy of the source beam, respectively.

The performed simulations are characterized by a low probability of scoring contributions to the quantity of interest. This is generally due to the small scoring volume and, in some cases, to the fact that the scoring volume is not irradiated by the primary source, but by the scattered radiation from bodies between the source and the detector. However,two warnings must be issued. Firstly, in PENELOPE, a parameter called maximum step length has to be defined. If the medium where the energy deposition has to be calculated is extended, setting this parameter is not needed; otherwise, for critical geometries, i.e. with thin bodies, it is reasonable to set this to one tenth of the thickness of the body. This is to ensure that the number of hard collisions within the body is at least 10. In all performed simulations this precaution has been implemented. Secondly, low probability of scoring leads to large statistical uncertainties. To reduce the uncertainty, larger simulation times are required. Therefore, variance reduction techniques are applied to speed up the simulation and, indeed, improve its efficiency.

7.3 Variance reduction techniques in PENELOPE and in MCNPX

In both codes variance reduction techniques are implemented.

In PENELOPE three techniques are available: particle splitting, Russian roulette and interaction forcing. Particle splitting is implemented to increase the likelihood of having a contribution by a particle when it approaches the region of interest. The particle is split into NSPLIT particles; this number is set by the user. Since an initial weight WGHT equal to one is given to primary particles, the generated particles by the splitting will have weight WGHT/NSPLIT. Russian roulette should be used when a particle goes away from the region of interest and is not likely to contribute, thus it is killed with probability PKILL and, if it survives, its weight is replaced by WGHT/(1-PKILL). Interaction forcing forces interactions to occur. This is equivalent to increasing the inverse mean free path (the interaction probability per unit path length). Therefore, to keep the simulation unbiased, a new weight $WGHT_2$ is assigned to secondary particles produced in forced interactions of a particle of weight WGHT. $WGHT_2$ is equal to WGHT/F where F is a factor higher than one and equal to the ratio between the mean free path of the real process and the shorter mean free path defined for the interaction forcing. Particle splitting and interaction forcing are used. After repeating the same test with different NSPLIT values, NSPLIT equal to 10 was chosen because the highest efficiency of the simulation is achieved. Interaction forcing was employed in very thin foil, where the interaction probabilities were very low. Notice that also the weight of the deposited energy is decreased by the factor F when forced interactions occur.

In MCNPX the DXTRAN sphere method is the name of a technique for variance reduction. The DXTRAN sphere is used when particles have a very limited chance of reaching a small region, the user can then specify a sphere that encloses this region. Two spheres have to be defined, one inside the other: an outer and an inner sphere. When a particle collides with the outer sphere, a splitting of the particle into two occurs: a special DXTRAN particle and a no-DXTRAN particle are generated. The DXTRAN particle is created and deterministically scattered towards the inner DXTRAN sphere. Its transport towards the inner sphere is forced, but not the collision, and a new weight is assigned to it (a fraction of the weight of the original particle). The no-DXTRAN particle continues its track with no change in its weight. The bias introduced is then compensated by adding a condition that if the no-DXTRAN particle crosses the inner DXTRAN sphere, it is killed. This method has been adopted by the user to calculate the dose in small regions of interest, such as the operator's eyes, where the interaction of scattered radiation from the patient is unlikely to occur.

The way to define the DXTRAN sphere for photons p is DXT:p x y z R_i R_o. x, y and z represent the point where the spheres are centered, R_i and R_o are the inner and outer radius of the two spheres. To avoid a massive loss of particles inside the spheres, it is important to set the difference between the inner and outer radius equal to the mean free path in the tissue of the region of interest, for the specific energy of the beam. In the cases analyzed, the mean energy of the beam is approximately 50 keV. For a photon with this energy, in muscle soft tissue, the mean free path is 4.46 *cm*. An example of syntax of the DXT sphere for the eye region is: DXT:P 11 31 88.1 10 14.46.

Another variance reduction technique in MCNPX is the importance of a particle. The default importance for all particles is one. The importance has not been changed in the programs implemented for the present study. Otherwise, if, for instance, the photon importance of cell 1 is 2, then a track will be split into two, and each new track will have half the weight of the original one before splitting.

Unfortunately, in spite of variance reduction techniques, to reach an accurate and reliable result for complex geometries, long calculation times are needed. The use of Monte Carlo calculation in real time is not generally feasible in clinical practice, hence Monte Carlo simulations have found their major application in research. As previously stated, they are very helpful in providing specific information on isolated parameters difficult to derive from measurements with dosemeters, because of the multi-parametric nature of clinical procedures. Thus, experimental measurements are essential for dose assessment and still represent the main source of data available in the literature.

Chapter 8

X-ray spectra and data analysis

8.1 X-ray spectra definition

Most of the MC calculations require the definition of the radiation sources, which are X-ray beams. The program XCOMP5 (Nowotny, Hofer, 1985) is used to generate the required X-ray spectra. At the INTE facility, the X-ray-tube-anode angle is 18° and its inherent filtration is $7mm$ of Beryllium. Apart from the intrinsic parameters of the tube, features of the generated beam are given by the user. For instance, for generating an RQR5 beam, $2.5mm$ of aluminum is needed as added filtration and a peak voltage of 70 kV has to be entered. The program provides the fluence spectrum of the beam, for energy steps of 1 keV. In Figure 8.1 the fluence spectra of N60 to N120 and RQR qualities from 5 to 9 generated by Xcomp5 and visualized by Matlab are presented.

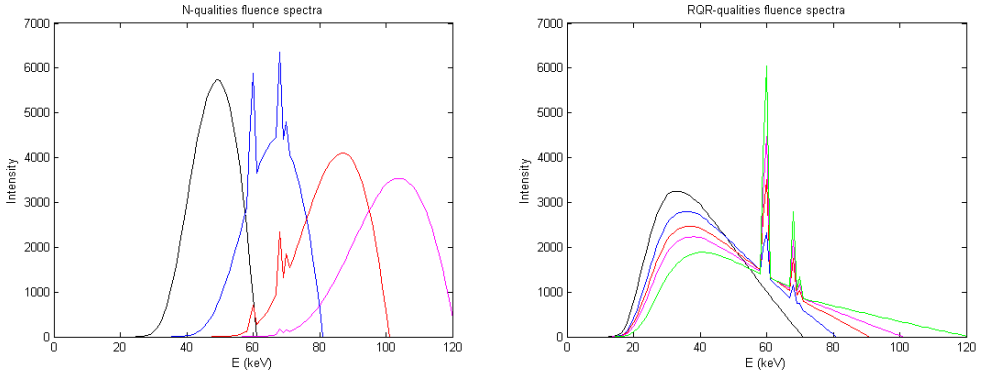

(a) N qualities (b) RQR qualities

Figure 8.1: Spectra from XCOMP database (Nowotny and Hofer, 1985)

8.2 Data analysis tool

Statistical analysis of data was performed with SPSS Statistics (IBM, 2013). SPSS is a software package used for logical batched and non-batched statistical analysis. In this work it has been used mainly to verify the statistical significance of difference in mean values. SPSS has a user-friendly interface and the main features are accessible by a pull-down menu. The most useful options used in this thesis were descriptive statistics, bivariate statistics, such as the t-test, and graphics generation. The output can be captured as data, text, or as graphic formats (i.e. box-plots). Matlab (MathWorks, 2000) numerical computing environment and Microsoft Excel have also been used for algorithm development, data visualization, data analysis, and numerical computation.

Part IV

Results

Chapter 9

Determination of conversion coefficients from air kerma to eye lens equivalent dose

As stated in the introduction, the set of air kerma to $H_{\mathrm{p}}(3)$ conversion coefficients $h_{\mathrm{p}K}(3)$ available in the literature is limited to certain qualities and phantoms. To overcome this problem, $h_{\mathrm{p}K}(3)$ for the cylindrical phantom for all RQR IEC-61267 (IEC, 2005) X-ray beams and for angles of incidence from 0° to 180° were calculated. The RQR2 to RQR9 IEC-61267 qualities were chosen because they provide a better approximation of the radiation spectra found in practice in interventional cardiology and radiology workplaces than ISO 4037-1 qualities and are often used in intercomparisons in this field. The study also discusses the influence of different approaches used in the literature for the calculation of conversion coefficients. The simulation study to obtain the conversion coefficients was initially performed using both PENELOPE (Salvat et al., 2006) and MCNPX (Pelowitz, 2005) MC codes.

The kerma-to-personal dose equivalent $H_{\mathrm{p}}(3)$ conversion coefficient is defined as the ratio of the quantities $H_{\mathrm{p}}(3)$ and the air kerma K_{a}:

$$h_{\mathrm{p}K}(3) = H_{\mathrm{p}}(3)/K_{\mathrm{a}} \tag{9.1}$$

The air kerma K_{a} and $H_{\mathrm{p}}(3)$ in the cylindrical ICRU tissue phantom were calculated to obtain the $h_{\mathrm{p}K}(3, RQR, 0°)_{cyl}$ conversion factors for normal incidence and for the radiation qualities RQR. Although K_{a} and $H_{\mathrm{p}}(3)$ are obtained per unit fluence, i.e. K_{a}/ϕ and $H_{\mathrm{p}}(3)/\phi$, they are referred to as K_{a} and $H_{\mathrm{p}}(3)$ for simplicity. In the set-up geometry the cylindrical phantom embedded in vacuum is irradiated by a 20 cm × 20 cm collimated square beam, placed 1 m from the phantom front-face. To assess $H_{\mathrm{p}}(3)$ values, a $0.5-mm-$thick sensitive volume was placed at 3 mm depth within the cylinder. Parallelepipeds of 1 mm width, 0.5 mm thickness, and 5 cm height were used as scoring volumes for both MC codes. The conversion coefficient depends on the energy, the directional distribution of the incident radiation and the phantom used in the calibration. $h_{\mathrm{p}K}(3, RQR, \alpha)_{cyl}$ values for different RQR radiation qualities and angles α from 0 to 180° were assessed only using MCNPX. PENELOPE was employed to compare the results only for normal incidence. The statistical uncertainty of the MC simulations was to within 0.1-1 % (1sd). It is worth mentioning that PENELOPE and MCNPX manage the simulation output process in different ways.

The requested PENELOPE output for the calculation of $H_{\mathrm{p}}(3)$ was the energy deposited in the detection material. This quantity was then divided by the mass of the scoring volume to obtain the absorbed dose at 3 mm depth. Cut-off energies were set to 1 keV for both electrons and positrons. On the other hand, for the calculation of the air kerma, transport of secondary electrons and positrons was disregarded by setting both cut-off energies equal to the maximum energy of the radiation spectrum, which is the voltage applied to the X-ray tube. For the MCNPX calculations, energy deposition tally F6 was used, employing the kerma approximation for both $H_{\mathrm{p}}(3)$ and K_{a}. $h_{\mathrm{p}K}(3)$ coefficients obtained by PENELOPE were calculated considering secondary electron transport, while $h_{\mathrm{p}K}(3)$ obtained by MCNPX disregarded secondary particles in order to evaluate the difference between the two approaches for these energies. The codes show very similar outputs when identical geometries are run.

To find out if analytic calculations might also be a valid method for the calculation of $h_{\mathrm{p}K}(3)$, conversion coefficients were calculated for RQR qualities and for a varying angle of incidence from 0 to 180° by

implementing the interpolation technique suggested by Behrens (Behrens, 2011). Conversion coefficients for mono-energetic photon beams were taken from Gualdrini (Gualdrini et al., 2013). The following steps were considered:

a) Firstly, the photon fluence spectra $d\phi/dE$ for the radiation qualities of interest were determined from the XCOMP5 program (Nowotny and Hofer, 1985). The fluence per unit energy $d\phi/dE_i$ is given for integer values of energy from 1 keV to the voltage applied to the X-ray tube to generate the radiation beam (Vmax), in steps of 1 keV.

b) Subsequently, the conversion coefficients $h_{\mathrm{p}K}(3, RQR, \alpha)_{cyl}$ were calculated from $h_{\mathrm{p}K}(3, E_i, \alpha)$ for mono-energetic photons for the ICRU cylindrical phantom by applying the following equation:

$$h_{\mathrm{p}K}(3, RQR, \alpha)_{cyl} = \frac{H_{\mathrm{p}}(3, RQR, \alpha)_{cyl}}{K_{\mathrm{a}}(RQR)} = \frac{\sum_{i=1keV}^{Vmax} \frac{d\phi}{dE}_i h_{\mathrm{p}K}(3, E_i, \alpha) E_i \frac{\mu_{en}(E_i)}{\rho}}{\sum_{i=1keV}^{Vmax} \frac{d\phi}{dE}_i E_i \frac{\mu_{en}(E_i)}{\rho}} \tag{9.2}$$

The formula represents the ratio between the dose equivalent at 3 mm depth and K_{a}, calculated for the radiation quality of interest RQR. $K_{\mathrm{a}}(RQR)$ is calculated from the photon fluence $d\phi/dE_i$ and the mass-energy absorption coefficients of air. The mass-energy absorption coefficients $\mu_{en}(E_i)/\rho$ for photons in air are obtained by log-log interpolation (logarithmic both in energy and in values) from available values (only for few energies) taken from Hubbell and Seltzer (1995) and folded with photon fluence and energies E_i. The $H_{\mathrm{p}}(3, RQR, \alpha)_{cyl}$ are calculated as the convolution of the conversion coefficients $h_{\mathrm{p}K}(3, E_i, \alpha)_{cyl}$ with photon fluence, energies E_i and $\mu_{en}(E_i)/\rho$. $h_{\mathrm{p}K}(3, E_i, \alpha)_{cyl}$ are obtained by using a cubic spline interpolation at low energies (for energies between 10 keV and 40 keV and for angles larger than 90°) and a linear-logarithmic interpolation for the rest of energies and angles (linear in values and logarithmic in energy). $h_{\mathrm{p}K}(3, RQR, \alpha)_{cyl}$ are then calculated as the ratio between $H_{\mathrm{p}}(3, RQR, \alpha)_{cyl}$ and $K_{\mathrm{a}}(RQR)$ for the specific RQR quality.

Results from MC calculations and interpolations are shown in Table 9.1. Only the coefficients for the qualities of interest for the calibration and for normal incidence are shown. The set of conversion coefficients obtained as mean values between MC codes (column 4) was then used for the set-up of a calibration procedure for the UPC-ELD.

RQR qualities	PENELOPE	MCNPX	MC average	Interpolation
RQR5	1.281	1.270	1.276	1.276
RQR6	1.349	1.336	1.343	1.343
RQR7	1.384	1.368	1.376	1.376
RQR8	1.406	1.394	1.400	1.403
RQR9	1.461	1.456	1.459	1.462

Table 9.1: Conversion coefficients $h_{\mathrm{p}K}(3, RQR, 0)_{cyl}$ in Sv/Gy from MC and interpolation methods for 0° angle of incidence and RQR5 to RQR9 qualities

The difference between PENELOPE and MCNPX $h_{\mathrm{p}K}(3, RQR, 0)_{cyl}$ were below 1%. The statistical uncertainty for both MC codes was within 1%, for one standard deviation. This result confirms the validity of the kerma approximation used in the following calculations. In Table 9.2 all conversion coefficients $h_{\mathrm{p}K}(3, RQR, \alpha)_{cyl}$ calculated with MCNPX for RQR qualities and for angles of incidence from 0 to 180° are listed.

The MCNPX output in Table 9.2 was compared to the values obtained by interpolation. For all the considered incident angles, $h_{\mathrm{p}K}(3, RQR, \alpha)_{cyl}$ differences were lower than 0.8%. This result highlights the fact that the analytical method is both a good and quick estimation tool for the calculation of conversion coefficients within the analyzed energy range, provided that conversion coefficients for mono energetic photon beams are available. As suggested by Behrens (Behrens, 2011), for angles larger than 90° an approximation with a cubic polynomial can better estimate conversion coefficients at low energies from 10 up to 40 keV, and thus avoid unrealistic results. Indeed, in this angle and energy range, the difference between analytical and simulated outputs is reduced from a maximum of 7% (linear interpolation on a log-lin scale) to values within 0.8% (cubic spline interpolation). Therefore, MC modelling has been considered the golden standard method even though interpolation results lead to very good approximations when this technique has been chosen carefully. Figure 9.1 shows an example of the two different interpolation techniques (linear and cubic) applied at low energies for an incident angle of 105°, for the RQR5 spectrum. If only linear interpolation

	$h_{pK}(3, RQR, \alpha)_{cyl}$							
Angles	RQR2	RQR3	RQR4	RQR5	RQR6	RQR7	RQR8	RQR9
0°	1.106	1.178	1.232	1.270	1.336	1.368	1.394	1.456
10°	1.099	1.172	1.226	1.268	1.337	1.369	1.396	1.455
15°	1.099	1.172	1.226	1.269	1.336	1.369	1.397	1.456
20°	1.094	1.167	1.221	1.262	1.329	1.363	1.390	1.449
30°	1.081	1.154	1.208	1.247	1.314	1.347	1.373	1.437
40°	1.060	1.140	1.186	1.228	1.295	1.330	1.358	1.418
45°	1.043	1.117	1.171	1.215	1.283	1.317	1.346	1.408
50°	1.019	1.093	1.149	1.195	1.263	1.296	1.324	1.388
60°	0.965	1.041	1.097	1.141	1.211	1.247	1.276	1.341
70°	0.883	0.945	1.016	1.055	1.128	1.166	1.197	1.265
75°	0.800	0.882	0.941	0.989	1.064	1.102	1.134	1.207
80°	0.705	0.787	0.859	0.902	0.981	1.020	1.052	1.128
90°	0.450	0.533	0.595	0.643	0.723	0.766	0.802	0.884
105°	0.131	0.186	0.232	0.269	0.330	0.365	0.396	0.467
120°	0.039	0.067	0.093	0.117	0.153	0.177	0.198	0.246
135°	0.015	0.030	0.046	0.062	0.086	0.102	0.117	0.151
150°	0.008	0.018	0.029	0.040	0.057	0.070	0.081	0.107
165°	0.005	0.013	0.022	0.031	0.046	0.056	0.066	0.088
180°	0.004	0.011	0.020	0.029	0.042	0.052	0.062	0.082

Table 9.2: $h_{pK}(3, RQR, \alpha)_{cyl}$ calculated with MCNPX for RQR qualities and for angles of incidence from 0° to 180°

had been chosen, it would have led to an overestimation of the $h_{pK}(3, RQR, 105)_{cyl}$ conversion coefficient.

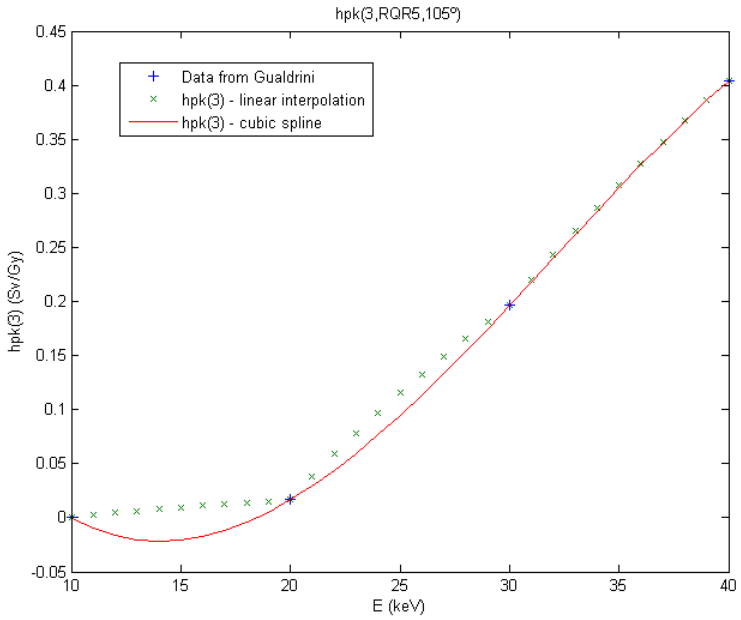

Figure 9.1: Application of two different interpolation techniques to $h_{pK}(3)$ for RQR5 and 105° angle of incidence

The influence of RQR reproduced at different laboratories has also been studied. As opposed to ISO 4037-1 qualities, IEC-61267 does not specify the filtration needed to produce RQR beams. RQR qualities are defined by the tube voltage and the nominal first half-value layer. In order to be reproduced, the additional filtration has to be adjusted to obtain a ratio between air kerma (or air kerma rate) with and without a filter of thickness equal to the nominal first half-value layer between 0.485 and 0.515. $h_{pK}(3)$ were calculated for the RQR spectra generated at the Secondary Standard Laboratory at the Universitat Politècnica de Catalunya (UPC) (Column 3 in Table 9.3), but to evaluate the influence of the filtration

used by different laboratories, calculations were repeated for the RQR spectra used by the Metrology Institute at the Physikalisch-Technische Bundesanstalt (PTB)in Germany. The information regarding the spectra generated at PTB are provided in PTB calibration certificates (Column 4 in Table 9.3). The inherent filtration for UPC and PTB beams is equal to 7 $mmBe$. In addition, results have also been compared with $h_{pK}(3)$ coefficients calculated by the French National Metrology Laboratory CEA LIST/LNE LNHB(5) for RQR7 and RQR9 nominal HVL values (Column 5, Table 9.3).

	Tube voltage	HVL (mmAl)			Added filtration (mmAl)		
	(kV)	UPC	PTB[a]	CEA[b]	UPC	PTB	CEA
RQR2	40	1.41	1.42		2.5	2.49	
RQR3	50	1.78	1.77		2.5	2.46	
RQR4	60	2.11	2.19		2.5	2.68	
RQR5	70	2.39	2.57		2.5	2.83	
RQR6	80	3.01	3.01		3.0	2.99	
RQR7	90	3.48	3.48	3.48	3.0	3.18	3.0
RQR8	100	3.86	3.96		3.0	3.36	
RQR9	120	4.98	5.00	5.00	3.5	3.73	3.39

Table 9.3: HVL and added filtration for the different standard laboratories and RQR qualities. *a* Data obtained from PTB calibration certificates (PTB, 2012). *b* CEA LIST/LNE LNHB (Vanhavere et al., 2012)

Results showed good agreement. Differences were below 1.5% for angles smaller than 90° and between 1 and 7% for larger angles. The larger disagreement was found for RQR5 and RQR8 qualities, where differences in added filtration are higher. The conversion coefficients given in Table 9.2 are calculated for RQR qualities as defined in our laboratory. From the statement above, it has been verified that up to an angle of incidence of 90° coefficients from Table 9.2 can be used by other laboratories to within an uncertainty of 2% (one standard deviation). This is the same uncertainty stated in ISO 4037-3 for ISO 4037-1 quality conversion coefficients. For larger angles of incidence specific conversion coefficients should be determined.

In addition, data were also compared with the conversion coefficients published in Table 2.7 in the ORAMED report (Vanhavere et al., 2012) for RQR7 and RQR9, for angles up to 90°. In this case, results agreed to within 0.6%.

Conversion coefficients shown in Table 9.1 and Table 9.2 were published in (Principi et al., 2015c) and are used in this thesis for the characterization of UPC dosemeters when using RQR qualities. For ISO N-qualities (Behrens, 2012a) are used.

Chapter 10

Performance verification of the UPC-ELD

10.1 Energy and angular response

10.1.1 Energy calibration and calculation of optimal energy calibration factors

The average energy of the scattered radiation fields encountered in IC/IR ranges from 20 to 100 keV (Eurados report ORAMED). Radiation qualities RQR5, RQR6, RQR7, RQR8, RQR9, N60, N80, N100 and N120 were chosen to study the energy response of the different dosimetric systems used in this thesis. The characteristics of these beams are presented in Part III. 279 pellets were irradiated, and 10 detectors were kept apart (not irradiated) for background radiation measurement. The calibration set-up for eye lens dosimetry was based on the suggested cylindrical phantom (Gualdrini et al., 2011) and was carried out for UPC-ELD and EYE-D holders. The UPC-WBD was irradiated using the ISO slab phantom for the assessment of $H_{\mathrm{p}}(10)$ and $H_{\mathrm{p}}(0.07)$. Three UPC-ELDs and one EYE-D were irradiated on the cylindrical phantom and two UPC-WBDs on the slab phantom, at each radiation quality. The energy responses were determined through the energy calibration factors for the studied radiation beams. The energy calibration factors are defined as the reference equivalent dose $H_{\mathrm{p}}(d)_{ref}$ divided by the measured quantity M_Q, for the specific beam quality Q.

$$N_{cal}(Q, H_{\mathrm{p}}(d)) = \frac{H_{\mathrm{p}}(d)_{ref,Q}}{M_Q} \tag{10.1}$$

The reference equivalent dose at a depth d, in units of μSv, is given by:

$$H_{\mathrm{p}}(d)_{ref,Q} = K_{\mathrm{a},ref} h_{\mathrm{p}K}(d, 0) \tag{10.2}$$

Where $K_{\mathrm{a},ref}$ is the reference air kerma, measured by a secondary standard ionization chamber. $h_{\mathrm{p}K}(d,0)$ is the conversion coefficient from air kerma to equivalent dose at depth d, for the radiation quality Q and for normal irradiation. The measured quantity is determined by using the equation:

$$M_Q = L_i f_i - < B > \tag{10.3}$$

Where L_i is the reading of the dosemeter i, f_i is the individual calibration factor for detector i, and $< B >$ is the mean reading of background detectors. It is given in units of electric charge (nC). Table 10.1 presents the energy calibration factors for each reference quality and for the different types of dosemeters.

The standard uncertainties of the energy calibration factors $N_{cal}(Q, H_{\mathrm{p}}(d))$(k=1) are calculated following the Guide to the expression of Uncertainty in Measurement (ISO/IEC, 2008). Details are given in Appendix B.

In addition, $N_{cal}(Q, H_{\mathrm{p}}(d))$ are represented in Figure 10.1 for WBD as a function of the ratio between $M(10)$ and $M(0.07)$, where $M(10)$ is the reading at $10mm$ depth, and $M(0.07)$ at $0.07mm$, in nC. This ratio takes into account the penetration depth of the radiation. It is function of the radiation quality and is used in the algorithm for $H_{\mathrm{p}}(10)$ calculation.

Based on typical IC/IR beam characteristics, the energy calibration factor for the estimation of $H_{\mathrm{p}}(0.07)$ is calculated as the average of the energy calibration factors for radiation qualities RQR and

Q	$N_{cal}(Q, H_p(0.07))$	$N_{cal}(Q, H_p(10))$	$N_{cal}(Q, H_p(3))$UPC-ELD	$N_{cal}(Q, H_p(3))$EYE-D
RQR5	6.08±0.16	16.15±0.43	5.40±0.14	5.70±0.24
RQR6	6.58±0.17	15.19±0.40	5.51±0.15	5.75±0.24
RQR7	6.38±0.17	13.23±0.37	5.58±0.15	5.91±0.25
RQR8	6.48±0.17	12.33±0.33	5.52±0.15	6.06±0.25
RQR9	6.36±0.17	10.67±0.28	5.90±0.16	6.06±0.25
N60	6.29±0.17	10.54±0.28	5.48±0.14	5.48±0.23
N80	6.87±0.18	8.64±0.23	6.40±0.17	6.46±0.27
N100	7.07±0.19	8.36±0.22	7.35±0.19	7.84±0.33
N120	7.95±0.21	8.94±0.24	7.82±0.21	8.13±0.34

Table 10.1: Energy calibration factors $N_{cal}(Q, H_p(d))$±u$(N_{cal}(Q, H_p(d)))$ (k=1) for each reference quality Q and at depth d, for the different types of dosemeters

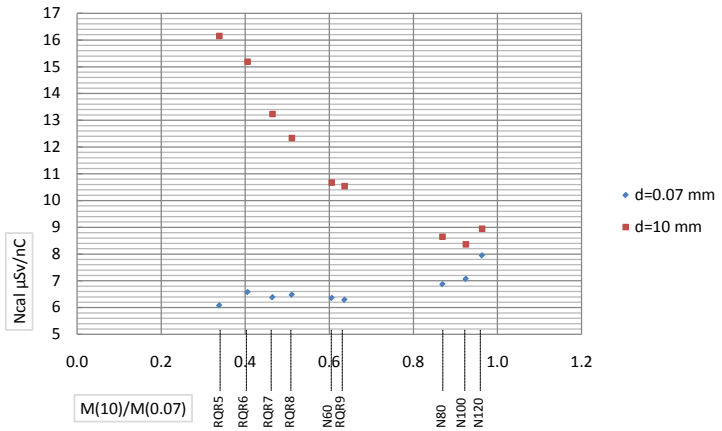

Figure 10.1: $N_{cal}(Q, H_p(d))$ vs. $M(10)/M(0.07)$ ratio for $H_p(10)$ and $H_p(0.07)$

N60 shown in Table 10.1:

$N_{cal}(H_p(0.07))$= 6.36 μSv/nC. The resulting uncertainty is u$[N_{cal}(H_p(0.07))]$ = 4.8% (k=1) (see Appendix B).

As regards the determination of $H_p(10)$, $N_{cal}(H_p(10))$ is clearly energy dependent. The calibration factor is determined through a least square fitting as a function of $M(10)/M(0.07)$: $N_{cal}(H_p(10)) = 20.36 - 14.56 \cdot M(10)/M(0.07)$ in μSv/nC. The relative uncertainty in the range of interest associated to the proposed algorithm is 0.8% (k=1). The combined uncertainty associated to $N_{cal}(H_p(10))$, u$[N_{cal}(H_p(10))]$=4.3% (k=1) (see Appendix B).

For $H_p(3)$, the relative energy calibration factor normalized to ^{137}Cs is given in Figure 10.2, for normal incidence (α=0).

Maximum deviation of the energy calibration factors for RQR and N60 qualities with respect to ^{137}Cs is around 10% for both dosemeters, whereas it increases up to 40% for N120 radiation quality. UPC-ELD tends to lower values with respect to data from the EYE-D, although both dosemeters give an energy response within the standard requirements. Based on these results, the energy calibration factor to obtain $H_p(3)$ for unknown photon radiation fields typical to IC/IR is calculated as the average of the calibration factors obtained for RQR5, RQR6, RQR7, RQR8, RQR9 and N60. This proposal provides a deviation in this range with respect to ^{137}Cs of 5%, calculated as the maximum deviation of $N_{cal}(Q, H_p(3))$ with respect to $N_{cal}(^{137}\text{Cs})$, divided by $N_{cal}(^{137}\text{Cs})$.

The energy calibration factors are:

For EYE-D: $N_{cal}(H_p(3))$ = 5.83 μSv/nC, with an associated relative uncertainty in the range of interest of 5.9% (k=1).

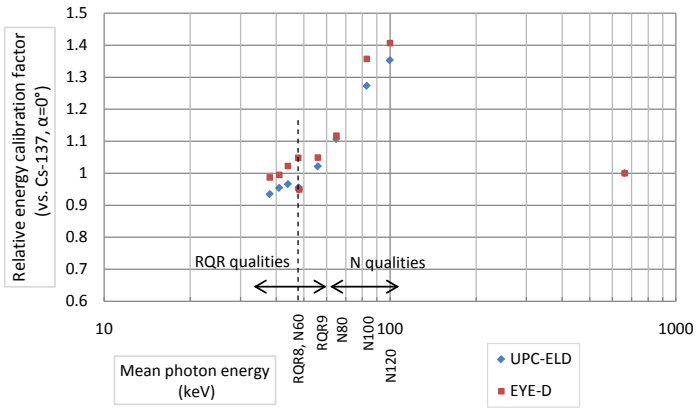

Figure 10.2: Relative energy response of UPC-ELD and EYE-D to ^{137}Cs

For UPC-ELD: $N_{cal}(H_{\mathrm{p}}(3)) = 5.57$ μSv/nC, with an associated relative uncertainty in the range of interest of 5.0% (k=1) (see Appendix B). The uncertainty of the EYE-D is larger than the uncertainty of the UPC-ELD because, as it was decided not to use it in the measurement campaigns, a single detector was used for the determination of $N_{cal}(Q, H_{\mathrm{p}}(d))$.

When the eye-lens dosemeter is used together with a UPC-WBD dosemeter, the radiation quality can be estimated using the ratio $M(10)/M(0.07)$, and thus a more energy specific calibration factor is used, as summarized in Table 10.1.

10.1.2 Angular response

Angular response was also evaluated for both UPC-ELD and EYE-D. In this case, irradiations were limited to RQR6 and N60 qualities. The dosemeters were located at 0°, 45° and 75° with respect to the normal incidence of the beam to the frontal face of the phantom, along the horizontal axis.
The ideal angular response is achieved when the dosemeters fulfill the equation:

$$\frac{N_{cal}(Q,\alpha)}{N_{cal}(Q,0)} = \frac{K_{\mathrm{a}} h_{\mathrm{p}K}(3,\alpha) M(0)}{K_{\mathrm{a}} h_{\mathrm{p}K}(3,0) M(\alpha)} = 1 \tag{10.4}$$

That is:

$$\frac{M(\alpha)}{M(0)} = \frac{h_{\mathrm{p}K}(3,\alpha)}{h_{\mathrm{p}K}(3,0)} \tag{10.5}$$

Where $M(\alpha)$ is the dosemeter reading for an incident angle α, whilst $M(0)$ is the reading at normal incidence. It thus follows that the optimal angular response is achieved when the ratio between readings at a certain angle α and for normal incidence is equal to the ratio between the conversion coefficients $h_{\mathrm{p}K}(3,\alpha)$ and $h_{\mathrm{p}K}(3,0)$. Conversion coefficients for the cylindrical phantom for N60 quality were taken from Behrens (Behrens, 2012a), while for RQR6 they were taken from Principi et al. (Principi et al., 2015c).
Figure 10.3, presents the ratio of the readings of the two tested eye lens dosemeters at an angle α compared with normal incidence for RQR6 and N60. In addition, the theoretical ratio, this is the ratio of the conversion coefficients, is also represented.

Table 10.2 lists the angular response for the studied configurations and the deviation with respect to the ideal angular response, which is unity.

In the case of the EYE-D, the largest deviation is 5% for 75° and RQR6, whilst for UPC-ELD a deviation of 8% is observed for 75° and both N60 and RQR6 qualities. The performance of the dosemeters was compared to the requirements of the IEC standard for passive photon dosimetry. The IEC standard IEC 62387-1 (IEC, 2012) requires that the energy and angular response for any type of passive photon dosimeters should be within 0.71 and 1.67 at any energy and angle. Both dosemeters fulfill these requirements.

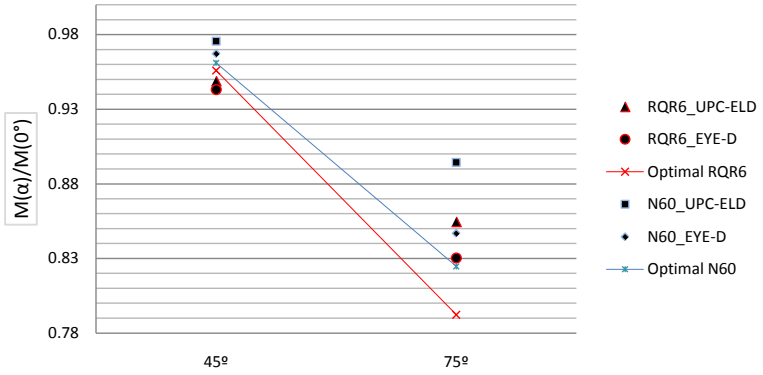

Figure 10.3: Angular dependence for UPC-ELD and EYE-D relative to normal incidence

	$\frac{h_{pK}(3,45)M(0)}{h_{pK}(3,0)M(45)}$	$\frac{h_{pK}(3,75)M(0)}{h_{pK}(3,0)M(75)}$	Deviation wrt ideal response	
			45°	75°
N60 UPC-ELD	1.015	1.084	2%	8%
N60 EYE-D	1.006	1.026	1%	3%
RQR6 UPC-ELD	0.992	1.079	-1%	8%
RQR6 EYE-D	0.987	1.048	-1%	5%

Table 10.2: Angular response for UPC-ELD and EYE-D relative to normal incidence and deviation with respect to the ideal angular response

10.2 Results of the UPC-ELD in the EURADOS 2014 eye lens intercomparison

Intercomparison exercises dedicated to individual monitoring services are aimed at comparing results with other participants and improving dosimetry systems. The final check of the performance of the UPC-ELD system for photon fields typical from medical applications was obtained through the results obtained from the first intercomparison exercise devoted to eye lens dosemeters, organized by EURADOS (Clairand et al., 2016). 20 European individual monitoring services from 15 different countries participated in this exercise. Nine individual monitoring services provided the EYE-D system, while the other participants provided different systems of various designs. UPC-ELD was also tested during the intercomparison. The dosemeters were located on the suggested cylindrical phantom for eye lens dose calibration (Gualdrini et al., 2011). Figure 10.4 shows the different tested types of eye lens dosemeters. The irradiations were carried out with several photon fields chosen to cover both the energy and angle ranges encountered in medical workplace using the cylindrical phantom: S-Cs, ISO X-ray narrow series N40, N60, N80 and RQR6 IEC diagnostic qualities. Finally, irradiations were performed with a realistic field representative of the scattered field at the level of the operator in IC/IR. They correspond to a field with mean energy of 42 keV and resolution of 52 keV, produced by a primary X-ray beam of 70 keV and a filtration of 4.5 mmAl + 0.2 mmCu, which corresponds to a mean energy of 48 keV and a resolution of 60 keV (Bordy et al., 2007). For irradiations with ^{137}Cs and RQR6, different ranges of doses in terms of personal dose equivalent $H_p(3)$ were given. Furthermore, some irradiations were performed at different angles: at 0°, 45° and 75° for RQR6 and at 0° and 60° for S-Cs. Table 10.3 summarizes the experimental set-ups used in the intercomparison.

UPC-ELDs were identified in the intercomparison with the code XAH.

Figure 10.5 shows the box plots with minimum, first quartile, median, third quartile and maximum responses, R, for each participant, anonymously identified, resulting from the intercomparison exercise. The response of a dosemeter was defined as the value of the dose measured by the participant and corrected for background and transit dose, $H_p(3)$, divided by the reference value given by the irradiation laboratory.

For the analysis of the global results, the performance limits according to the ISO 14146 standard, commonly known as *trumpet curves*, were adopted:

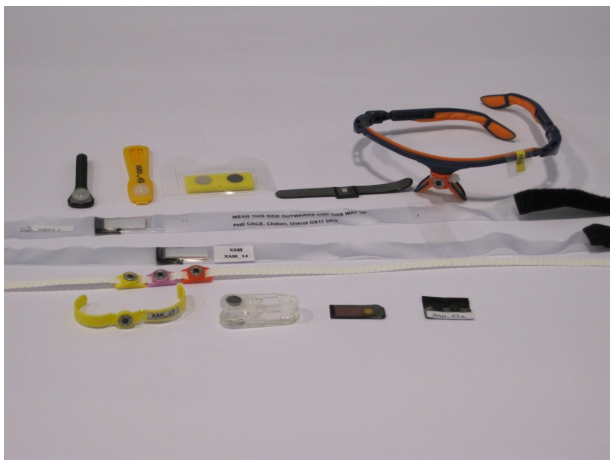

Figure 10.4: Tested types of dosemeters during EURADOS-2014 eye lens intercomparison

Set-up	Radiation quality	Number of irradiated dosemeters	Range Hp(3) (mSv)
1	S-Cs; 0°	2	0.4 - 0.5
2	S-Cs; 0°	2	2.0 - 2.2
3	S-Cs; 60°	2	2.0 - 2.1
4	N-40; 0°	2	3.0 - 3.1
5	N-60; 0°	2	3.0 - 3.1
6	N-80; 0°	2	3.0 - 3.1
7	RQR6; 0°	2	2.6 - 2.7
8	RQR6; 45°	2	2.5 - 2.6
9	RQR6; 75°	2	2.1 - 2.2
10	Realistic field (Bordy et al., 2007)	2	0.9 - 1.0

Table 10.3: Experimental set-ups for the EURADOS-2014 eye lens intercomparison

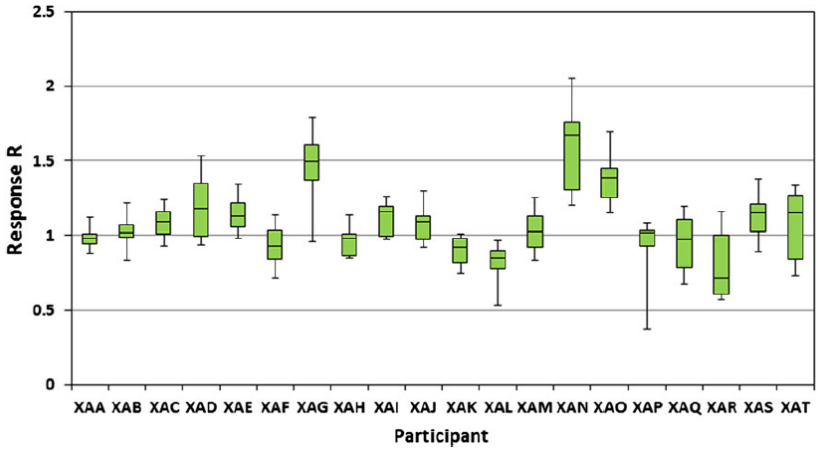

Figure 10.5: Distribution of the response R for dosimetry systems from all participants (Clairand et al., 2016).

$$\frac{1}{F}\left(1-\frac{2H_0}{H_0+H_c}\right) \leq R \leq F\left(1+\frac{H_0}{2H_0+H_c}\right) \tag{10.6}$$

H_c is the conventional true value, R is the response, F is set equal to 1.5 following the recommendations of the ICRP 75 report and H_0 is the *lower limit of the dose range for which the system has been approved* as mentioned in the ISO 14146 standard (ISO, 2000). For this IC, a value of H_0 of 0.085 mSv was chosen for all participants, assuming a *lower limit of the dose range* of $1mSv$ in a year, and a monthly issuing frequency. For the UPC-ELD, the response R as a function of the reference doses H_c is displayed in Figure 10.6 and the *trumpet curves* were built up according to the equation Equation 10.6.

Results show that the response provided by the UPC-ELD fulfills the ISO 14146 standard requirements, as R remains within the *trumpet curves* for all configurations under study. In general,

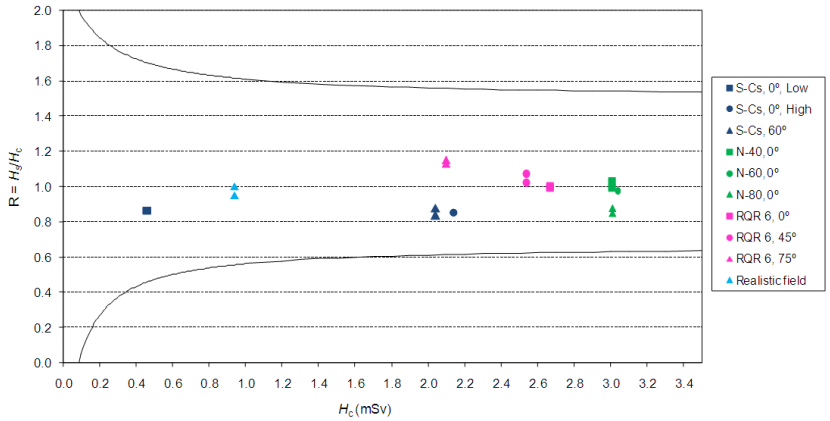

Figure 10.6: Response R as a function of reference doses H_c for the UPC-ELD

17 dosimetry systems out of the 20 participating provided 90% of their response in accordance with the ISO 14146 standard requirements, which can be considered a globally satisfactory result for this first eye lens IC. However, a relatively large variability is observed among participants, as the median of responses ranges from 0.72 to 1.67. The results for the UPC-ELD are in all cases within the IEC 62387-1 and ISO 14146 requirements. Thus, it can be concluded that it is a suitable system for eye lens dosimetry in photon fields.

Chapter 11

Measurements on phantom in a realistic clinical set-up

The aim of this part of the study is to evaluate different possible approaches in order to have a good estimate of the eye lens dose during interventional procedures. In particular, the influence of both the type and the position of the dosemeter has been analysed. Before starting measurements on operators, measurements on a phantom in a realistic clinical set-up were performed in order to:

- Determine the best position for the eye lens dosemeter (ELD), in other words where the recorded dose is as close as possible to the dose of the most exposed eye/eye lens (since the ELD cannot be placed directly on the eye of the operator)
- Compare the UPC-ELD with EYE-D measurements
- Determine the relation between eye lens dose with patient dose measured in terms of DAP or KAP, in different configurations
- Determine the relation of eye lens dose with whole body quantities, i.e. $H_p(10)$ and $H_p(0.07)$ measured with an unprotected WBD
- Determine whether the active personal dosemeter (DoseAware; Philips Medical System, The Netherlands, http://www.healthcare.philips.com/) can provide a good enough estimate of eye lens dose

Active personal dosemeters are very useful to optimize procedures and to improve awareness of personnel exposure. Compared with passive systems, they provide an immediate feedback of the dose received. However, previous works (Vanhavere et al., 2012) have highlighted some limitations when used in pulsed radiation fields, in the energy and dose range characteristics of the monitored scattered fields. In this preliminary study we considered it to be interesting to include the DoseAware active personal dosemeter (APD) in order to validate its use in the medical campaigns. In fact, if electronic DoseAware data are comparable with UPC-WBD measurements, they might possibly be used for providing real time monitoring (the information collected is automatically stored in a centralized local data base).
The manufacturer claims linearity is ensured from 40 μSv·h^{-1} up to 300 mSv·h^{-1} and there is a 20% variation in energy response between 33 keV and 100 keV and reports an angular dependence of more than 30% for angles greater than 50°. The energy responses of the dosemeters were previously checked at a secondary standard calibration laboratory but no specific correction factor was used since the response was within the manufacturer's specification. Previous work (Chiriotti et al., 2011) showed differences with UPC-WBD within 10%-15% in scattered radiation fields used in cardiology.

11.1 Experimental set-up

Measurements were carried out at San Carlos University Hospital in Madrid with a Philips Allura (http://www.healthcare.philips.com/) FD-10 X-ray system. Measurements were performed for low-dose fluoroscopy mode (88-114 kV; HVL 8.0-10 $mmAl$) and image acquisition mode (68-84 kV; HVL 3.5-4.0 mm Al) and for two projections, Posterior-Anterior (PA) and Left-Lateral (LLAT) or Left-Anterior-Oblique at 90° (LAO-90). When lateral irradiations are performed (LLAT) more penetrating beams are needed and the voltage of the tube is increased. The beam resulted in a field size of $25cm^2$ at the level of the patient's back surface. Geometric schemes of the two configurations are presented in Figure 11.1, where

both lateral and top views are presented for PA projection, and Figure 11.2 where a side view is given for LLAT projection.

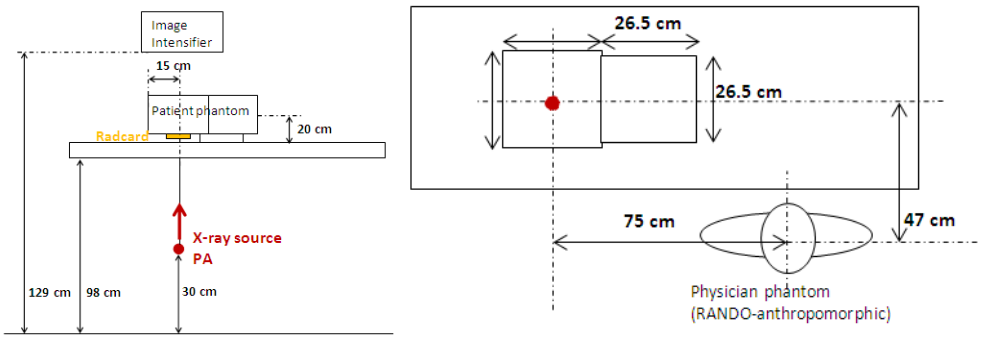

(a) PA - Lateral view (b) PA - Top view

Figure 11.1: PA projection

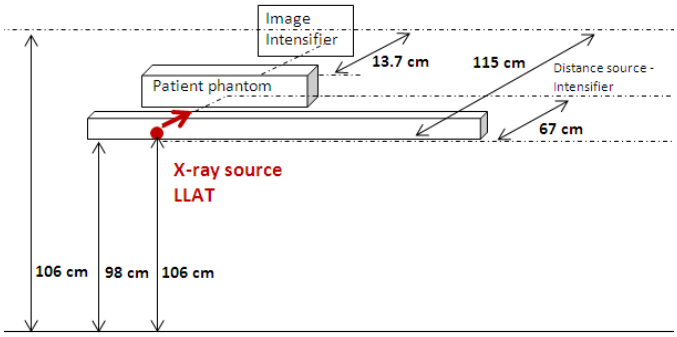

Figure 11.2: LLAT projection - Lateral view

The patient entrance surface air kerma K_a was monitored by using a calibrated Radcal ionization chamber model 20x6-60E connected to an electrometer model 20x26C (Radcal corp. Monrovia. California. USA, http://www.radcal.com/). The main features of the performed experiments are listed in Table 11.1.

Id. experiment	Mode	Added filtration	voltage	Radcal (mGy)	Protection	Projection
1	fluo	0.9mmCu+1mmAl	88 kV	45.5	No	PA
2	cine	–	68kV	77.6	No	PA
3	cine	–	68kV	245.0	CS, Apron,Collar	PA
4	cine	–	68kV	253.9	Glasses,Apron,Collar	PA
5	fluo	0.9mmCu+1mmAl	88 kV	43.4	No	PA
6	cine	–	68 kV	92.2	No	PA
7	fluo	0.9mmCu+1mmAl	88 kV	45.8	No	PA
8	cine	–	68 kV	94.5	No	PA
9	fluo	0.9mmCu+1mmAl	114 kV	50.0	No	LLAT
10	cine	–	84 kV	368.24	No	LLAT

Table 11.1: Main features of the performed experiments. CS stands for ceiling screen.

A 30·60·20 cm^3 PMMA slab phantom on the treatment couch was used to simulate patient-scattered radiation. The cardiologist was simulated by an anthropomorphic phantom model Rando (The Phantom laboratory, Salem, NY, USA, http://www.phantomlab.com/), which was situated on the right-hand side of the X-ray tube at a distance of 90 cm. The UPC-WBD was used as reference dosemeter for $H_p(0.07)$ and $H_p(10)$ measurements. They were located on the chest (on the right and left side), on the left shoulder and at the center of the collar of the Rando phantom. The three APDs were positioned on the chest, at the top of the UPC-WBD, on the left side of the collar and below the UPC-WBD located on

the shoulder.

The UPC-ELD batches were located:

- On the left eye (LE)
- On the right eye (RE)
- On the left lateral side of the head (LL), close to the left ear
- On the forehead or *middle eye* (ME), i.e. between the two eyes

The EYE-D was positioned on the left lateral side of the head. The EYE-D was used only for cases 1 and 2 in Table 11.1. The reference value for $H_p(3)$ was the measurement provided by the UPC-ELD on the left eye. Figure 11.3 (a) clarifies the positioning of the dosemeters, while Figure 11.3 (b) shows personal protection means (lead apron, glasses and protective collar) used in experiment 4.

(a) Without personal protections (b) With personal protections (Lead glasses, Collar protection, Lead apron)

Figure 11.3: Positioning of the dosemeters (EYE-D, UPC-ELD, UPC-WBD, active dosemeters) on the RANDO phantom

Measurements were carried out in two stages. For all cases, the table shielding below the couch was correctly placed, as, in practice, is generally used by cardiologists. During the first set of measurements (experiments 1 to 4), the attenuation because of the ceiling suspended screen and of the goggles was evaluated by doing measurements both when they were used and when they were not. In spite of long irradiations, when protection was properly used, measurements were close to the detection limit of the dosemeters, so in the second stage of the study only the table shielding was used. For experiment 4, when the goggles were used, the LL dosemeter was positioned on the internal side of the goggles, which is below the lateral protection. A Thermo EPD MK2 electronic personal dosemeter (Thermo Scientific Inc.. US, http://www.thermoscientific.com/) was also used to monitor the scatter radiation in real time Figure 11.3 (a). The reading of this dosemeter (50-70 μSv) was used to decide when to stop irradiation.

11.2 Optimal ELD positioning for eye lens dose measurement

$H_p(3)$ measured with the UPC-ELD situated on the LE is generally considered the best estimate of the maximum eye lens dose and thus the other measurements are compared to it. In fact, values show that the most exposed eye for the tested set-up (cardiologist on the left-hand side of the table, PA and LLAT projections) is the left eye. In Table 11.2 the ratio between the dose measured at the LE, $H_p(3,LE)$, and the doses measured in terms of $H_p(3)$ for the other positions, are shown.

Id. experiment	1	2	3	4
Mode	LD	Cine	Cine	Cine
Projection	PA	PA	PA	PA
Protection means			CS	Go
H_p(3,LE)/H_p(3,LL)	0.93	1.00	1.09	0.90
H_p(3,LE)/H_p(3,ME)	1.20	1.34	1.55	0.22
H_p(3,LE)/H_p(3,RE)	1.49	1.97		

Table 11.2: LD: Low-Dose fluoroscopy; Cine: acquisition; CS: ceiling suspended screen; Go: goggles. Ratio between H_p(3,LE), and H_p(3) for the other positions

The UPC dosemeter at the LL position provides a good estimate of the eye lens dose at the LE, while the dosemeters located at the other positions tend to subestimate the dose. Especially, the reference H_p(3) measured on the LE is twice the H_p(3) measured by the dosemeter on the right eye for the cine mode. It is also shown that for the PA projection a dosemeter on the forehead (ME) would provide an underestimate of more than 20% of the maximum dose to the eye lens, for this configuration. However, when protection is used, different results may be expected. When the ceiling screen is employed (case 3) the eye lens dosemeter on LL position subestimates the dose measured on the LE. It depends on the positioning of the ceiling screen in this specific case. Furthermore, ME dose is about four times higher than LE dose when goggles are used. This is strictly depending on the model and fit of the goggles worn (see Figure 11.3 (b)).

Table 11.3 summarizes all the ratios of H_p(3,LL)/H_p(3,LE) both for PA projection (cases 1, 2 and 5 to 8) and LLAT projection (case 9 and 10), collected during the whole study.

H_p(3,LL)/H_p(3,LE)			
Projection	Average±sd	Range	N
PA	1.08±0.05	1.14-0.98	6
LLAT	1.1±0.1	1.18-1.04	2

Table 11.3: H_p(3,LL)/H_p(3,LE) for PA (cases 1, 2 and 5 to 8) and LLAT (case 9 and 10)

11.3 Dependence of eye lens dose with patient dose (KAP)

Table 11.4 shows the estimated H_{lens} from $H_p(3,LE)_{UPC}$ measurements and the associated standard uncertainty, u, (k=1) for each set of measurements. Standard uncertainty u is calculated here taking into account the standard deviation of the two detectors of each UPC-ELD and the standard deviation of the background correction. Results show great variability for the H_p(3)/KAP[1] ratios ranging from 0.1 when CS is used (highest operator protection) to 6.2 for LLAT projection in fluo mode (highest peak voltage) for set-up 10. The ratio between H_p(3) and the KAP (if the radiation beam size is the same) is generally higher in low-dose fluoroscopy mode than for image acquisition mode. Likewise, H_p(3) is higher for the LLAT projection than for the PA projection because the operator is closer to the X-ray tube (for the implemented set-up) and because the beam is more energetic, thus it generates more backscatter.

Id. experiment	1	2	3	4	5	6	7	8	9	10
Mode	LD	Cine	Cine	Cine	LD	Cine	LD	Cine	LD	Cine
Projection	PA	PA	PA	PA	PA	PA	PA	PA	LLAT	LLAT
Protection means			CS	Go						
KAP (Gy·cm^2)	6.2	10.7	33.7	35.0	6.0	12.7	6.5	12.7	6.9	12.7
H_p(3)±u (μSv)	20±1	18±2	3±0.6	7±0.6	25±1	27±1	34±3	30±1	43±3	49±6
$\frac{H_p(3)}{KAP}$(μSv·Gy^{-1}cm^{-2})	3.2	1.7	0.1	0.2	4.2	2.1	5.3	2.4	6.2	3.8

Table 11.4: Summary of the ten set of measurements' conditions and the estimated H_{lens} and H_{lens}/KAP. H_p(3) measured by the UPC-ELD on the left eye of the Rando phantom was used as estimate of the H_{lens}± combined standard uncertainty (k=1). CS: ceiling suspended screen; Go: goggles

[1] air kerma-area product (KAP) calculated from the Radcal K_a measurement and the field area

When the ceiling suspended screen was positioned between the X-ray tube and the Rando phantom (experiment 3) $H_p(3)$ ranged between 1-3 μSv, values close to the detection limit of the dosemeters. Therefore, it was verified that the screen, correctly positioned, provided very good protection for the operator's upper part. When goggles were used, but no ceiling suspended screen was employed (experiment 4), for the same KAP, $H_p(3)$ to the left eye and to the side of the goggles was between 7-8 μSv, while on the external left side of the goggles (unprotected) $H_p(3)$ was of the order of 50 μSv. As expected, due to the attenuation of the radiation by the protection, $H_p(3)$/KAP is much lower for experiments 3 and 4 compared with the other cases. From these results it can be concluded that KAP will, in general, not be a good parameter for eye lens dose assessment. When used, it must be known beforehand if protection is being used or not.

11.4 Relation of eye lens dose with whole body dose

A paired sample t-test verified that the mean value of the two quantities $H_p(10)$ and $H_p(0.07)$ can be considered equal to within a 95% confidence interval of (-0.29 - 0.44), which means there is no statistical difference between these two quantities (p=0.7 > 0.05=α.). Thus, the mean value of $H_p(10)$ and $H_p(0.07)$ is calculated for each position and compared to H_p(3,LE). Table 11.5 summarizes the influence of UPC-WBDs position in estimating H_{lens}. It reports the ratio of the different dose measurements in the selected body positions with $H_p(3)$ measured on the left eye. For this evaluation only TLD data were used although similar conclusions could be derived from DoseAware measurements.

Projection	Position	$H_p(d)$position/H_p(3,LE)		
		Average±sd	Range	N
PA (cases 1, 2, 5, 6, 7, 8)	Chest Left side	1.3±0.3	1.82-0.94	6
	Left shoulder	1.9±0.3	2.45-1.61	6
	Center of collar	0.9±0.2	1.26-0.78	6
LLAT (cases 9, 10)	Chest Left side	1.8±0.3	2.04-1.62	2
	Left shoulder	2.5±0.6	2.91-2.10	2
	Center of collar	1.0±0.2	1.19-0.86	2

Table 11.5: Ratios between $H_p(d)$ measured at various positions and $H_p(3)$ measured at the left eye, for PA and LLAT projections

The best estimate of H_p(3,LE) would be given by $H_p(10)$ or $H_p(0.07)$ measured by a WBD at a certain position where the lowest spread of values is achieved. In the case of $H_p(d,collar)/H_p$(3,LE) the standard deviation sd is equal to 0.2 both for PA and LLAT configurations and the value of the ratio is close to unity. This implies that the whole body dose measured at collar level might be a good estimate of the dose to the left eye. The left side of the chest seems to be a better position than the left shoulder which shows a larger overestimate and a larger variability. However, none of the studied positions provide a better estimate than $H_p(3)$ measured at the LL position, as previously shown in Table 11.2. In addition, it must be kept in mind that these results do not include measurements performed when the ceiling suspended screen or the lead glasses were used.

11.5 Comparison of whole body and eye lens doses from different dosimetric systems

It was verified that there was no significant difference (p>0.05) between the UPC-WBD and DoseAware performance for fluoroscopy and image acquisition mode measurements. Table 11.6 shows the mean value, standard deviation and range of the ratio between $H_p(10)$ measured with DoseAware and with UPC-WBD considering the different positions and experiments.

To compare the performance of UPC-ELD with standard EYE-D at the same position the ratio $H_p(3,LE)_{UPC}/H_p(3,LL)_{EYE-D}$ was also calculated. Because of the good estimate of $H_p(3)$ provided by UPC-ELD, the EYE-D was not used in all experiments. Experiments 3 and 4 (where protection tools were used) were not included in the calculations because readings were close to the dosemeter detection limit.

	Average±sd	Range	N
$H_p(10)_{DoseAware}/H_p(10)_{UPC-WBD}$	1.02±0.21	1.35-0.65	24
$H_p(3)_{UPC-ELD}/H_p(3)_{EYE-D}$	1.07±0.13	1.28-0.94	8

Table 11.6: Comparison of *a)* $H_p(10)$ measurements with the electronic DoseAware detector and the UPC-WBD *b)* $H_p(3)$ measurements with the EYE-D holder and the UPC-ELD

11.6 Recommendations for the hospital measurement protocol

The left lateral part of the head is shown to be the optimal site on which to locate the eye lens dosemeter. In clinical practice, the positioning of the eye lens dosemeter is even more important than in phantom studies because during the procedures, protection such as the ceiling suspended screen can be moved and thus will protect only a part of the head/upper body. The eye lens dosemeter therefore has to be positioned as close as possible to the area to be monitored (the left eye). Consequently, for this study, the left lateral side will be the optimal position for performing eye lens dose measurements in hospital campaigns. Details will be provided in section 11.7. Both UPC-ELD and EYE-D supply similar results, but for simplicity in its use, only the UPC-ELD will be employed in measurements campaigns in hospitals. As regards the best position to locate the WBDs to be correlated with the eye lens dose, both thyroid and chest dosemeters provided acceptable results. However, after discussions with the staff to be monitored, it was agreed to locate the dosemeter at chest level, on the left side of the apron (usually on the pocket of the apron), as it is more comfortable for the operators to wear it on the thorax than the neck and it prevents the need to use a different protocol for staff who do not wear thyroid protection.
It is also seen that the DoseAware electronic device responds satisfactorily in realistic fields in interventional scattered field cardiology, for the studied configurations. When available, electronic devices will be used together with the passive dosemeter. However, the mean value of $H_p(10)$ and $H_p(0.07)$ from the UPC-WBD will be used as a reference for WB dose monitoring.

11.7 Preliminary measurements on physicians

The scope of this part of the study was to confirm that a TLD located on the left side of the head estimates the maximum dose to the eye lens, as the left eye is the most exposed eye due to it being the closest to the X-ray tube. Four physicians from Clinico San Carlos Hospital in Madrid participated in this measurement campaign. Since all of them wore normal glasses, the ELDs were taped on the left and right lateral eyepieces of the glasses. The monitoring period varied depending on the physicians' workload, but was generally about two weeks. Data collected are summarized in Table 11.7. Physicians were identified as phys_*a*, *b*, *c* and *d*. In column 2 and 3 the performed procedures together with the cumulated KAP during the follow-up period are presented. In column 4, 5 and 6 the dose measured at the left lateral (LL) and the right lateral (RL) eyepiece of the glasses with the UPC-ELD and the ratio H_p(3,LL)/H_p(3,RL) are shown, respectively.

	Performed procedures	KAP (Gy·cm^2)	H_p(3,LL) (μSv)	H_p(3,RL) (μSv)	H_p(3,LL)/H_p(3,RL)
phys_*a*	6 PTCA, 8 diagnostic, 1 Valvuloplasty	1107	653	188	3.5
phys_*b*	8 PTCA, 2 diagnostic	452	140	57	2.5
phys_*c*	5 PTCA, 9 diagnostic	532	378	101	3.7
phys_*d*	1 PTCA, 3 Valvuloplasty	368	383	108	3.6

Table 11.7: Right and left eye lens dose monitoring in 4 physicians. PTCA stands for Percutaneous transluminal coronary angioplasty

Data show the left eye received doses about 3 times higher than the right eye. Therefore, during the following campaigns in IC/IR, $H_p(3)$ at the right eye will not be measured and only UPC-ELDs will be used.

Chapter 12

Measurement campaign in real clinical conditions

The measurements described in this chapter were performed at four Spanish hospitals: Vall d'Hebron, Clinico San Carlos, Princesa and Clinica Universidad de Navarra. In total, 24 physicians and 13 nurses participated. A common protocol was employed for all measurement campaigns.

12.1 General features

According to the conclusions of the preliminary studies on phantom presented in chapter 11 a common protocol was established to monitor medical staff during clinical procedures. All participants wore UPC-ELDs and UPC-WBDs which were individually identified. The protocol followed was the same for all campaigns. The UPC-ELDs were located on the external left side of normal glasses when worn by the operators. When normal goggles were not worn by the worker, the dosemeter was fixed to the left side of the cap. Two dosemeters were assigned to each operator when workers wore lead glasses in order to test their efficiency in protecting the eyes in clinical conditions, . For (b)− and (c)− type glasses, represented in Figure 12.1, one dosemeter was fixed to the left external lateral part of the eyewear, while the other was located on the internal side of the lateral protection, beneath the shielding. In the case of type (a) wraparound glasses, a dosemeter was situated on the external left eye piece, while the other was located on the internal side of the left front glass, since there is no shield on this side, in a position that did not produce visual impairment (Figure 12.1 (a), arrow). The left side was chosen because, as verified in the preliminary tests, it is often the closest side to the X-ray tube and the dose measured is a good estimate of the maximum eye dose. Uncertainties in $H_{\mathrm{p}}(3)$, calculated following the Guide to the Expression of Uncertainty in Measurement (ISO/IEC, 2008), are of the order of 6% (see Appendix B). The lower detection limit of the dosemeters in the study is 10 μSv , at a confidence level of 95%. The WBD for the estimation of the quantities $H_{\mathrm{p}}(0.07)$ and $H_{\mathrm{p}}(10)$ was located on the lead apron, on the left side of the thorax.

Data for the estimation of attenuation of lead glasses were collected from six physicians from the hemodynamic units of three of the four hospitals under study.

(a) Wraparound type lead glasses (b) Lead glasses with side protection (c) Lead glasses with side protection, but with smaller frontal and lateral lenses compared with type b glasses

Figure 12.1: Different types of lead glasses

In addition to the above-mentioned dosimeters, all participants wore their own dosemeter from the official dosimetry service situated under the lead apron, for whole-body monitoring of effective dose.

Measurements were conducted at the four above mentioned hospitals in Spain. The monitoring period varied depending on the workload and availability of the participants. Preferably, at least two measurements were performed for each participant to obtain more data and improve the statistics of the results. The main features of the campaigns are summarized in Table 12.1.

Hospital	Monitoring period	Participants	Frequency of dosemeter change
Vall d'Hebron	1 week	6 physicians 4 nurses (phys_1 to 6; nurses 1 to 4)	Weekly
Vall d'Hebron	1 week	8 physicians 2 nurses (phys_1 to 4, 6 to 9; nurses 5 and 6)	UPC-WBD Daily for phys; UPC-ELD after each procedure for phys; WBD and ELD weekly for nurses
Vall d'Hebron	7 weeks	3 physicians 1 nurse (phys_3, 9, 10 and nurse 6)	Weekly
San Carlos	4 weeks	5 physicians	Variable, as a function of physicians workload
La Princesa	5 weeks	5 physicians	Variable, as a function of physicians workload
C.U.Navarra	5 weeks	4 physicians 7 nurses	Weekly

Table 12.1: Monitoring period, number of participants and frequency of dosemeter change

Table 12.2 provides details about which medical field each monitored worker belonged to. P stands for physicians and N for nurses.

Hospital	Hemodynamic	Vascular cardiology	Endoscopy	Electrophysiology
Vall dHebron	10 P, 6 N	—	—	—
San Carlos	5 P	—	—	—
La Princesa	2 P	2 P	1 P	—
C.U.Navarra	2 P 2 N	1 P 1 N	—	1 P 4 N

Table 12.2: Number and type of participants (P=physicians; N=nurses) depending on the field

12.2 Vall d'Hebron study

The measurements were performed at the Hemodynamic Department at the Vall d'Hebron Hospital in Barcelona. The department is provided with three different operating rooms with three Philips Allura X-ray systems: one FD10, one FD10/10 and one Clarity FD10. The total number of participants was 16. The monitoring was divided in three phases, as shown in Table 12.1.

- a first phase lasting one week in which WBD and ELD were changed weekly.
- a second period of one week in which ELDs were changed after each procedure and WBD daily (for physicians); dosemeters were changed weekly for nurses. The aim of this phase was to analyze the influence of the type of procedure on the eye lens dose.
- a third period lasting 7 weeks in which monitoring was performed on a weekly basis. It included three physicians and one nurse. ELDs were changed weekly, both for physicians and nurses. Data obtained in this third phase will be used to determine annual doses to the eye lens and correlation with whole body measurements.

During the first two-week monitoring period, detailed data were collected for each procedure thanks to a careful follow up of the operators' work. Eye lens dose exposure was monitored for nine physicians and six nurses. The number of procedures that were followed up was 43 during these first two weeks, with a total of 60 sets of monitoring data from physicians and 43 sets from nurses. In most procedures there were two operators and one nurse. This level of detail was not achieved during the third follow-up (7-weeks period). In this case, the dosemeters were delivered to the workers and changed weekly, when feasible, as the operators were already familiar with the use of the TLD batches after the first two-week follow-up period. The number of procedures followed up during the 7-weeks-period was 228. The main monitored procedures were coronary angiography (CA) and percutaneous transluminal coronary angioplasty (PTCA). Patients were both adults and children, in the age range 4-80 years old. As mentioned above, in this hospital only one physician wore lead glasses, whereas all other physicians used both a lead apron and a thyroid collar. Only one nurse wore the thyroid protection. The frequency of the usage of personal protective equipment for the 16 participants is shown in Figure 12.2 (a). Furthermore, it was observed that ceiling suspended screens were frequently not appropriately positioned, or only used

for a fraction of the time (Figure 12.2 (b)). Sometimes, the screen was not used at all, though available, because it impeded the physician's work. Meanwhile, the table shield available under the bed was always employed.

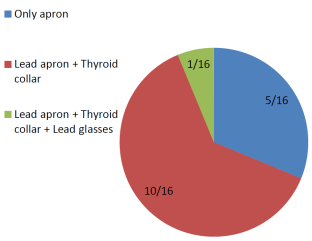

(a) Use of personal protective equipment

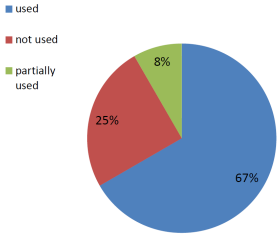

(b) Use (%) of the protective screen for the monitored procedures during the first two-week period

Figure 12.2: Statistics of the use of protective equipment

12.2.1 Data collection

The information acquired during the first two-week monitoring period included:

1. Identification number of the operator
2. Whether the patient was pediatric or adult
3. Tube configuration (monoplane or biplane system)
4. Type of intervention (PTCA, valvuloplasties,)
5. Protection tools used (ceiling suspended screen, lead glasses, thyroid collar)
6. Position along the patient (1st, 2nd and 3rd operator position, according to Figure 12.3)
7. Catheter access route (femoral F or radial R access, on the left or right side)
8. Kerma area product (KAP)
9. Air kerma (Kair)
10. Fluoroscopy time (T_{fluo})
11. Whether the operator leaves the room during image acquisition
12. Beginning and end time of the intervention

In Figure 12.3 sketch of a possible configuration is represented: two physicians are in the room, at the 1st (the closest to the tube) and the 2nd position, while the nurse is at the 3rd position.

An example of the detailed dataset for each monitored procedure performed during the first two weeks is given in Table 12.3 and Table 12.4.

Table 12.3 corresponds to the first week of monitoring, in which only weekly doses are available, whereas in Table 12.4 values of eye lens doses per procedure are shown from the second week of follow-up. The identification numbers of the physicians are listed in column 1. Details on: patient, whether adult or pediatric; monoplane or biplane tube configuration; type of procedure; use of ceiling screen CS; position of the physician; catheter access; KAP and air kerma values, the 'in-room' percentage, which indicates the fraction of time the monitored person was inside the operating room and time of fluoroscopy; are given.

Table 12.3 provides measured dose values during the 1st-week follow-up in columns 12 to 14.

In Table 12.4 measured $H_p(3)$ per procedure from the second week are given in column 13 and daily $H_p(0.07)$ and $H_p(10)$ are listed in columns 14 and 15. In column 16 $H_p(3)$ values normalized by KAP are also indicated.

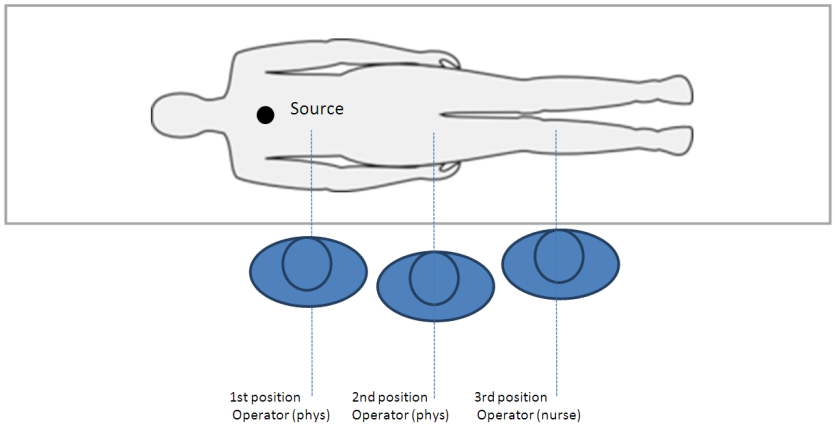

Figure 12.3: Positioning of the operators along the patient table. A sketch of a possible configuration is represented: two physicians are in the room, at the 1^{st} (the closest to the tube) and the 2^{nd} position, while the nurse is at the 3^{rd} position

ID	Patient	Tube	Procedure	Use of CS [y=yes n=no p=partially]	Position	Access	KAP mGycm^2	K_a mGy	% In room	T$_{fluo}$	$H_p(3)$ μSv	$H_p(0.07)$ μSv	$H_p(10)$ μSv
	Adult	Mono	ACTP	y	2nd	right F	32049	329.066	100%				
	Adult	Mono	ACTP+Diagnostic	y	1st	right R			57%				
phys_1	Adult	Mono	Valvuloplasty	n	1st	right F	22972	204.05	100%	15'31"			
	Adult	Mono	Valvuloplasty	n	1st	left F	21824	188.66	58%	16'14"			
	Adult	Mono	Diagnostic	y	2nd	left F	11242	106	100%	15'52"			
	Adult	Mono	ACTP+Diagnostic	y	2nd	left F	161781	2129	100%	37'50"			
phys_1											442	132	134
	Adult	Mono	Diagnostic	y		left R	56574	635	0%	11'04"			
	Adult	Mono	ACTP+Diagnostic	p	2nd	left R	185163	3153	100%	40'37"			
	Adult	Mono	ACTP+Diagnostic	y	2nd	right F	224914	3114.42	77%	29'16"			
phys_2	Adult	Biplane	Diagnostic	y	1st	left R	168996	997-front; 874-lat	22%	22'19"			
	Adult	Biplane	ACTP	y	2nd	left R	451557	1962-front; 3842-lat	100%	6'44"			
	Adult	Mono	ACTP+Diagnostic	y	1st	left R	45582	827.55	40%	11'14"			
	Adult	Mono	Diagnostic	y	1st	left F	25413	427.33	100%	6'32"			
phys_2											485	197	186
	Pediatric	Mono	ACTP+Diagnostic	y	1st	left F	20978	214.4	100%	51'19"			
phys_3	Pediatric	Mono	ACTP	n	1st	right F	7158	123.99	100%	8'34"			
	Pediatric	Biplane	ACTP	n	1st	right F	130423	145-front; 1189-lat	100%	15'44"			
	Pediatric	Biplane	ACTP	n	2nd	right F	202161	190-front; 1704-lat	100%	23'35"			
phys_3											1421	318	287
phys_4	Adult	Mono	Valvuloplasty	n	2nd	right F	22972	204.05	100%	15'31"			
	Adult	Mono	Valvuloplasty	n	1st/2nd	left F	21824	188.66	100%	16'14"			
phys_4											62	12	1
	Adult	Mono	ACTP+Diagnostic	y	1st/2nd	right R			37%				
	Adult	Mono	ACTP+Diagnostic	y	2nd	left R	136292	1753.53	100%	13'19"			
	Adult	Mono	Diagnostic	y	1st	right R	4661	33.345	100%	2'19"			
	Adult	Mono	Diagnostic	y	1st	left R	44747	633.879	100%	4'51"			
phys_5	Adult	Mono	ACTP+Diagnostic	y	1st	left R	108034	1256.73	100%	13'			
	Adult	Mono	Diagnostic	p	2nd	left F	11242	106	100%	15'52"			
	Adult	Mono	ACTP+Diagnostic	y	2nd	left R	161781	2129	100%	37'50"			
	Adult	Mono	Diagnostic	y	1st	left R	17562	269	100%	6'12"			
	Adult	Mono	Diagnostic	y	1st	left F	12191	199.75	100%	2'7"			
phys_5											404	173	171
	Adult	Mono	Diagnostic	y	2nd	right F	64509	742.65	50%				
phys_6	Adult	Mono	Diagnostic	y	1st	left R	56574	635	100%	11'04"			
	Adult	Mono	ACTP+Diagnostic	y	2nd	left R	185163	3153	75%	40'37"			
	Adult	Mono	Diagnostic	p	1st/2nd	left R	45582	827.55	100%	11'14"			
phys_6											149	71	70

Table 12.3: Data sheet for physicians monitored during week 1. PTCA stands for Percutaneous transluminal coronary angioplasty; F or R access means either femoral or radial artery access of the catheter

ID		Patient	Tube	Procedure	Use of CS [y=yes n=no p=partially]	Position	Access	KAP mGycm^2	K_a mGy	% In room	T$_{fluo}$	$H_p(3)$ μSv	$H_p(0.07)$ μSv	$H_p(10)$ μSv	$H_p(3)$/KAP (μSv Gy^{-1}cm^{-2})
phys_1	day_1	Adult	Mono	ACTP	n	2nd	right F	259884	760.86	100%	14'55"	189			0.7
		Adult	Biplane	ACTP+Diagnostic	y	1st	right F	73143	310 ap; 558 lat	100%	5'54"	118			1.6
	day_1												150	156	
	day_2	Adult	Biplane	ACTP	y	1st	right F	161407	458 ap; 1036 lat	100%	24'31"	460			2.9
		Adult	Biplane	Valvuloplastia	n	1st/2nd	right F	394562	954 ap; 2076 lat	100%	39'20"	572			1.4
	day_2												788	806	
phys_2	day_1	Adult	Mono	Diagnostic	y	2nd	left R	52664	730	50%	19'13"	14			0.54
	day_1												15	13	
phys_3	day_1	Pediatric	Mono	Biopsia	n	2nd	Jugular	2164	34	50%	8'44"	13			6.1
		Pediatric	Biplane	Diagnostic	n	2nd	right F	4375	33 ap; ? Lat	100%	13'31"	9			2.1
	day_1												18	15	
	day_3	Pediatric	Mono	ACTP	y	1st/2nd	right F	98602	358.96	100%	23'09"	267			2.7
		Pediatric	Mono	ACTP	n	1st	right F	9634	81.85	100%	15'09"	37			3.8
	day_3												50	51	
phys_4	day_4	Adult	Mono	ACTP	n	1st/2nd	left R	203681	3036	75%	30'45"	120			0.8
		Adult	Mono	ACTP+Diagnostic	y	1st/2nd	right R	220695	3873	50%	19'54"	66			0.6
	day_4												75	81	
	day_2	Adult	Mono	Diagnostic	p	1st/2nd	left R	29932	480	100%	10'04"	53			1.8
		Adult	Mono	Diagnostic	y	1st	left R	10255	159	100%	4'26"	20			2.0
		Adult	Biplane	ACTP+Diagnostic	y	1st	left R					70			
	day_2												99	97	
phys_6	day_3	Adult	Mono	Diagnostic	y	1st	left R	42060	697	100%	5'56"	79			1.9
		Adult	Mono	Diagnostic	y	1st	left R	21367	367	100%	6'25"	31			1.5
		Adult	Mono	Diagnostic	y	1st/2nd	left R	52664	730	100%	19'13"	170			3.2
	day_3												332	321	
	day_4	Adult	Biplane	ACTP	n	1st/2nd	right F	161407	458 ap; 1036 lat	100%	24'31"	21			0.1
		Adult	Mono	ACTP+Diagnostic	y	1st/2nd	right R	220695	3873	50%	19'54"	50			0.4
	day_4												63	65	
	day_1	Adult	Mono	Diagnostic	y	1st	right R	9231	144	100%	8'31"	19			2.0
		Adult	Mono	Diagnostic	y	1st	left R	12782	157	100%	4'09"	23			1.8
		Adult	Biplane	ACTP+Diagnostic	y	1st	right R	102109	1496	100%	27'46"	73			0.7
	day_1												49	46	
phys_7	day_2	Adult	Mono	Diagnostic	p	1st	left R	29932	480	50%	10'04"	8			0.5
		Adult	Mono	ACTP+Diagnostic	y	1st	left R					157			
	day_2												29	32	
	day_4	Adult	Biplane	ACTP	y	1st	left R	73109	1238	100%	16'04"	77			1.0
		Adult	Mono	ACTP+Diagnostic	y	1st/2nd	right R	220695	3873	50%	19'54"	97			0.9
	day_4												83	91	
phys_8	day_1	Pediatric	Mono	ACTP	y	1st/2nd	right F	98602	358.96	100%	23'09"	251			2.5
	day_1												36	37	
phys_9	day_2	Adult	Mono	ACTP	n	1st	right F	259884	760.86	100%	14'55"	782			3.0
	day_2												47	52	
	day_3	Adult	Mono	Diagnostic	y	1st	left R	52664	730	25%	19'13"	28			0.5
		Adult	Mono	ACTP	y	1st	right R	118959	1300	100%	15'49"	132			1.1
	day_3												30	27	
	day_4	Adult	Mono	ACTP	n	1st/2nd	left R	203681	3036	100%	30'45"	231			1.1
	day_4												34	37	

Table 12.4: Data sheet for physicians monitored during week 2

Two physicians and one nurse that had participated in the second week follow-up participated in a third follow-up phase. An additional physician (phys_10), who was wearing lead glasses, wraparound style joined in the study. Table 12.5 shows data of weekly measured eye lens doses, in this last phase.

	ID	Patient	N Procedures	KAP (Gycm^2)	$H_p(3)$ (μSv)	$H_p(0.07)$ (μSv)	$H_p(10)$ (μSv)	$H_p(3)$/KAP (μSv Gy^{-1}cm^{-2})	$H_p(3)$/N (μSv proc^{-1})
week_1	phys_3	Pediatric	3	62					
	phys_9	Adult	21	3294	2934	851	791	0.9	140
	phys_10	Adult	5	1614	3608	683	738	2.2	722
	nurse_6		13	1520	156	161	159	0.1	12
week_2	phys_3	Pediatric	2	107	664	1112	1188	4	133
	phys_9	Adult	20	2924	1749	1326	1448	0.6	87
	phys_10	Adult	2	1168	1395	310	301	1.2	698
	nurse_6		10	787	89	110	88	0.1	9
week_3	phys_3	Pediatric	3	112					
	phys_9	Adult	18	1294	1416	225	230	1.1	79
	phys_10	Adult	5	795	905	199	176	1.1	181
	nurse_6		7	530	79	81	75	0.1	11
week_4+5	phys_3	Pediatric	2	30	711			5	168
	phys_9	Adult	37	3669	1187	603	627	0.3	32
	phys_10	Adult	8	2397	1596	621	572	0.7	199
	nurse_6		17	1740	349	229	202	0.2	21
week_6+7	phys_3	Pediatric	3	208	841			4	280
	phys_9	Adult	35	3271	1267	422	421	0.4	36
	phys_10	Adult	8	2766	1517	482	486	0.5	190
	nurse_6		9	756	66	63	55	0.1	7

Table 12.5: Data collected from the third follow-up period

$H_p(3)$ for phys_10 shown in Table 12.5 corresponds to the reading from the UPC-ELD worn on the unprotected part of the glasses. Phys_3 (pediatric) did not change his dosemeter after week 1 and week 3, thus the registered measurements of week_2 and week_4 represented the cumulative dose for two consecutive weeks (weeks 1 and 2, and weeks 3 and 4). Hence, Hp(3) per unit KAP (column 9) and $H_p(3)$ divided by the number of procedures (column 10) is obtained as the cumulative $H_p(3)$ in the two consecutive weeks divided by the corresponding KAP or number of performed procedures during the two-week monitored period, respectively.

12.2.2 Data analysis for the 1st and 2nd follow-up

Mean eye lens dose $<H_p(3)>$ per procedure (in μSv) obtained from the first week of monitoring (week_1) and the second week of monitoring (week_2) are shown for each participant in Table 12.6. $<H_p(3)>$ was obtained as the sum of all $H_p(3)$ per procedure and divided by the number of the monitored procedures per person. $H_p(3)$, $H_p(0.07)$, $H_p(10)$ and KAP, cumulated during week_1 and 2, are also listed. Ratios of $H_p(3)/H_p(0.07)$ and $H_p(0.07)/H_p(10)$ are given for further consideration. $<H_p(3)>$, calculated over two consecutive working weeks, shows high variability even for the same physician.

	phys_1	phys_2	phys_3	phys_4	phys_5	phys_6	phys_7	phys_8	phys_9
$<H_p(3)>_{week\_1}$ (μSv)	74	69	355	31	45	37			
$H_p(3)_{cumulated\ week\_1}$ (μSv)	442	485	1421	62	404	149			
$H_p(0.07)_{cumulated\ week\_1}$ (μSv)	132	197	318	12	173	71			
$H_p(10)_{cumulated\ week\_1}$ (μSv)	134	186	287	1	171	70			
$KAP_{cumulated}$ (Gy cm^2)	343	891	361	45	563	273			
$H_p(3)/H_p(0.07)$	3.3	2.5	4.5	5.3	2.3	2.1			
$H_p(0.07)/H_p(10)$	1	1.1	1.1	8.7	1	1			
$H_p(3)$/KAP (μSv Gy^{-1}cm^{-2})	1.29	0.54	3.94	1.38	0.72	0.55			
$<H_p(3)>_{week\_2}$ (μSv)	335	14	81	93		62	65	251	130
$H_p(3)_{cumulated\ week\_2}$ (μSv)	1339	14	326	185		494	453	251	1173
$H_p(0.07)_{cumulated\ week\_2}$ (μSv)	938	15	68	75		494	161	36	111
$H_p(10)_{cumulated\ week\_2}$ (μSv)	962	13	66	81		483	169	37	115
$KAP_{cumulated}$ (Gy cm^2)	889	26	114	263		482	370	99	596
$H_p(3)/H_p(0.07)$	1.4	0.9	4.8	2.5		1	2.8	7.1	10.6
$H_p(0.07)/H_p(10)$	1	1.1	1	0.9		1	1	1	1
$H_p(3)$/KAP (μSv Gy^{-1}cm^{-2})	1.51	0.54	2.86	0.7		1.02	1.23	2.54	1.97

Table 12.6: $H_p(3)$ per procedure, cumulated $H_p(3)$, $H_p(0.07)$, $H_p(10)$, KAP and $H_p(3)/H_p(0.07)$, $H_p(0.07)/H_p(10)$, $H_p(3)$/KAP during week_1 and_2

Large differences in $<H_p(3)>$ between the two weeks were observed for most of the participants. Some of the differences, in particular, the high $<H_p(3)>$ value of phys_1 second week and phys_3 first week,

can be explained by analyzing the operations performed. During the second week phys_1 performed an infrequent, lengthy procedure which entailed a recorded $H_p(3)$ higher than the cumulative eye lens dose during the first week (572 μSv in one single procedure on day_2 of the second week vs. 442 μSv cumulated during the first week). Thus this value is considered an outlier and disregarded for the estimation of annual eye lens dose. As regards phys_3, in the first week he was the only physician in the room, while during the second week he worked as the second position operator.

High variability in the $H_p(3)_{cumulated}$ is also highlighted. This is associated with the weekly workload, which is generally largely variable through the year, and also to the complexity of the procedures. Higher $H_p(3)$ usually corresponds to lengthy procedures, which generally require large fluoroscopy times, hence high KAP. The variation of KAP between the two weeks is about a factor of 3: 889 vs. 241 Gy cm^2 and 361 vs. 114 Gy cm^2 for phys_1 and phys_3 respectively. $H_p(10)_{cumulated}$ and $H_p(0.07)_{cumulated}$ are also listed in Table 12.6. No statistical differences were observed between $H_p(10)$ and $H_p(0.07)$ ($p = 0.54$), except for phys_4 who presented an unexpected $H_p(0.07)/H_p(10)$ ratio of 8.7. Accordingly, dose values from phys_4 were disregarded when analyzing the relation between $H_p(3)$ and whole body doses. Large differences are observed between $H_p(3)/H_p(0.07)$ ratios, with values ranging from 0.9 to 10.6. The range of variation of these values is broader than that obtained with measurements on phantoms. This difference is associated with the fact that in clinical conditions more parameters vary simultaneously.

For instance, the large variability of $<H_p(3)>$ and $H_p(3)/H_p(0.07)$ may be explained by the fact that the use of radiation protection tools in routine practice is not always appropriate. The ceiling suspended screen provides good protection, but it is not always well placed to protect the eyes. The box plot in Figure 12.4 shows the distribution of KAP per procedure for all physicians, for the second week of monitoring, when data from single procedures were available for both KAP and $H_p(3)$. Figure 12.5 also provides the distribution of $H_p(3)$ normalized by the corresponding KAP for single procedures. When KAP was not registered and when $H_p(3)$ values were below the detection limit of 10 μSv, data were disregarded and not included in the figures. KAP can be defined as an indicator of the complexity of the procedure, and is highly variable even for the same physician. Data for phys_3 show that even though procedures do not require particularly large fluoroscopy time and KAP, high $H_p(3)$/KAP ratios are recorded. Phys_3 performs pediatric interventions and thus is usually closer to the tube because of the small size of the patient. He also uses the biplane system more frequently and often does not employ the ceiling suspended screen. This consequently leads to higher eye lens doses, even though the amount of KAP is the same. Therefore, the length and complexity of the procedure may be indicated by the KAP values, but there are other parameters that also affect the dose. Hence, from these preliminary considerations, KAP cannot be considered to be an exhaustive indicator of the eye lens dose.

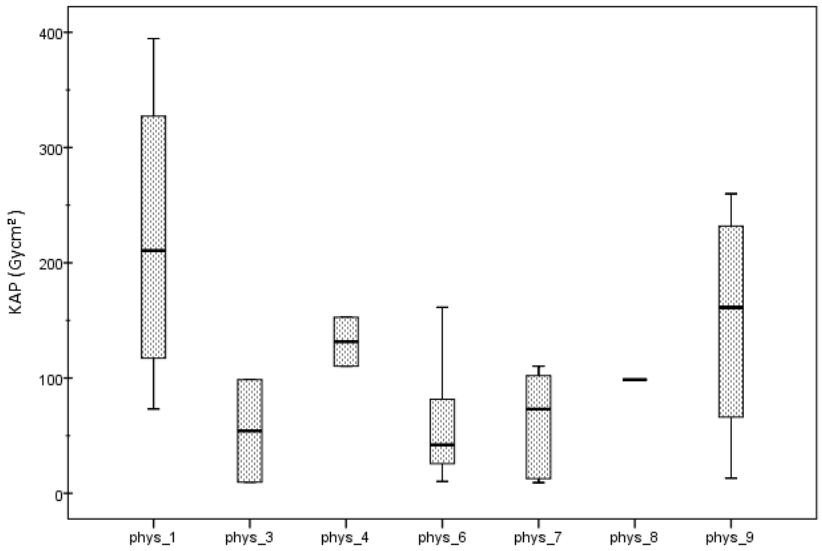

Figure 12.4: Box plot of the distribution of KAP per procedure for all physicians monitored during the second week

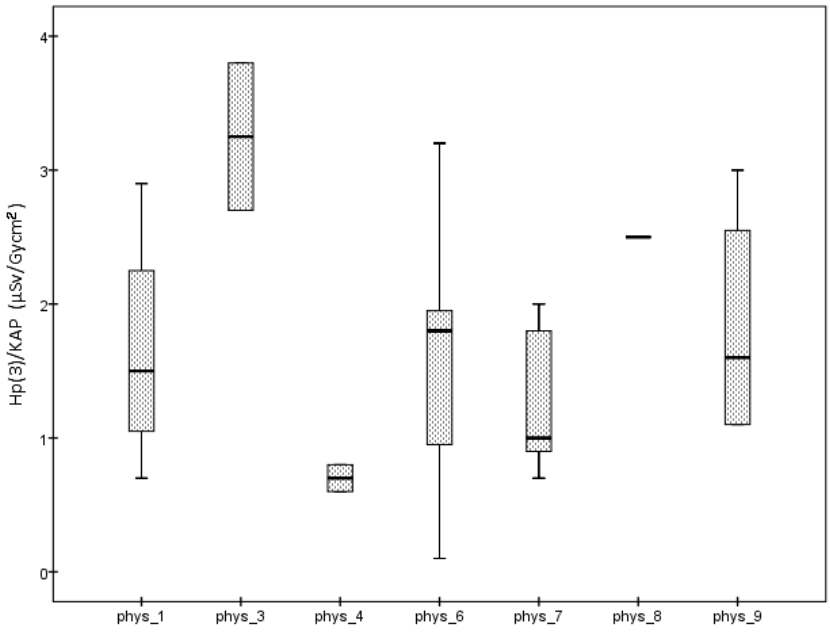

Figure 12.5: Box plot of the distribution of $H_{\mathrm{p}}(3)$/KAP per procedure for all physicians monitored during the second week

12.2.2.1 Effect of the position of the operator, patient size and ceiling suspended screen use on eye lens dose and access route

One of the main limitations in analyzing IC/IR personal monitoring data is the multi-parametric dependence of dose on other factors, such as:

- The position of the operator with respect to the source or with respect to other operators in the room.
- The use of protection tools, such as personal or shielding equipment installed in the room.
- The duration and difficulty of the intervention, which enlarge the fluoroscopy time (it also depends on the experience of the operators).
- The intensity and characteristics of the radiation field.

Thus, the parameters influencing the dose vary simultaneously during a single procedure and there is also variation among procedures. The non-static configuration of the operator and of the ceiling suspended screens introduces variability. Some of these parameters have been taken into account for data analysis.

Table 12.7 presents mean, standard deviation and range of $H_{\mathrm{p}}(3)$/KAP values per procedure for physicians, and distinguishes between:

- Pediatric physicians and non-pediatric ones (lines 3 and 4)
- Radial, femoral and jugular access (lines 5 to 7)
- Physicians at the 1^{st} or 2^{nd} position (line 10).

To increase the number of data, values from week_1 and 2 were considered. The t-test was used to verify that the differences found in the dataset presented in Table 12.7 have statistical significance. Firstly, normality of the data distribution was proven. The Shapito-Wilk test was used to verify if the distribution of the data is normal when the sample number was less than 50. If significance is greater than 0.05, then a Gaussian distribution can be assumed. In all cases, the condition of a normal distribution was fulfilled, except for the operator at the second position. In this case, significance was below 0.05 (0.008) and the Mann-Whitney U test was used instead of the t-test.

The position of the operators in the room next to the patient plays an important role in understanding the collected doses: generally, the closer they are to the source, the larger the dose. During this measurement

campaign, two physicians and one nurse were usually inside the operating room during the intervention. The presence of two physicians is determined by 1− the complexity of the procedure. In this case, two experienced physicians are in the room; or 2− the training of physicians with only a few (or no) years of experience. In this case, one inexperienced physician and one experienced physician are in the room, at the 1^{st} and 2^{nd} position, respectively. The 1^{st} position operator is the physician who stands closest to the X-ray tube. The nurse is generally located at the patient's feet (3^{rd} position). Furthermore, apart from the positioning with respect to the operators in the room, the location of the physician performing the procedure depends on the size of the patient (whether pediatric or adult) and the preferred access route (radial, femoral or jugular). Another limitation when evaluating the results is the use and positioning of the room protection equipment, especially the ceiling suspended screen.

	$H_p(3)$/KAP (μSv Gy^{-1}cm^{-2})						
		Mean	Max	Min	Sd	N	p (2-tallies)
patient	Pediatric	3.5	6.1	2.1	1.4	6	0.001
	Non pediatric	1.3	3.2	0.1	0.8	29	
access	Radial	1.3	3.2	0.5	0.7	18	0.023
	Femoral	2.1	3.8	0.1	1.1	10	
	Jugular	6.1				1	
	$H_p(3)$/KAP 1^{st} position/ $H_p(3)$/KAP 2^{nd} position						
		Mean	Max	Min	Sd	N	p (2-tallies)
	$1^{st}/2^{nd}$	4	6.4	1.5	2.3	7	0.038

Table 12.7: Mean, maximum, minimum, standard deviation of $H_p(3)$/KAP mean and number N of samples for pediatric/non pediatric, different access and relative position

Data show a difference between eye lens dose for physicians working in pediatric units and those who usually work with adults of a factor 2.7. The maximum $H_p(3)$/KAP of 6.1 for pediatric patients corresponds to an operation with jugular access. In this specific case, the physician had to stay very close to the tube, and the presence of the screen would have disturbed his work. Sometimes, in the case of pediatric intervention, the use of the protective screen is found cumbersome by the operators and is indeed not used. This fact contributes to higher $H_p(3)$/KAP. As regards the access route, although data from the bibliography (Vanhavere et al., 2011) state that eye lens doses are usually lower when catheter access is carried out on the femoral route rather than for radial access, due to the greater distance from the source (even though when ceiling screen is present the difference is not statistically significant); data from the present work show the opposite. The reason may lie in the fact that femoral access is preferred by experienced physicians who, on the other hand, do not use protective screens as often as inexperienced physicians do. The use of biplane system was preferred to monoplane tube by Phys_1, who show high $H_p(3)$/KAP . Furthermore, during this monitoring period, the radial route was never used by pediatric physicians, who were physicians that received the highest eye lens dose levels per unit KAP. In summary, we believe that our sample is too small to draw conclusions on the influence of catheter access, and is an example of the difficulties encountered in generalizing observations from one hospital to another.

The position of the operator, if two physicians are present in the operating room, also affects the dose. On average, the operators at the 2^{nd} position receive a dose to the eye lens that is 4 times lower than the operators at the 1^{st} position. This was found for all 7 monitored interventions where 1st and 2nd operators were both present and monitored. During the second week follow-up, the whole interventional procedure was witnessed by the author of this thesis and the use of the suspended shield was registered. The distribution of $H_p(3)$/KAP collected for single procedures is represented in Figure 12.6, data were separated on whether the shield (suspended screen) was employed or not. $H_p(3)$ values lower than 10 μSv were disregarded for this analysis as they are close to the lower detection limit. Operators at the first position and the second position together with nurses are analyzed separately, in the light of previous results. As the nurse $H_p(3)$ values per procedure were not available, $H_p(3)$/KAP were obtained from weekly values. When the operators moved between the first and second position, the most frequent position was chosen; if the time at the second and at the first position was the same, the value was disregarded.

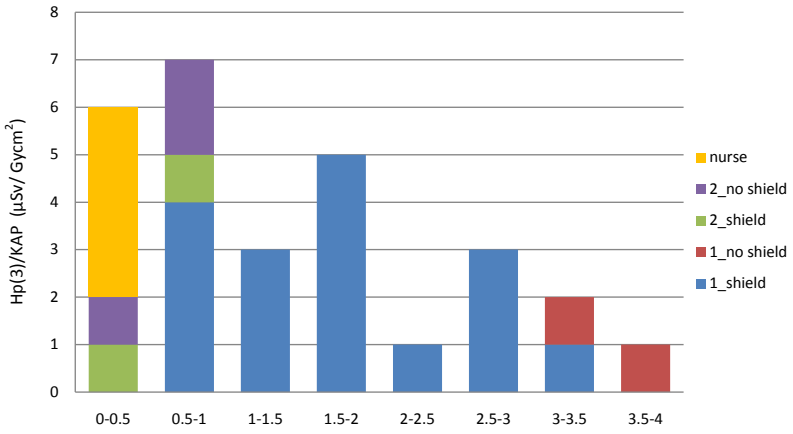

Figure 12.6: Distribution of $H_p(3)$ per unit KAP for: operator at first position, shielded by the ceiling suspended screen (1_shield); operator at first position, unshielded (1_no shield); operator at second position, shielded (2_shield); operator at second position, unshielded (2_no shield); nurses, considered as being independent of the shielding (nurse)

The distribution shows that nurses clearly receive the lowest doses, followed by the operator at the second position. There is no clear trend for physicians at the second position. No differences are observed whether the ceiling suspended screen was used or not (p = 0.8) for nurses or second position operators. Operators at the first position that do not use room shielding are the ones that received the highest amount of scattered radiation to the eyes, even though only two measurements are available. The t-test proves that the difference between 1_s and 1_n is statistically significant (p = 0.01). Equal variances are assumed for these tests, as the number of samples is small. Operators at the second position are compared with the group of nurses, with the use of the screen being disregarded. A t-test analysis shows that no statistical difference (or very weak significance) is seen between these two groups (nurses and the operator at the second position, p = 0.05). The descriptive statistics are given in Table 12.8.

	Position	N	Mean	sd	Median	Min	Max
$H_p(3)$/KAP (μSv Gy^{-1}cm^{-2})	1_n	2	3.41	0.56	3.41	3.01	3.8
	1_s	17	1.69	0.82	1.77	0.52	3.23
	2_n	3	0.55	0.36	0.73	0.13	0.78
	2_s	2	0.49	0.06	0.49	0.45	0.54
	n	4	0.18	0.03	0.17	0.14	0.21

Table 12.8: Descriptive statistics depending on the position of the operators (1 or 2) and on the use or not of the ceiling suspended screen (_s or _n)

The database demonstrates a reduction of eye lens dose by a factor of 2.2 when the ceiling suspended shield is used, obtained as ($<H_p(3)>_{1\_noshield}$/KAP) /($<H_p(3)>_{1\_shield}$/KAP) for the operator at the first position. The attenuation provided by the screen is not as high as expected, considering that an attenuation factor of 17 was calculated for measurements on a phantom.

12.2.2.2 Estimation of annual eye lens dose

Annual eye lens doses were extrapolated from measured $H_p(3)$ and the annual workload for all monitored physicians and nurses was provided by the hospital. Table 12.9 summarizes the mean measured $H_p(3)$ per procedure ($<H_p(3)/N>$) and the corresponding standard deviation (1 sd) for the nine physicians during the follow-up period corresponding to the two weeks of monitoring. The estimated annual eye lens dose is then obtained by multiplying $<H_p(3)/N>$ by the number N_{year} of procedures performed in one year.

Data show that four physicians out of nine exceeded the new recommended limit of 20 mSv y^{-1}. $<H_p(3)/N>$ ranges from 42 to 251 μSv procedure^{-1}, while the estimated annual doses range between 8 and 61 mSv y^{-1}. Large variability of the measured $H_p(3)/N$ is observed, as previously assessed. The standard deviation of $H_p(3)/N$ is of the order of 80%, even for the same physician. This variability is mainly associated with the high KAP values recorded in some procedures, where a long fluoroscopy time

	$<H_p(3)/N> \pm 1$ sd (μSv)	N_{year}	$H_p(3)_{year}$ (mSv)
Phys_1	164±129	369	61
Phys_2	42±39	303	13
Phys_3	218±163	149	32
Phys_4	62±45	253	16
Phys_5	45±42	182	8
Phys_6	49±46	253	12
Phys_7	65±53	325	21
Phys_8	251±187	77	19
Phys_9	130±102	385	50

Table 12.9: Mean measured $H_p(3)$ per procedure ± 1 sd, number of procedures per year N_{year} and estimated annual dose for physicians based on the first follow-up

is required, and to the inappropriate use of shielding. Two values of $H_p(3)$ equal to 780 and 540 μSv were removed to derive the annual dose, since they were considered to be outliers, and not considered to be significant of standard procedures. If these values had been included, the estimated annual dose would have increased up to 75 mSv for physician 1 and up to 113 mSv for physician 9. This highlights the fact that a larger period of monitoring is needed for a more reliable estimate of the annual eye lens dose. Table 12.10 presents the estimated annual eye lens dose for nurses. In this case, none of the nurses exceeds the recommended 20 mSv y^{-1} and the range of variability among the different monitored nurses is small.

	$H_p(3)/N$ (μSv)	N_{year}	$H_p(3)_{year}$ (mSv)
Nurse 1	11	209	2
Nurse 2	18	193	3
Nurse 3	14	171	2
Nurse 4	22	105	2
Nurse 5	13	176	2
Nurse 6	24	171	4

Table 12.10: $H_p(3)$ divided by the number of procedures N, number of procedures per year and estimated annual dose for nurses

12.2.3 Data analysis for the 3^{rd} follow-up period

Previous data analysis highlights the influence of the chosen monitoring period in dose assessment. As the workload varies from week to week, it is difficult to estimate annual doses if short monitoring periods are used and it is possible to run into large over or underestimation of the annual eye lens dose. For this reason, monitoring over a longer period of seven weeks was undertaken and annual doses obtained from the third follow-up period are compared with previous results. Table 12.11 provides the mean and standard deviation of $H_p(3)$ per procedure, number of procedures per year and estimated annual $H_p(3)$ for the third follow-up period, which lasted for 7 consecutive weeks.

	$H_p(3)/N \pm 1$ sd (μSv)	N_{year}	$H_p(3)_{year}$ (mSv)
Phys_3	171±83	149	25
Phys_9	65±44	385	25
Phys_10*	56±18	191	11
Nurse 6	13±5	171	2

Table 12.11: $H_p(3)$ divided by the number of procedures ± 1sd (third follow-up), number of procedures per year and estimated annual dose values. *Phys_10 wore lead goggles, $H_p(3)$ was estimated by using the dosemeter in the internal part

In this case, two physicians out of three exceed the 20 mSv y^{-1}. The mean $H_p(3)$ per procedure for phys_3 and _9 was lower than in the first two-week follow-up. The longer the measuring period, the more reliable the estimation of annual $H_p(3)$. Table 12.11 highlights the fact that the standard deviations associated with $H_p(3)$ per procedure for a weekly monitoring period are lower when compared with those

in Table 12.9 for a shorter monitoring period. Results in Table 12.9 and Table 12.11 show that for all monitored physicians the estimated annual eye lens dose exceeds $3/10^{th}$ of the recommended limit of 20 mSv, which corresponds to 6 mSv. Thus, regular monitoring is highly recommended. This is not the case for nurses, whose annual dose is always below 6 mSv.

The attenuation factor due to the use of lead goggles for phys_10 was estimated weekly, along the 7-week period (3 data values available). The mean ratio between $H_p(3)$ measured of the external left earpiece and behind the lead glass of the goggles is 3.5 and ranges from 2.5 to 4.8.

12.3 Measurement campaign at other Spanish hospitals

Eye lens doses and whole body doses were measured at other Spanish hospitals following the same protocol as the one employed for the 3^{rd} phase of the Vall d'Hebron study. In this case, data are not as detailed as previously described for the first two-week follow-up. Dosemeters were delivered to the operators who used and returned them after an established period of time, shown in Table 12.1. The main aims at this point were: 1− The comparison of $H_p(3)$ with $H_p(0.07)$ or $H_p(10)$; 2− The comparison of $H_p(3)$ with KAP; 3− the estimation of annual eye lens dose from data collected and annual workload.

12.3.1 Correlation with whole body quantities and KAP

One of the aims of this study was to determine whether the measured eye lens dose can be correlated to whole body doses or KAP. All available weekly data from our database are used for this analysis. Thus, data from single procedures from week 1 and week 2 follow-ups at Vall d'Hebron have been added to obtain weekly data. Physicians and nurses were studied separately. WBD gave very close values of $H_p(10)$ and $H_p(0.07)$ for the same measurement. No statistical differences were observed ($p > 0.05$). Therefore, both quantities could be used to verify the correlation with $H_p(3)$. $H_p(0.07)$ was chosen. Figure 12.7 represents $H_p(3)$ measured outside the lead glasses as a function of $H_p(0.07)$ measured on the lead apron for physicians for each of the hospitals that participated in the study. A least square fit was performed to derive the linear relationship between $H_p(0.07)$ and $H_p(3)$, without intercept. The slope of the line was considered the best correction factor to assess $H_p(3)$ from $H_p(0.07)$ measurements. The square of the Pearson coefficient (R^2) is used to measure the strength of the linear relationship between $H_p(3)$ and $H_p(0.07)$. The analysis of data from the Vall d'Hebron Hospital show statistically significant differences between the eye lens dose for pediatric physicians and no- pediatric ones. Also the position of the operator, whether at first or second position, entails differences in the exposure and thus in the eye lens equivalent dose (see subsubsection 12.2.2.1). Thus, only data for physicians at first position, excluding pediatric physicians, were considered for Vall d'Hebron hospital in this comparison. The fitted equation and R^2 are indicated in the figures.

Figure 12.8 represents $H_p(3)$ measured outside the lead glasses as a function of $H_p(0.07)$ measured on the lead apron for nurses for the two hospitals where nurses were monitored. $H_p(3)$ better correlates with $H_p(0.07)$ for nurses (R^2 = 0.8, 0.9) than for physicians (R^2 = 0.7-0.9), while the ratio between $H_p(3)$ and $H_p(0.07)$ was found to be close to one. In fact, for nurses, the trend in data is similar for both hospitals. Correlations with KAP were also analysed. Figure 12.9 and Figure 12.10 show the experimental data, the fitted equation and the R^2. The correlation of $H_p(3)$ with respect to KAP is, in general, worse than with $H_p(0.07)$. R^2 ranges between 0.5 and 0.7 for physicians and it is 0.5 for nurses. The ratio between $H_p(3)_{out}$ and $H_p(0.07)$ and the ratio between $H_p(3)_{out}$ and KAP are listed in Table 12.12 and Table 12.13 for both physicians and nurses, respectively. Mean, maximum, minimum, standard deviation sd and standard deviation of the mean $sd_{\bar{x}}$, median and N values are tabulated for each ratio. The value N stands for the number of data values collected (not for participants).

Data from Table 12.12 for $H_p(3)_{out}/H_p(0.07)$ show variability of the mean ratios for physicians at each hospital, within 11% and 35%. Except for $H_p(3)_{out}/H_p(0.07)$ for Navarra hospital which presents the largest variability, there is a good consistency between the mean and the median. The highest $H_p(3)/H_p(0.07)$ is obtained for the Vall d'Hebron Hospital. Although we cannot explain this difference between this hospital and data from other hospitals, the main discrepancy observed during the measurement campaigns was the unusual and in some cases misplaced positioning of the ceiling suspended screen at the Vall d'Hebron Hospital. This latter fact could mean that the thorax may be better protected than the head and high $H_p(3)_{out}/H_p(0.07)$ ratios are justified. Furthermore, the biplane system was employed in some cases. As regards $H_p(3)_{out}$/KAP ratios, the spread of values for physicians ranges from 11 and 23% and mean values range from 0.6 to 1.9.

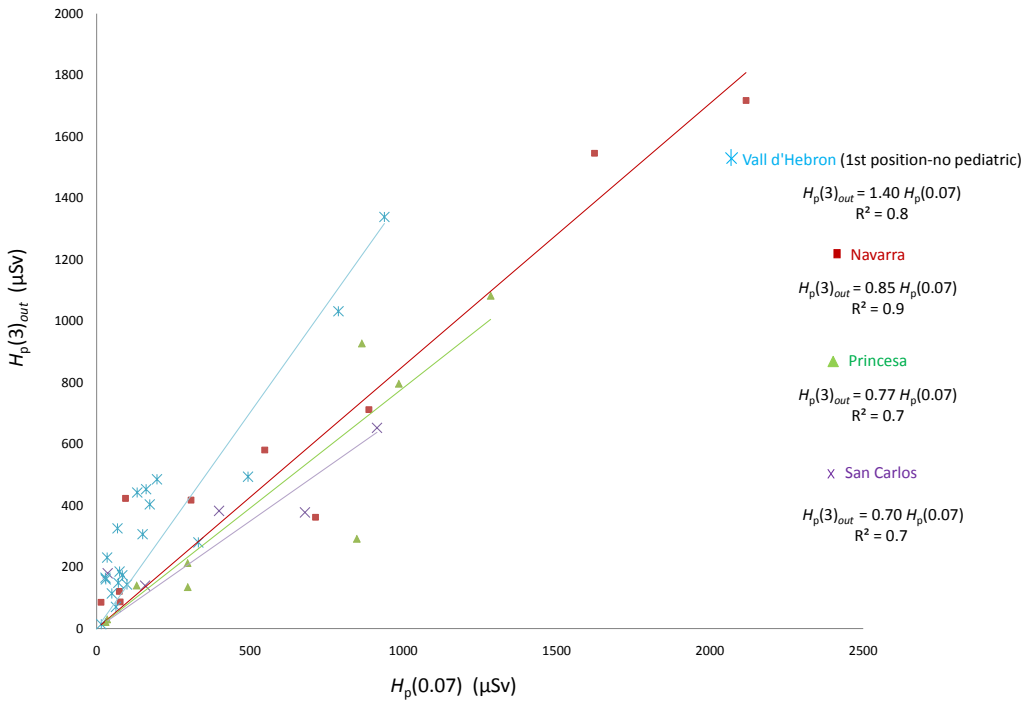

Figure 12.7: Relation between $H_{\mathrm{p}}(3)$ measured outside the lead glasses $H_{\mathrm{p}}(3)_{out}$ and $H_{\mathrm{p}}(0.07)$ measured on the lead apron for physicians for the four hospitals in the study

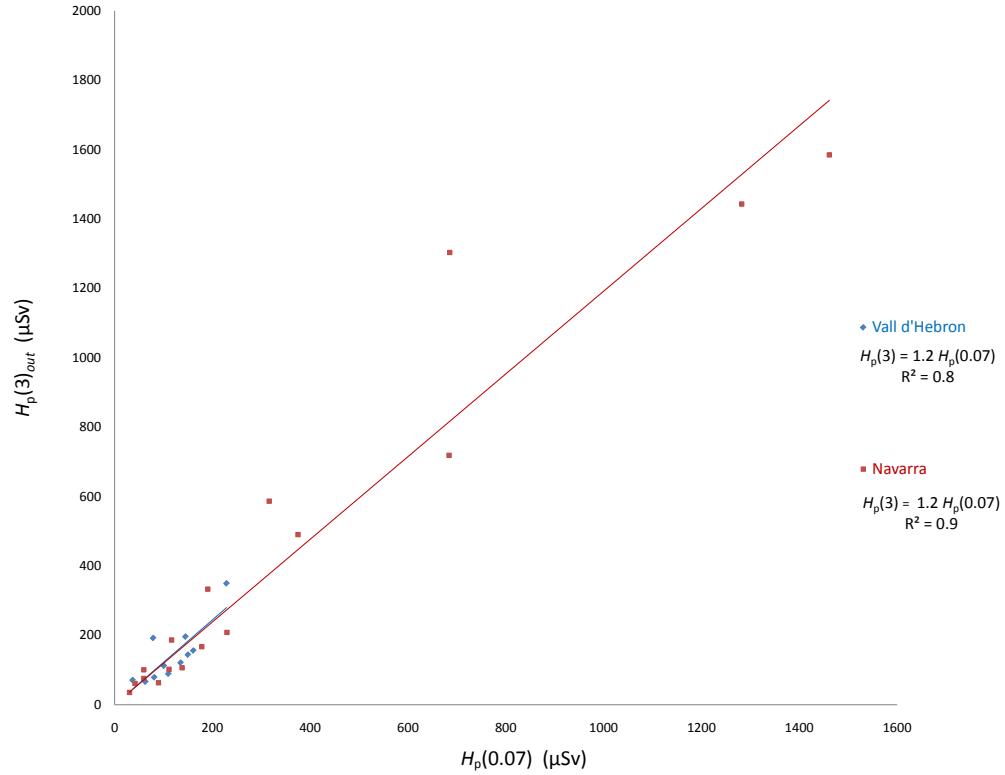

Figure 12.8: Relation between $H_{\mathrm{p}}(3)$ measured outside the lead glasses $H_{\mathrm{p}}(3)_{out}$ and $H_{\mathrm{p}}(0.07)$ measured on the lead apron for nurses, for the two hospital in the study

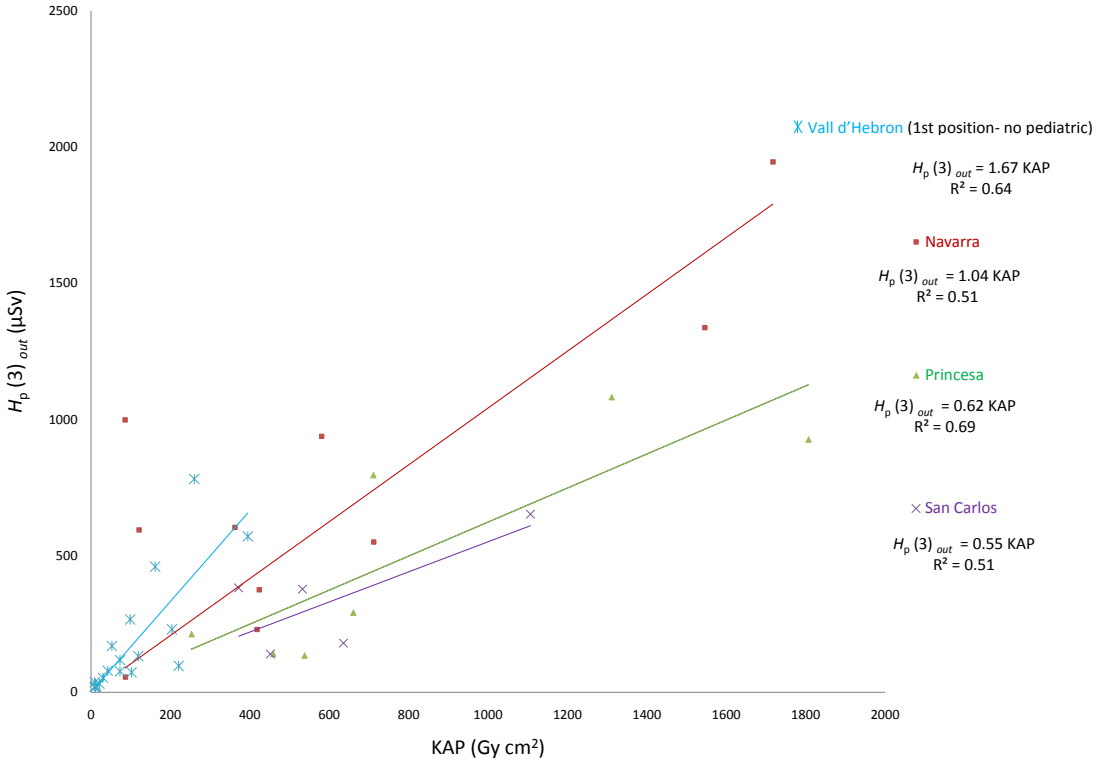

Figure 12.9: Relation between $H_{\mathrm{p}}(3)$ measured outside the lead glasses $H_{\mathrm{p}}(3)_{out}$ and KAP for all physicians from the four hospitals under study

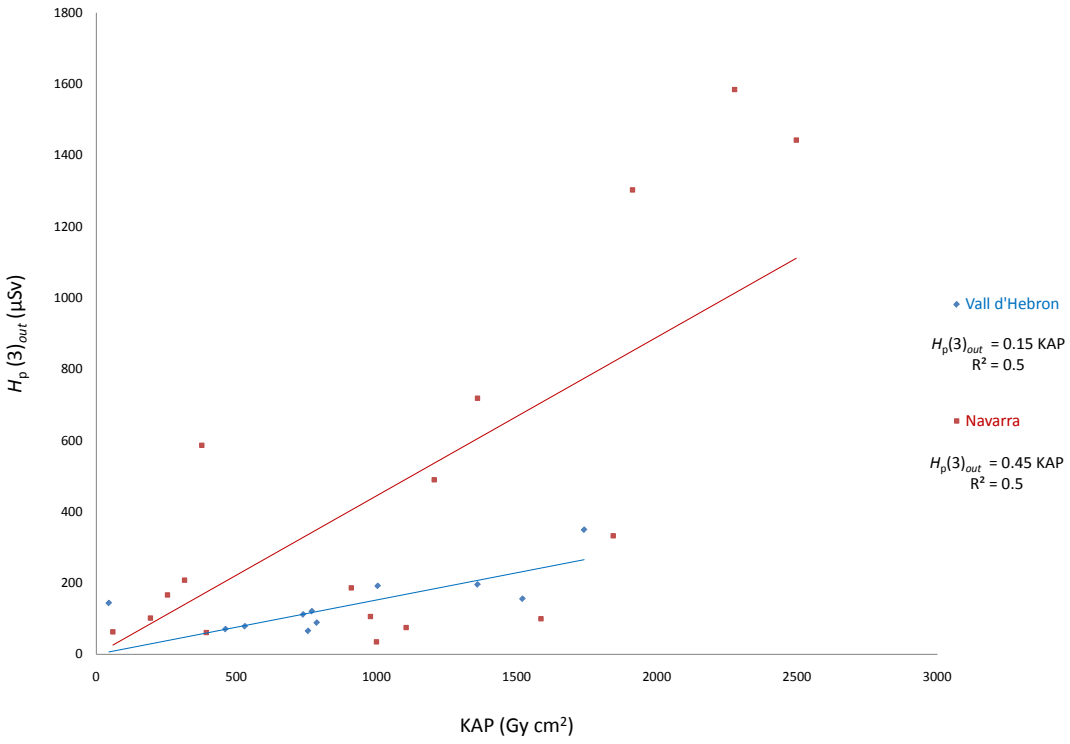

Figure 12.10: Relation between $H_{\mathrm{p}}(3)$ measured outside the lead glasses $H_{\mathrm{p}}(3)_{out}$ and KAP for nurses, for the two hospital in the study

	Vall d'Hebron only no pediatric-1st operator		Navarra		Princesa		San Carlos	
	$\frac{H_p(3)_{out}}{H_p(0.07)}$	$\frac{H_p(3)_{out}}{KAP}$	$\frac{H_p(3)_{out}}{H_p(0.07)}$	$\frac{H_p(3)_{out}}{KAP}$	$\frac{H_p(3)_{out}}{H_p(0.07)}$	$\frac{H_p(3)_{out}}{KAP}$	$\frac{H_p(3)_{out}}{H_p(0.07)}$	$\frac{H_p(3)_{out}}{KAP}$
Mean	2.6	1.9	1.6	0.9	0.7	0.6	0.78	0.7
Max	6.8	3.8	6.0	1.8	1.1	1.1	0.96	1.0
Min	0.8	0.4	0.5	0.1	0.4	0.2	0.56	0.3
sd	1.7	0.9	1.7	0.6	0.3	0.3	0.18	0.3
$sd_{\bar{x}}$ (%)	15%	11%	35%	19%	11%	21%	12%	23%
Median	2.2	1.8	1.1	1.0	0.8	0.8	0.8	0.7
N	20	18	9	10	10	8	4	4

Table 12.12: Mean, maximum, minimum, standard deviations sd and $sd_{\bar{x}}$ (%), median and N values of the ratios between $H_p(3)_{out}$ and $H_p(0.07)$ and between $H_p(3)_{out}$ (in μSv) and KAP (in Gycm^2) for physicians

	Vall d'Hebron		Navarra	
	$H_p(3)_{out}/H_p(0.07)$	$H_p(3)_{out}$/KAP	$H_p(3)_{out}/H_p(0.07)$	$H_p(3)_{out}$/KAP
Mean	1.27	0.42	1.26	0.48
Max	2.43	3.2	1.9	1.56
Min	0.81	0.08	0.7	0.04
sd	0.5	0.92	0.38	0.41
$sd_{\bar{x}}$ (%)	12%	66%	7%	20%
median	1.04	0.15	1.15	0.53
N	11	11	7	7

Table 12.13: Mean, maximum, minimum, standard deviations sd and $sd_{\bar{x}}$ (%), median and N values of the ratios between $H_p(3)_{out}$ and $H_p(0.07)$ and between $H_p(3)_{out}$ (in μSv) and KAP (in Gycm^2) for nurses

Nurses are exposed to a more homogeneous radiation field than physicians because of different proximities to the source. Mean $H_p(3)_{out}/H_p(0.07)$ is close to unity, and a low spread of values is observed (7% and 12% for Navarra and the Vall d'Hebron Hospitals, respectively). However, as regards the relation between $H_p(3)$ and KAP, the variability is higher than with physician and the correlation worst, in particular in the case of Vall d'Hebron. This is due to the fact that, in general, the increase in KAP is related to an increase of complexity of the clinical procedure and this has higher impact on physicians' doses than on nurses'.

12.3.2 Estimation of attenuation coefficients for lead glasses

The protection efficiency of the lead glasses was estimated as the correction factor (CF) defined as the ratio of the dose to the eyes when lead glasses were used and when they were not:

$$CF = \frac{H_p(3)_{in}}{H_p(3)_{out}} \tag{12.1}$$

Measured CF in real clinical conditions for types of lead glasses shown in Figure 12.1 are presented in Table 12.14. The number of collected data values are shown in line 6. For the wraparound lead glasses (Figure 12.1 (a)), the measured CF ranged between 0.21 and 0.41, with a mean value of 0.31. Meanwhile, for the (b) and (c) models, the CF ranged from 0.25 to 0.72, with a mean value of 0.37. The highest CF (0.72), which indicates the lowest protection efficiency, belongs to the (c) model that has the least efficient protection design with smaller frontal and lateral lenses when compared to the other glasses. The mean CF is about 0.5 (i.e. they halve the doses) for Type (c) glasses, while for the (a) and (b) models it is approximately 0.3 (i.e. they reduce dose to 1/3).

12.3.3 Estimation of annual eye lens dose

The estimated annual dose is calculated for San Carlos, Navarra and Princesa Hospitals Table 12.15. Values of $H_p(3)$/N (μSv procedure^{-1}) are multiplied by the number of procedures per year N_{year} to

Glasses model	CF		
	Wrap around glasses	Lateral shielding - large lenses	Lateral shielding - small lenses
	Figure 12.1 (a)	Figure 12.1 (b)	Figure 12.1 (c)
Mean	0.31	0.32	0.54
Min	0.21	0.25	0.36
Max	0.41	0.52	0.72
N	3	7	3

Table 12.14: Ratio of $H_p(3)$ values with and without lead glasses (CF) obtained in experimental measurements. Mean, minimum, maximum and number N of data values collected for each model of glasses are listed

obtain an estimation of the annual $H_p(3)_{year}$. When $H_p(3)$ data collected inside the protective glasses are available, then the estimate of the $H_p(3)_{in,year}$ is given. Values are given in Table 12.15 both for physicians and for nurses. In the latter case, only nurses from the Navarra Hospital were monitored. Data show that 8 physicians over 14 surpassed the recommended 20 mSv annual eye lens dose. Even though physicians wore lead glasses, in two cases, the protection provided was not enough to reduce the dose below 20 mSv (cases Pr_3, Nav_3), in some cases the dosemeter inside the goggles is probably located on a part of the glasses to avoid disturbing the physician and is therefore not very well protected, the attenuation factor might thus be highly underestimated. In the case of nurses, three nurses out of six exceeded the 20 mSv y^{-1} limit, in contrast with what was observed in Vall d'Hebron Hospital.

	$H_p(3)$/N (μSv procedure^{-1})	N_{year}	$H_p(3)_{year}$ (mSv)
Physicians			
Pr_1*	5	200	1
Pr_2*	19	700	13
Pr_3*	33	700	23
Pr_4	46	300	14
Pr_5	92	300	28
Nav_1*	38	429	16
Nav_2	279	444	124
Nav_3*	58	566	30
Nav_4	11	908	10
SC_1	41	667	27
SC_2	14	625	9
SC_3	27	700	19
SC_4	77	417	32
SC_5	8	639	5
Nurses			
Nav_1	72	665	48
Nav_2*	117	677	79
Nav_3	87	336	29
Nav_4	13	655	9
Nav_5*	19	267	5
Nav_6	5	752	4

Table 12.15: $H_p(3)$ is estimated by using the dosemeter in the internal part of the glasses ($H_p(3)_{in,year}$). $H_p(3)$ divided by the number of performed procedures, number of procedures per year and estimated annual doses calculated for physicians from the Princesa Hospital (Pr), Navarra (Nav), San Carlos (SC) and nurses from the Navarra Hospital (Nav). *Physicians wearing lead goggles

Chapter 13

Analysis of variability through Monte Carlo calculation

MC analysis allows the study of the influence of different parameters on eye lens exposure during an interventional procedure. This part of the work, performed in collaboration with the EURADOS working group 12 (Dosimetry in Medical Imaging), complements the experimental measurements and aims to study the influence of operator position, height and body orientation on eye lens exposure by using Monte Carlo simulations. The protection efficiency of lead glasses in real clinical conditions and the relation between $H_{\mathrm{p}}(3)$ and $H_{\mathrm{p}}(10)$ measured at thorax level on the lead apron are also examined. More specifically the following parameters were studied:

- The effect of operator position with respect to the patient when lead glasses are not worn;
- The influence of the presence of the image intensifier, tube voltage and operator height;
- The protection efficiency of lead glasses for different operator positions and body orientations with respect to the patient;
- $H_{\mathrm{p}}(10)$ on the left and the centre of the thorax and its comparison with $H_{\mathrm{p}}(3)$.

The IC/IR scenario described in Part III was simulated, as defined within the framework of the European projects ORAMED and ELDO. A first study was carried out in order to evaluate the influence of operator position and body rotation on eye lens dose when lead glasses were not worn. The main aim of this part was to investigate how the eye lens dose can be reduced by optimizing the relative position of the operator with respect to the X-ray source. Several distances (0, 20, 40 and 70 cm) between the operator and the X-ray source were considered together with the following operator body orientations: 0, 10, 30, 45 and 60 degrees, facing towards and away from the tube. A simplified sketch of the configurations is illustrated in Figure 13.1. The selected distances represent the position of the operator for jugular access (0 cm), radial access for pediatric (20 cm) and adult patients (40 cm) and femoral access (70 cm). A 90 kV peak-voltage X-ray beam with 3 mmAl added filtration was used. The reference operator height is 178 cm. Postero-Anterior projection and thorax irradiation were considered for these simulations.

Depending on the relative position of the operator, the image intensifier can provide attenuation of the scattered radiation that reaches the operator's eye. In order to investigate this, a $2-mm-$thick cylindrical lead shell filled with air and an input window of $1.5mm$ aluminium were used to represent the image intensifier. Simulations were repeated by replacing the lead and aluminium materials by air, for the above-mentioned distances. Rotation of the operator with respect to the source was not considered. For all the other cases, the image intensifier was simulated.

The effect of tube voltage on the operator eye lens was studied by repeating calculations for a 110 kV peak voltage radiation beam with $3mm$ aluminium added filtration at distances of 0, 20, 40, 70 cm and 0° rotation. Eye lens dose values were compared against the beam with a lower voltage (90 kV). The higher voltage is usually used for a larger patient. In order to study the influence of eye lens exposure for an operator who is either shorter or taller than the reference operator, calculations for operator heights of 158, 168 and 188 cm were also included. Simulations were performed for distances of 0, 20, 40, 70 cm and 0° rotation. For the study of the efficiency of the lead glasses, the wraparound style was modelled as defined in Koukorava et al. (2014) with $0.5mm$ lead and $7.5mm$ lens size. Two field dimensions were studied resulting in a 30 and 20 cm diameter field at the level of the patient's thorax, for Postero-Anterior (PA) and Left-Lateral (LLAT) projections, respectively.

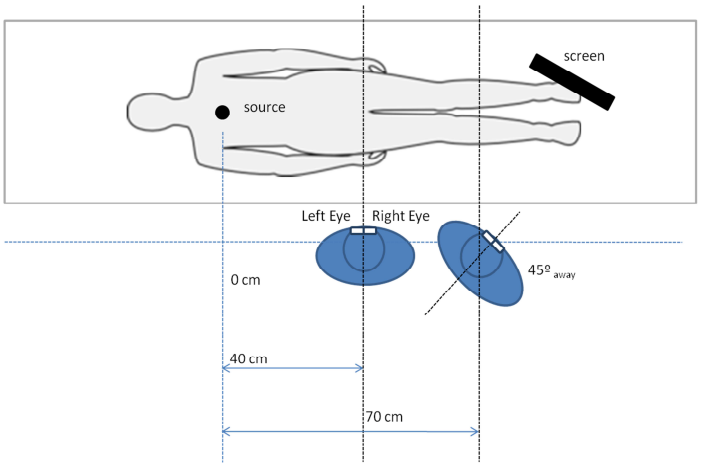

Figure 13.1: Simplified geometry with some of the possible configurations of the clinical simulated scenario. In this figure the operator is at 40 *cm* distance and 0° orientation (no rotation) and at 70 *cm* distance and rotated 45° away from the source (facing towards the image screen)

When using lead glasses, ISO 15382 (ISO, 2015) recommends the use of a dosemeter worn, preferably, behind the lead part of the glasses. However, this option is usually not very practical as it is a bit cumbersome. An alternative solution is to wear a dosemeter close to the eye on an unprotected part and to apply a proper correction factor that takes into account the protection provided by the glasses. In this study, the protection efficiency of the lead glasses was hence estimated as the correction factor (CF) as defined in subsection 12.3.2. CF is the ratio of the dose to the eyes when lead glasses are used and when they are not.

In order to study the relation between whole body dose, measured at the thorax above the lead apron, and eye lens dose, two thin tally volumes were positioned on the apron, at the center (MT) and at the left (LT) of the thorax. A $1-cm-$thick soft tissue layer was placed above each of them to estimate $H_{\mathrm{p}}(10)$ at the two positions. $H_{\mathrm{p}}(10)$ was used as it was found from experimental measurements that no statistical differences were observed when $H_{\mathrm{p}}(0.07)$ was used. Furthermore, active dosemeters are usually calibrated in terms of $H_{\mathrm{p}}(10)$ and results can be compared with published data. The dose to the left eye (LE) to calculate the personal dose equivalent $H_{\mathrm{p}}(3)$ and to the left lateral position (LL), were compared with doses at MT and LT.

Distances of 40 and 70 *cm* between the operator and the X-ray source were considered together with operator body orientations of 0, 30 and 45 degrees, facing towards and away from the tube. Only radial access (40 *cm*) and femoral access (70 *cm*) were considered for these simulations as they represent the most common configurations in clinical practice. Postero-Anterior projection and thorax irradiation were simulated. LLAT projection at 40 *cm* and 70 *cm* distance without rotation was also considered.

Energy deposition tally (F6 tally) in kerma approximation mode was used to determine the energy deposition to the left eye (LE), to the left lateral position (LL), to the middle thorax (MT) and to the left side of the thorax (LT). Correction factors from whole body dose, measured by dosemeters placed on the lead apron, were used to extrapolate eye lens dose.

13.1 Results of the influence of operator position, height and body orientation on eye lens dose

Table 13.1 shows the ratio of the left and right eye lens personal dose equivalent calculated using MC simulations. Data were obtained for a PA projection for the operator at the different studied positions in the configuration facing away from the tube (columns 2 to 5) and facing towards the tube (columns 6 to 8). The latter is quite an unlikely scenario in interventional cardiology and radiology practice. In this case, the left eye is generally the most exposed, but the ratios between the two eyes is almost 1

when the operator is facing towards the tube. The cumulative dose in the left and right eye is similar and differences are sometimes within statistical uncertainty. The statistical uncertainty of the simulation results was 1% (1 sd) in most cases, except for the cases of 45 and 60° rotation facing away from the tube where the uncertainty was 3% (1 sd). Simulations were performed without lead glasses since the aim of this part of the study was to evaluate the influence of operator position and rotation on left and right eye lens dose when no protection is used.

At 0 *cm* distance (jugular access-typical position) and 0° and 10° rotation, there are no differences between the left and right eye dose, while for larger angles the eye closest to the tube receives the greatest dose. When the operator is looking away from the tube (Table 13.1, column 2), when the monitoring screen is set to his/her right, the most exposed eye is the left one. In realistic clinical conditions, the operator always turns towards the screen when hitting the X-ray pedal in order to visualize the progress of the catheter and to perform the intervention. At distances of 20, 40 and 70 *cm* for an operator turning away from the tube, which represents the most likely situation in routine practice, the left eye is always the most exposed one. In addition, as shown in Table 13.1 (col. 3 to 5), the ratio between the dose to the left eye and right eye increases with both angle and distance, even though when the angle changes from 45° to 60° away from the tube, the dose remains almost constant. In these latter cases, the dose to the right eye is almost negligible, since it is mainly due to backscatter from the head (McVey et al., 2013).

$H_p(3, LE)/H_p(3, RE)$							
	away from the tube				*towards the tube*		
Angles (°)	0 *cm*	20 *cm*	40 *cm*	70 *cm*	20 *cm*	40 *cm*	70 *cm*
0	1.0	1.2	1.3	1.5	1.2	1.3	1.5
10	1.0	1.2	1.5	2.3	1.0	1.2	1.4
30	1.1	1.6	2.8	5.4	1.1	1.1	1.2
45	1.3	3.6	6.6	13.1	1.0	1.2	1.1
60	2.2	4.3	6.0	12.6	0.8	0.9	1.0

Table 13.1: $H_p(3, LE)/H_p(3, RE)$ ratios for away from the tube and for towards the tube for the PA projection and when lead glasses are not worn. LE stands for Left Eye and RE for Right Eye

Figure 13.2 shows the normalized dose values with respect to the LE dose at 40 *cm* distance and for 0° rotation. Values correspond to the configuration facing away from the tube. This configuration yields the highest dose to both eyes in the case of PA projection. It can be seen that increasing the rotation of the head diminishes the dose to both eyes when the operator is standing at distances of more than 40 *cm* away from the X-ray tube. This was also verified by Koukorava et al. (2014). Rotations higher than 45° entail a drop in dose of more than 50% for the left eye compared with the 0° rotation. The relative lower dose between 0 *cm* and 20 *cm* compared with the dose at 40 *cm* can be explained by the simulations performed both with and without the image intensifier. Eye lens dose with and without the image intensifier is lower by a factor of 3 at 0 *cm* distance. This effect decreases when the distance is increased and it is null for 40 and 70 *cm* distance of the operator from the source. Thus, it can be confirmed that the image intensifier works as a shield when it is near the operator. In the present simulations this effect can be seen for distances lower than 40 *cm* from the X-ray beam axis for the PA projection.

Both eye lens dose values were found to increase by about 25% when tube voltage was increased from 90 kV to 110 kV with 3*mm* Al filtration for all tested situations and operator-field distances of 0, 40, 70 *cm* and 0° rotation. Table 13.2 highlights the influence of operator height on the left eye lens dose. It shows the ratio between the left eye lens dose for three different phantom heights (158, 168 and 188 *cm*) and the left eye lens dose of the reference phantom height (ref = 178 *cm*). The phantom height plays a crucial role in diminishing the cumulative doses. Calculations show that eye lens dose decreases when the vertical distance between the operator's eyes and the patient increases. This effect is important when the operator is close to the X-ray tube (0 and 20 *cm*): in this case the left eye dose can change by a factor of 2 in the case of a $10 - cm$ shorter operator (168/ref case). This effect is mitigated by increasing the lateral distance (e.g. from radial to femoral access). However, a taller operator (column 4) leads to doses to the left eye lens that are reduced by a factor of 2 at 0 and 20 *cm* distance; this reduction is lower for 40 and 70 *cm* distances.

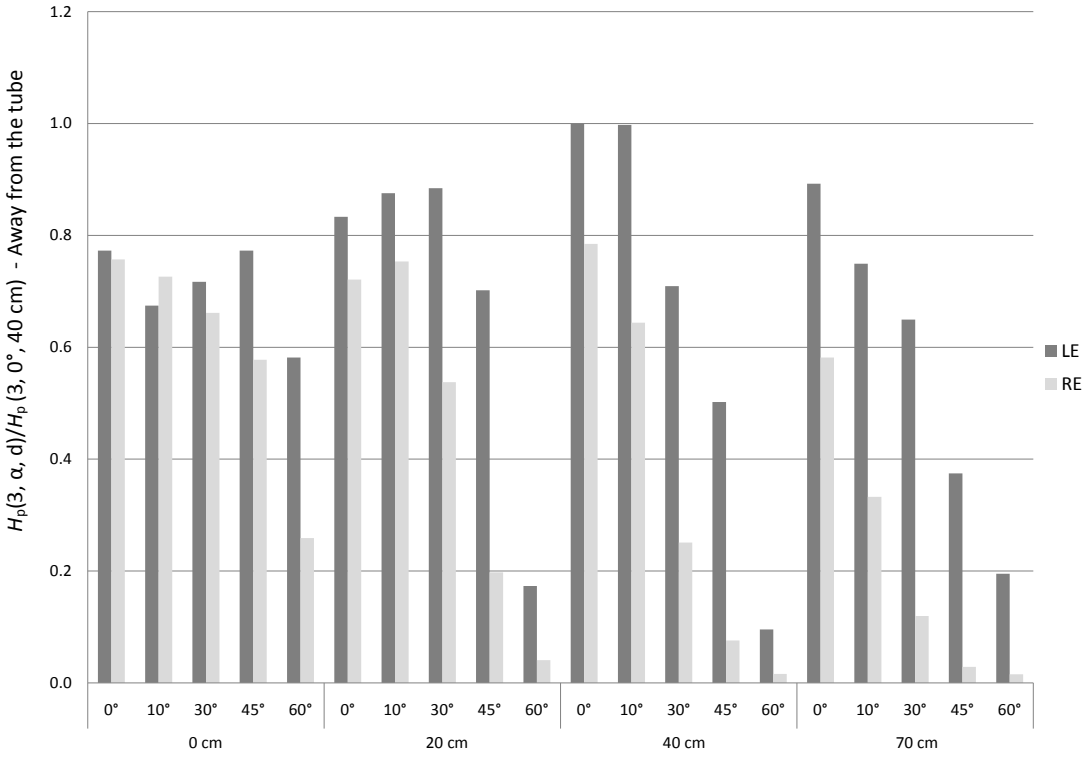

Figure 13.2: Eye lens dose distribution for all distances normalized with respect to the left eye dose at 40 *cm* distance and 0° rotation for the PA projection, and for when lead glasses are not worn

Distance	158/ref	168/ref	188/ref
0 *cm*	3.2	2.0	0.5
20 *cm*	2.8	1.9	0.5
40 *cm*	1.9	1.4	0.6
70 *cm*	1.3	1.2	0.8

Table 13.2: LE dose ratios for different operator heights (158 *cm*, 168 *cm* and 188 *cm*) and a reference height of 178 *cm*

13.2 Protection efficiency of lead glasses

MC results of $H_p(3)$ values with and without lead glasses (CF) for PA and LLAT irradiation are shown in Table 13.3. Some relevant data from Koukorava et al. (Koukorava et al. (2014)) are also included for comparison. It can be seen that, at 0°, the protection effectiveness of the glasses for the left eye is higher as distance increases, whilst it decreases for the right eye (as shown in Figure 13.2, without glasses the right eye is the least exposed). Likewise, the protection effectiveness of lead glasses is generally increased when the operator faces the X-ray tube as opposed to when looking away. This is due to the fact that a larger amount of scattered radiation directly strikes the lens of the glasses. Similar observations were found by Koukorava et al (Koukorava et al., 2014). Such a protective effect is reduced at 70 *cm* distance, where no relevant difference is observed within CF at different angles.

If we consider the most likely operator positions, which are 0, 40 and 70 *cm* distance for rotation angles up to 45°, the correction factor for the most exposed eye (the left one), for $0.5 - mm-$thick wraparound-style lead glasses, ranges from 0.11 to 0.58. The lowest protection (0.58) belongs to the femoral access configuration (70 *cm*) with 45° rotation away from the tube. Figure 13.2 shows that this value corresponds to the lowest dose and thus reduction of the protective efficiency should be of no concern.

Measured CF in real clinical conditions for types of lead glasses shown in Figure 12.1 are presented in Table 12.14.

		CF				
		PA		LLAT		
		LE	RE	LE	RE	Reference
0 *cm*	0°	0.51	0.52	–	–	Koukorava et al. (2014)
40 *cm*	0°	0.2	0.78	0.23	0.92	Koukorava et al. (2014)
	30°_towards	0.27	0.31	0.21	0.39	Present work
	30°_away	0.34	1.19	0.32	0.98	Present work
	45°_towards	0.32	0.22	0.29	0.29	Present work
	45°_away	0.41	0.88	0.40	0.79	Present work
	60°_towards	0.53	0.2	0.45	0.2	Present work
	60°_away	0.58	0.8	0.31	0.58	Present work
70 *cm*	0°	0.15	0.89	0.12	0.97	Koukorava et al. (2014)
	30°_towards	0.15	0.24	0.11	0.31	Present work
	30°_away	0.25	0.95	0.28	0.92	Present work
	45°_towards	0.15	0.16	0.11	0.18	Koukorava et al. (2014)
	45°_away	0.42	0.78	0.58	0.7	Koukorava et al. (2014)
	60°_towards	0.17	0.16	0.12	0.12	Present work
	60°_away	0.84	0.82	0.89	0.76	Present work

Table 13.3: Ratio of $H_p(3)$ values with and without lead glasses (CF) for PA and LLAT irradiation (data from Kourokava et al. (Koukorava et al., 2014) are also included for comparison).

13.3 Results on the relation between $H_p(3)$ and $H_p(10)$ measured on the thorax

Calculations were performed for PA projection considering rotation of the head, of 30° and 45°, whereas the rest of the body remains at 0°. Simulations were repeated for the LLAT projection only for 0° rotation of the head and body (no rotation). Correction factors are determined as the ratio between the dose at the left eye (LE) and at the left lateral sensor (LL) and the dose at middle thorax (MT) and left thorax (LT), when the operator was wearing the protective apron, but not the lead glasses. Results are shown in Table 13.4. In column 6 the $H_p(3)$ ratio between LL and LE is also presented. The LL sensor overestimates the dose to the eye lens of approximately 30%. This overestimation is higher when the head is rotated away from the tube and LE receives a lower amount of radiation than other configurations, such as for 70 *cm* and 45°_ away.

			$\frac{H_p(3,LE)}{H_p(10,MT)}$	$\frac{H_p(3,LE)}{H_p(10,LT)}$	$\frac{H_p(3,LL)}{H_p(3,LE)}$	$\frac{H_p(3,LL)}{H_p(10,MT)}$	$\frac{H_p(3,LL)}{H_p(10,LT)}$
PA	40 *cm*	0°	0.58	0.39	1.29	0.75	0.65
		30°_towards	0.44	0.39	1.22	0.54	0.48
		30°_away	0.52	0.46	1.29	0.68	0.59
		45°_towards	0.43	0.38	1.26	0.54	0.48
		45°_away	0.29	0.25	1.30	0.37	0.33
	70 *cm*	0°	0.93	0.84	1.29	1.21	1.09
		30°_towards	1.00	0.91	1.16	1.17	1.05
		30°_away	0.77	0.70	1.40	1.08	0.98
		45°_towards	1.02	0.92	1.18	1.20	1.08
		45°_away	0.45	0.40	2.11	0.94	0.85
LLAT	40 *cm*	0°	0.95	0.82	1.34	1.27	1.10
	70 *cm*	0°	1.25	1.30	1.34	1.68	1.75

Table 13.4: Ratio of $H_p(3)$ and $H_p(10)$ values measured at different positions. The $H_p(3,LL)/H_p(3,LE)$ ratio is also included. LE stands for Left Eye, MT for Middle Thorax, LT for Left Thorax, LL for Left Lateral

Table 13.5 shows mean, minimum, maximum values for 40 and 70 *cm* distances together for the PA projection. Mean_all represents the average value obtained from all data from Table 13.4 disregarding the direction of the rotation of the head, whereas mean_away, mean_towards and mean_0° are the values

for rotation away from the tube, towards the tube and 0° respectively (averaged between 40 and 70 *cm*).

	$\frac{H_p(3,LE)}{H_p(10,MT)}$	$\frac{H_p(3,LE)}{H_p(10,LT)}$	$\frac{H_p(3,LL)}{H_p(3,LE)}$	$\frac{H_p(3,LL)}{H_p(10,MT)}$	$\frac{H_p(3,LL)}{H_p(10,LT)}$
Mean_all	0.64	0.56	1.3	0.85	0.76
Min	0.29	0.25	1.16	0.37	0.33
Max	1.02	0.92	2.11	1.21	1.09
Mean_away	0.5	0.5	1.5	0.8	0.7
Mean_towards	0.7	0.6	1.2	0.9	0.8
Mean_0°	0.8	0.6	1.3	1.0	0.9
sd	0.27	0.25	0.27	0.31	0.29

Table 13.5: Mean, minimum, maximum and standard deviation sd of $H_p(3)$ and $H_p(10)$ ratios measured at different positions for PA projection

For the PA projection results show that $H_p(3,LE)/H_p(10,MT)$ ratios are higher than $H_p(3,LE)/H_p(10,LT)$ as the left thorax is more exposed to scattered radiation than the middle thorax, as the radiation strikes from the left side. For the configurations where the physician is looking away from the tube, the $H_p(3)/H_p(10)$ ratios are lower than for the configuration 'towards the tube', as the eyes are less exposed in the 'away from the tube' case, whilst the thorax is equally exposed. The lowest value of 0.29 corresponds to the configuration at 40 *cm* distance for 45° rotation away from the tube. In this case, the physician is close to the field and the thorax is much more exposed than the head because of the rotation. The higher the rotation of the head away from the tube, the lower is $H_p(3)/H_p(10)$, as the eye lens dose decreases. This effect is mitigated at 70 *cm*. For the configuration 'towards the tube' and for 40 *cm* distance, $H_p(3)/H_p(10)$ is independent from the rotation angle (for the studied cases). The same can be stated for 70 *cm*. However, at this distance the exposure of the body to the field is more homogeneous for this specific projection and eyes and thorax are equally exposed (ratios close to unity while close to 0.5 for 40 *cm*). In order to extrapolate $H_p(3,LL)$, that is the eye lens equivalent dose that might be measured by an eye lens dosemeter located at the left temple, a correction factor of 0.76 should be applied to $H_p(10,LT)$, that is the dose measured by a whole body dosemeter positioned on the lead apron. This correction factor is derived from the mean of all $H_p(3,LL)/H_p(10,LT)$ and it ranges between 0.33 (40 *cm*, 45°_ away) and 1.09 (70 *cm*, 0°). Thus, a large variation is observed for these cases.

For the LLAT projection, the ratios increase significantly with respect to the PA projection. The eyes are generally more exposed than the thorax, especially at 70 *cm*. A mean value of 1.43 is derived from $H_p(3,LL)/H_p(10,LT)$ at 40 and 70 *cm* distance. This shows that, for the studied cases, the use of different projections influences the values of $H_p(3)/H_p(10)$, and highlights the difficulty of the application of a proper correction factor.

Although it is not very frequent in real practice, PA calculations were repeated considering the rotation of the whole body (head and thorax). Results are shown in Table 13.6. When both head and thorax rotate away from the tube, the eye lens dose to the left eye $H_p(3,LE)$ overestimates the dose to the thorax at 10*mm* depth by a factor of 5 for MT and 3 for LT. These values are doubled for $H_p(3,LL)/H_p(10,MT)$ and $H_p(3,LL)/H_p(10,LT)$, as the $H_p(3,LL)$ is 50% higher than $H_p(3,LE)$ for these configurations. Thus, in these cases, the radiation that reaches the thorax is highly attenuated by the body itself and there is the possibility of incurring in a high underestimation of the eye lens dose estimate by applying the $H_p(3)/H_p(10)$ factor. In the scenarios where the operator is facing towards the tube, $H_p(3,LE)/H_p(10,MT)$ and $H_p(3,LE)/H_p(10,LT)$ are equal to 0.7 and these ratios slightly increase using the LL sensor (0.8).

	$\frac{H_p(3,LE)}{H_p(10,MT)}$	$\frac{H_p(3,LE)}{H_p(10,LT)}$	$\frac{H_p(3,LL)}{H_p(3,LE)}$	$\frac{H_p(3,LL)}{H_p(10,MT)}$	$\frac{H_p(3,LL)}{H_p(10,LT)}$
Mean_all	2.5	1.7	1.2	4.4	2.5
Mean_away	5.3	3.2	1.5	11.4	6.0
Mean_towards	0.7	0.7	1.2	0.8	0.8
Mean_0	0.8	0.6	1.3	1.0	0.9
sd	3.4	1.6	0.3	7.4	2.8

Table 13.6: Mean values and standard deviation sd of $H_p(3)$ and $H_p(10)$ ratios measured at different positions for PA irradiation considering the rotation of the whole body

Part V

Discussion

Chapter 14

Summary of results and comparison with earlier published data

The main results of this thesis are analyzed and compared with earlier published data. Achievements and limitations are discussed and future studies are proposed.

14.1 Optimal positioning for maximum eye lens equivalent dose assessment

The study on phantom has shown the fact that an eye lens dosemeter at the left lateral (LL) position provides the best estimate of the eye lens equivalent dose at the most exposed eye (the left one for the studied cases). On the other hand, a dosemeter located at the forehead or at the right temple subestimate the dose at the left eye. In Domienik et al. study (Domienik et al., 2012) 10 TLDs were placed on a head band between the left and the right temple of physicians working in IR suites. Their results show that in 50% of the studied cases the TLD at the left temple (LL) registered the highest eye lens dose. The dose measured at the different sites decreases as the distance of the TLD from the X-ray tube increases. In none of the measured cases the maximum eye lens dose was found in one of the five TLDs between the forehead and the right temple. These results obtained in clinical condition agree with measurements performed on phantom and the pilot study performed in San Carlos University Hospital within the frame of this thesis .

14.2 Use of active personal dosemeters

The use of active personal dosemeters could be of great help to increase awareness of workers while they are being exposed and to optimize the procedures when an increased signal is observed. The comparison of $H_{\mathrm{p}}(10)$ measurements with UPC-WBD and with the electronic DoseAware detector in the preliminary phantom studies provided a mean value of $H_{\mathrm{p}}(10)_{DoseAware}/H_{\mathrm{p}}(10)_{UPC-WBD}$ equal to 1.02 (sd = 0.21). The result was obtained from 24 measurements corresponding to typical interventional procedures and it is in agreement with the value obtained in previous works done by our team: (1.11±0.10) (Sanchez et al., 2014). It confirms that the DoseAware electronic device responds satisfactorily well to realistic interventional cardiology scattered fields. The observed performance is better than the data pubished by Struelens et al. (Struelens et al., 2011) who performed some tests on operators. In their work, they reported a median value for the DoseAware of 0.61, obtained from a set of 5 measurements at one hospital. Similar responses were found for other active personal dosemeters, the authors admitted that the study could have some limitations associated with the low registered dose or with the shielding of one dosemeter compared with another. To complete our study it would be interesting to undertake a systematic campaign of measurements assigning both active and passive dosemeters to workers. This additional work has just started within the framework of EURADOS WG12 and preliminary results are promising and confirm our phantom data.

14.3 Assessment of eye lens equivalent dose using a whole body dosemeter situated on the lead apron

The most common and convenient procedure used at present for assessing eye lens equivalent dose is the use of a second WBD situated on the apron on the chest or the collar. Many studies have been published in recent years to analyze this procedure. Three major approaches or a combination of approaches are followed to address this issue, namely, measurements with phantoms, measurements in clinics and MC calculations. The three methodologies and, in particular, a combination of MC simulation and experimental results are used in different parts of this study. MC simulations have proven to be useful to study the individual influence of specific parameters, such as X-ray tube projection, operator position, type of lead glasses, etc. However, calculations fail to realistically reproduce clinical practice. The geometry of the patient and operator movements must be simplified compared with real clinical conditions. On the other hand, data from clinical practice are obviously realistic, but suffer from great variability of different parameters depending on patient, operator, difficulty of the procedure, adopted practice etc. Thus, large differences in measurements are not only found among the various hospitals and operators but also for the same operator.

To provide insight into the limitations and usefulness of the assessment of eye lens dose using a WBD situated on the lead apron, several papers from the literature were selected and compared with our data. Phantom and workers' measurements and MC calculations will be compared separately. For the comparison, preferably eye lens doses assessed as $H_p(3)$ measured close to the eye and $H_p(10)$ or $H_p(0.07)$ measured at chest or collar level will be chosen since they are the most frequently preferred positions. Measurements performed on other parts of the body, such as the shoulder or the extremities, will not be considered in the discussion. section 11.4 showed that the left shoulder position presented a larger variability than the chest or neck. When both $H_p(10)$ and $H_p(0.07)$ are reported, only $H_p(0.07)$ will be considered. As is verified in this study, the difference between the two quantities for low energy photon fields is not significant. Likewise, if the eye lens dose is assessed as $H_p(0.07)$, it will also be analyzed provided that it corresponds to a measurement close to the eye (Behrens et al., 2012).

14.3.1 Relation between eye lens and whole body doses on phantom

Table 14.1 provides a summary of results corresponding to recently published correction factors from eye lens dose measurements on phantoms. Correction factors CF are given in H_{eye}/H_{thorax} or $H_{eye}/H_{thyroid}$. The operational quantities will be specified henceforth in the text. The number N of performed irradiations and the type of projections or simulated procedures is also provided.

Author	N of irradiations	Projections/procedures	CF (mean ± sd) H_{eye}/H_{thorax}	CF (mean ± sd) $H_{eye}/H_{thyroid}$
This thesis Principi et al. (2015b)	8	PA	0.80±9%	1.14±6%
		LLAT	0.56±7%	1.02±12%
		PA,LLAT	0.74±8%	1.10±5%
Strocchi et al. (2016)	9	Vertebroplasty Periangliar Cerebral arteriography	0.71	
Cemusová et al. (2016)	24	PA	0.76±5%	1.12±5%
		LLAT	0.85±10%	1.13±9%
		PA,LLAT,AP,RLAT	0.73±15%	0.93±15%
Farah et al. (2013)	48	CA/PTCA, RFA, PM, ICD	0.87±87%	3.36±41%
		CA/PTCA, RFA	0.69±52%	3.98±41%

Table 14.1: Comparison of recently published data on the relation of the eye lens dose with whole body dose measured at chest or neck level on phantoms

The best estimate of $H_p(3)$ measured at the left eye in our study is given by $H_p(10)$ or $H_p(0.07)$ measured by a WBD at collar level. This is when the lowest spread of values is found (sd = 5%). In Strocchi et al.'s work (Strocchi et al., 2016), several projections corresponding to vertebroplasty, periangliar and cerebral angiography procedures were simulated on the RANDO phantom. Both eye lens dose and chest were given in units of $H_p(0.07)$ from TLD measurements. The CF $H_p(0.07)_{eye}/H_p(0.07)_{chest}$ averaged over all the simulated procedures was 0.71. In Cemusová et al.'s study (Cemusová et al., 2016), eye lens dose was measured with an EYE-D dosemeter in terms of $H_p(3)$, whilst $H_p(10)$ and $H_p(0.07)$ at chest and neck level were measured with a conventional

TL-WBD. The anthropomorphic phantom representing the physician wore a thyroid collar and a protective apron, thus WBD were located above the protection. Data were calculated for AP, PA, LLAT and RLAT projections. The CFs obtained in these three studies indicate that, disregarding the procedures/projections, a common factor of about 0.7 describe the dependence between eye lens dose and thorax dose and around 1.1 between eye lens equivalent dose and thyroid equivalent dose. Within 2 sd, the three papers are consistent. The ELDO study Farah et al. (2013) included a large number of measurements (48 irradiations) on anthropomorphic phantoms in typical interventional settings and considered different tube projections and configurations, beam energies and filtration, operator positions and access routes and used both mono-tube and biplane X-ray systems. No protection means were employed. Results showed that eye lens equivalent dose correlated best with $H_p(10)$ measured on the left side of the phantom at collar level. In Table 14.1 values for all procedures and specifically for CA/PTCA and RFA with mono-tube are reported. The CF for the dose at the thorax of 0.87 for all procedures show high standard deviation (87%). This variability is considerably reduced when only a type of procedure is selected, i.e. CA/PTCA (CF = 0.69±52%). The CF for equivalent dose at neck proposed by Farah et al. Farah et al. (2013) is much higher than CF from other studies. In Martin review from 17 different studies on the relation with H_{eye} and $H_{thyroid}$, the ratios of eye lens dose to whole body dose were between 0.24 and 1.25. Table 14.1 proves that for specific set-ups (ex. PA) the spread between results is small. However, when different positions are considered together, as it is the case in the ELDO study, the spread in the results increases and will be closer to what can be found when monitoring workers.

14.3.2 Relation between eye lens and whole body doses on physicians

As was mentioned in Part IV, one of the main difficulties when analyzing eye lens monitoring in clinics is the great variability of the results. One of the most important factor contributing to this variability of the eye lens dose and to high spread of the CFs is the use of shields (eyewear, suspended screen). These issues cannot be properly quantified by measurements on phantoms. A close follow up was organized and detailed data provided for some of the procedures. When the radiation protection officer is present during monitoring it is much easier to understand and justify some of the results. In Table 14.2, a summary of our main results is presented. $H_p(3)$ and $H_p(0.07)_{thorax}$ show good correlation for all hospitals. However, mean $H_p(3)/H_p(0.07)$ vary from 0.7 to 2.6. Considering all hospitals together, the correlation is still good (0.7) but increases up to 0.9 when disregarding the Vall d'Hebron Hospital measurements. As indicated in section 12.3, the proposed correction factor to assess $H_p(3)$ from $H_p(0.07)$ is derived from the slope of the fitted equations. From Table 14.2, we recommend to use the following equation: $H_p(3) = 0.8 \cdot H_p(0.07)_{thorax}$

		$H_p(3)_{out}/H_p(0.07)_{thorax}$				
Hospital	N of procedures	Mean	sd %	Median	Slope Figure 12.7	R^2
Vall d'Hebron*	51	2.6	15	2.2	1.40	0.8
Navarra	49	1.6	35	1.1	0.85	0.9
Princesa	80	0.74	11	0.79	0.77	0.7
San Carlos	68	0.78	12	0.80	0.70	0.7
All	248	1.8	14	1.09	0.84	0.7
All except V.H.	197	1.08	21	0.84	0.77	0.9

Table 14.2: Number of procedures N, mean, standard deviation (%), median and R^2 of the ratios between $H_p(3)$ measured outside the glasses ($H_p(3)_{out}$) and $H_p(0.07)$ for physicians. *Only no pediatric-1st position physicians

In Table 14.3, results from our study are compared with other authors' works for physicians. The square of the Pearson coefficient, when available, was used to measure the strength of the linear relationship between $H_p(3)$ and $H_p(0.07)$ measured on the lead apron. When data on neck dose are provided, they are also included. However, in this study, the thorax positioning was preferred because of the acceptability by the workers to wear a dosemeter at the chest rather than at the collar.

Comparison here is more difficult and the information provided in the different papers is often not comparable. Most of published data correspond to measurements performed with a WBD situated on the neck, whereas our data correspond to measurements on the chest. For interventional cardiology, doses at the thyroid or chest are higher than the eye lens doses, as we found in our study except for Vall d'Hebron Hospital. For other interventional procedures and for pediatrics, the eye lens equivalent dose is higher than the thyroid equivalent dose. In (Efstathopoulos et al., 2006), a ratio of 1.86 was found

Author	N of procedures	Procedure	CF (mean ± sd) H_{eye}/H_{thorax}	CF (mean ± sd) $H_{eye}/H_{thyroid}$
Efstathopoulos et al. (2006)	43 (only 1 physician followed)	IR	0.52	1.86
Lie et al. (2008)		IC	0.75	
Kong et al. (2014)	31	IR (anaesthetists)	1.42	2.49
Thrapnasnioti et al. (2016)	35 physicians	IC	0.64±0.43	
Buls et al. (2002)	54	IR		1.22
Sulieman et al. (2008)		IR		1.46

Table 14.3: $H_{\mathrm{p}}(3)/H_{\mathrm{p}}(d)$ measured at different positions and through different campaigns

for electrophysiology operators using bilateral femoral access. CF suggested by Lie and Thrapnasnioti are in agreement with values obtained from measurements on phantom of about 0.7 (Lie et al., 2008; Thrapnasnioti et al., 2016). In Kong et al. work, when single procedures are followed, a CF of 1.42 is achieved for the dose at chest for anaesthetists assisting IR procedures (Kong et al., 2014). In their study, a correlation coefficient of R^2=0.64 is published. Furthermore, the relation between eye dose and neck dose highlighted a large CF of 2.49 (R^2=0.61). Buls et al. (Buls et al., 2002) and Sulieman et al. (Sulieman et al., 2008) published correction factors $H_{eye}/H_{thyroid}$ of 1.22 and 1.46 respectively, where in all set-ups over-couch irradiation was predominant. In these cases, the upper part of the operator was the most exposed. The spread of $H_{\mathrm{p}}(3)_{out}/H_{\mathrm{p}}(0.07)_{chest}$ and $H_{\mathrm{p}}(3)_{out}/H_{\mathrm{p}}(0.07)_{thyroid}$ ratios found in the literature for measurements on physicians confirms the difficulties in assessing eye lens dose using a WBD situated on the lead apron and the problems in finding a unique correction factor, valid for all clinical conditions. Even when good correlation is found (Table 14.2), great variability among values is observed, thus highlighting the possibility of causing large over- or under-estimation of eye lens dose depending on the chosen correction factor. Mean and median $H_{\mathrm{p}}(3)_{out}/H_{\mathrm{p}}(0.07)_{chest}$ for all nurses (Vall d'Hebron and Navarra hospitals) is found to be 1.27 and 1.12 (with sd=6.4% and R^2=0.9). Less variability is observed than for physicians. Therefore, $H_{\mathrm{p}}(0.07)$ measured on the apron, on the left side of the thorax, can be considered as being a good estimator of eye lens dose for nurses.

14.3.3 Relation between eye lens and whole body doses with Monte Carlo simulations

Clerinx et al. (Clerinx et al., 2008) performed 62 simulations, including eight different projections: AP, PA, RLAT, LLAT and four 45° oblique. Simulations were performed for a distance lower than 50 *cm* from the worker to the center of the patient entry field for most cases (53 out of 62), while for all other cases the distance was 71 *cm*. The correlation between H_{eye} and $H_{\mathrm{p}}(0.07)$ measured at neck level ($H_{\mathrm{p}}(0.07)_{neck}$) was analyzed. For most cases, $H_{eye}/H_{\mathrm{p}}(0.07)_{neck}$ is 0.73, calculated as the regression coefficient obtained by least squares fitting. The square of the Pearson coefficient is 0.98. It follows that $H_{\mathrm{p}}(0.07)$ measured at the neck (above the thyroid collar if worn) overestimates the eye lens dose by approximately 25%. Different ratios are observed for a specific projection. The largest $H_{eye}/H_{\mathrm{p}}(0.07)_{neck}$ is found for the RLAT projection. A value of 1.2 was calculated for the LLAT projection. It is important to emphasise the fact that the number and type of simulated projections influence the value of the factor. For most projections, $H_{\mathrm{p}}(0.07)_{neck}$ tends to overestimate the eye lens dose. They are also in good agreement with the phantom results in Table 14.1. Based on the general agreement between different MC and phantom studies, as well as with some of the clinical measurements, (Martin, 2011) and (IAEA, 2013), recommend adopting a correction factor of 0.75 in practice for $H_{\mathrm{p}}(0.07)$ measured at neck.

The results from Clerinx's study cannot be quantitatively compared to our simulations, as in the case of this thesis the relation of eye lens dose with the dose at thorax level was studied but not at the neck. However, they are consistent. In fact, also in the present work, the highest $H_{eye}/H_{\mathrm{p}}(0.07)_{thorax}$ is found for the lateral projection. In the author's opinion, MC simulation and phantom measurements are very powerful methods, but they reproduce static scenarios and thus are always less accurate than actual measurements. Considering the large spread of correction factors derived from the real monitoring data (Table 14.2), a single correction should only be used for low exposed staff that are exposed to low radiation levels, in order to confirm that more precise monitoring is not needed.

14.4 Lead glasses efficiency

Protective lead glasses are often recommended in IC/IR procedures, especially in those cases where the ceiling screen is not practical for clinical work. For an appropriate assessment of eye lens dose, ISO 15382 recommends wearing a dosemeter behind the protection (ISO, 2015). However, this is often not very practical, and thus an alternative proposed option is to wear a dosemeter either on the outside or next to the lead glasses, and then apply a correction factor (CF) to take into account the efficiency of the eye wear. Part IV determines the efficiency of three types of lead glasses by MC simulation and through the monitoring of several physicians. Since a clinical procedure involves different positions and body orientations of the operator with respect to the radiation source, a mean CF is calculated from MC results in Table 13.3. Two hypotheses are considered. Firstly, the mean value of all CFs for the left eye is calculated including all distances and angles and the two projections, Postero-Anterior PA and Left-Lateral LLAT. Secondly, and based on feedback from routine practice, the mean CF is obtained by using only the most likely operator positions (i.e. 40 cm and 70 cm) and body orientations (0°, 30° and 45° away from the tube). Following these hypotheses, mean, standard deviation, maximum and minimum values of CF are presented in Table 14.4 in columns 2 and 3. For the first hypothesis, the mean CF value is 0.33 (sd = 0.22). For the second hypothesis, it is 0.31 (sd = 0.15) which shows that both results are consistent. Furthermore, the two results agree with findings from the work of Koukorava at al. (column 4) (Koukorava et al., 2014). These data are also consistent with our experimental results for the wraparound glasses (Table 14.4, column 5).

	MC calculated CF			Measured CF				
	This study hyp.1	This study hyp.2	Koukorava et al. (2014) hyp.2	This study	Magee et al. (2014)	Moore et al. (1980)	Thornton et al. (2010)	Rooijen et al. (2014)
Mean	0.33	0.31	0.32	0.31	0.22	0.24	0.14	0.32
SD	0.22	0.15	0.18	0.10	0.05	0.07	0.04	0.24
Max	0.89	0.58	0.58	0.41	0.53	0.29	0.19	0.62
Min	0.11	0.12	0.12	0.21	0.15	0.14	0.10	0.12

Table 14.4: Mean, standard deviation, maximum, minimum values of CF obtained for wraparound glasses with: Monte Carlo (MC) calculations, for hypotheses 1 and 2 (hyp.1: all MC, hyp.2: MC for 0, 30, 45° away from the tube), experimental measurements performed in this study and data from the literature

Other published experimental studies are also shown for comparison in Table 14.4, columns 6 to 9. These were performed on anthropomorphic phantoms and for wraparound glasses (Magee et al., 2014; Thornton et al., 2010; Rooijen et al., 2014; Moore et al., 1980). In these works, other types of glasses were also studied but are not taken into account in this comparison. In Magee et al. (Magee et al., 2014) three different scenarios were considered: the operator 30 *cm* from the source, 0° rotation; 68 *cm* from the source and 0° rotation; 68 *cm* with the operator tilted towards the tube by an angle of 60°. The CF ranged between 0.15 and 0.53, with a mean value of 0.22. This result is similar to the range found in the present study for measurements on operators in real clinical conditions. Furthermore, the highest protection efficiency of lead glasses (0.15) is attributed to the configuration with the operator looking towards the tube; this is in line with our MC value of 0.17 (PA projection) obtained for 70 *cm* and 60° rotation towards the tube. Furthermore, in the study by Moore et al. (Moore et al., 1980), a 3MR pelvic phantom was used to generate the scattered radiation field, while a phantom head simulated the position of the radiologist's head. Three different geometric configurations were studied: rotation of the operator of 0°, 30° and 60° towards the tube. No details regarding the distances of the operator to the tube were given, but as a patient pelvic phantom was used, radial/femoral access of the operator, i.e. about 55*cm* distance from the source, could be assumed. Their CF values ranged from 0.14 to 0.29 with a mean value of 0.24 obtained as an average of three geometric configurations. The authors showed that the larger the rotation is, the lower the attenuation efficiency becomes.

Additionally, in Thornton et al. (Thornton et al., 2010) the scenarios simulated were jugular, radial and femoral accesses; again no detailed information about the distances from the source was given. No rotation of the head was considered. This study provides the smallest CF range (0.10 - 0.19) compared with the other publications. The highest attenuation (0.1) is obtained for jugular access, as opposed to the results of the present work, where a CF of 0.5 was obtained considering 0 *cm* distance of the operator from the tube and no operator rotation (column 3, line 3). It is probably not overbold to consider that the influence of the image intensifier position has an important role in this case, as this difference in the two values could be due to the different relative positions of the eyes and the image intensifier in the two studies. Thornton's values for radial and femoral access of 0.19 and 0.11 agree with our MC results of 0.20 and 0.15, respectively.

Finally, Van Rooijen et al. (Rooijen et al., 2014) used two different geometrical configurations. Firstly,

a $50-cm-$distance was set between the source and the operator who was not tilted and had a height of $1.85m$. Secondly, the distances were maintained, but the operator head was tilted 45° away from the tube. The scattered radiation from the patient was produced by a PMMA slab phantom. Wraparound-type glasses, named model 4 and 5 in the quoted paper, were considered. Such types of glasses are similar to the MC model of this study. A mean CF of 0.32 (column 9) was obtained. This result is in agreement with our experimental measurements and our mean Monte Carlo CF value (columns 1 to 4 in Table 14.4) but remains larger than the other phantom measurements (columns 6 to 8). This difference may be due to the geometrical configuration involving an operator rotation of 45° away from the tube. Indeed, as previously mentioned, the efficiency of the lead glasses is reduced for head rotation away from the source and the highest CF value corresponding to this set-up was about 0.62.

In addition, the studies by Moore et al. (Moore et al., 1980) and Van Rooijen et al. (Rooijen et al., 2014) included few measurements on operators in clinical scenarios. Moore et al (Moore et al., 1980) only provided one value with a corresponding measured CF of 0.19. This value is smaller than the average CF value of 0.31 obtained in this study. Van Rooijen et al. (Rooijen et al., 2014) presented CF values for wraparound glasses (model 5 in the original paper) ranging from 0.18 to 0.90, with a mean value of 0.48. This range is broader than our measurements (CF range 0.21 - 0.41), but still consistent with MC values (0.15 - 0.84, for PA). However, as explained in their paper, Van Rooijen et al. (Rooijen et al., 2014) indicated that the dose reduction for the left eye lens is probably underestimated because the dosemeter was placed in a poorly shielded position. Based on this consideration, a mean CF of 0.48 for the wraparound model, as proposed, may be too high.

In spite of the shortcomings of both MC and experimental measurements, Table 14.4 shows good consistency between the two approaches, with CF mean values ranging from 0.14 to 0.33 (line 3). Based on our MC calculations, our measurements and the data available in the literature, a correction factor of 0.3 is recommended for radiological protection purposes for wraparound glasses. This CF value is obtained by averaging all values from the first row of CFs in Table 14.4. However, it is important to underline the fact that the number of collected data from our experimental campaigns is very limited and should be increased. The recommended correction factor provides a first solution to assess eye lens dose when lead glasses are worn and the dosemeter is situated in an unprotected position. This finding is in agreement with the recommendation from ISO 15382 (ISO, 2015), which proposes a value between 0.2 and 0.3 as correction factor. However, for non-wraparound glasses, such as type 3c glasses with smaller lenses, a more conservative CF value of 0.5 is recommended. Unfortunately, there are few clinical data available to reinforce our proposal. Further measurements in clinical practice would improve our knowledge.

14.5 Ceiling suspended screen attenuation

Phantom experiments highlight the efficiency of ceiling suspended screens to protect physicians. An attenuation factor of 17 on the eye lens dose is found for the PA projection, twice the efficiency of the lead glasses for the same conditions. The improper or miss-placement of the ceiling screen was considered to be one of the main justifications for the variability of the dose of the first operator, and training on how to use it one of the most effective tools for staff dose reduction. The protection provided by the screen is quantified by comparing $H_{\mathrm{p}}(3)$/KAP measured for single procedures in Vall d'Hebron Hospital when screen was used and when it was not. Physicians at first and second position are considered separately in Table 14.5. For physicians at first position, mean $H_{\mathrm{p}}(3)$/KAP from unshielded procedures is 3.4 and mean $H_{\mathrm{p}}(3)$/KAP for shielded procedures is 1.7. The attenuation factor associated with the use of the suspended screen is approximately 2. The difference between the mean values is statistically significant (p = 0.01, for $\alpha = 0.05$), but the attenuation is much lower than it was found for phantoms. For physicians at the second position, as expected, no statistical difference is observed associated with the use of the ceiling shielding (see chapter 12).

In clinical practice, several parameters change for each specific procedure. Thus, factors other than shielding may also contribute to the variation in $H_{\mathrm{p}}(3)$/KAP. The low attenuation during measurements in hospitals, could be due to the fact that the screen was not always well placed to protect the upper part of the body while using X-rays. In several studies, the contribution of the suspended screen to the attenuation of the eye lens dose was quantified. Within the framework of the ORAMED project, data from 34 hospitals were recollected, covering almost 1300 procedures. Results showed a reduction factor of (1.6 - 2.3) for CA/PTCA procedures, calculated as the ratio between eye lens dose without the shield and eye lens dose in presence of the shield (Vanhavere et al., 2011). The attenuation is enhanced up to 7 when the tube is above the operating table (Carinou et al., 2011). Simulations campaign were also conducted in order to determine the attenuation provided by the screen. Koukorava et al. in 2011

	Position/Shielding	N	Mean	SD	p (2-tailed)
$H_p(3)$/KAP (μSv Gy^{-1}cm^{-2})	1st_shield	17	1.69	0.82	0.01
	1st_no	2	3.41	0.56	
	2nd_shield	2	0.49	0.06	0.86
	2nd_no shield	3	0.55	0.36	

Table 14.5: Number N of procedures, mean $H_p(3)$/KAP, standard deviation and statistical significance p for shielded and unshielded procedures for physicians at first and second position

(Koukorava et al., 2011) assessed that the shield can reduce the eye lens dose a factor of 12 for PA and LLAT projections. This value was obtained for a specific and ideal configuration. In 2014 a more comprehensive study was carried out in order to obtain a more realistic result (Koukorava et al., 2014). Different projections, positioning of the screen and operator's distance from the X-ray source were taken into account. A total number of 25 simulations were performed. Results showed that the attenuation factor, averaged over the 25 simulation's outputs, was 2.3. Carinou et al (Carinou et al., 2015) in their review paper they summarized the influence of this protection reported in several studies. High variability was acknowledged. Attenuation factors ranged from 1.3 to 33 times with the most frequent range being between 3 and 11. However, the highest reported values of protection correspond to measurements on phantom or MC simulations. Martin's review (Martin, 2016) showed protection factors from 4 to 33. Within the reported wide variability, for a practical approach to radiation protection, measurements on clinical practice should be preferred thus an attenuation of the order of 2 - 4 should be considered. A correct use of the ceiling suspended screen should be promoted within physicians.

14.6 Estimation of annual eye lens dose

The distribution of the estimated annual eye lens doses of physicians monitored in this study is shown in Figure 14.1.

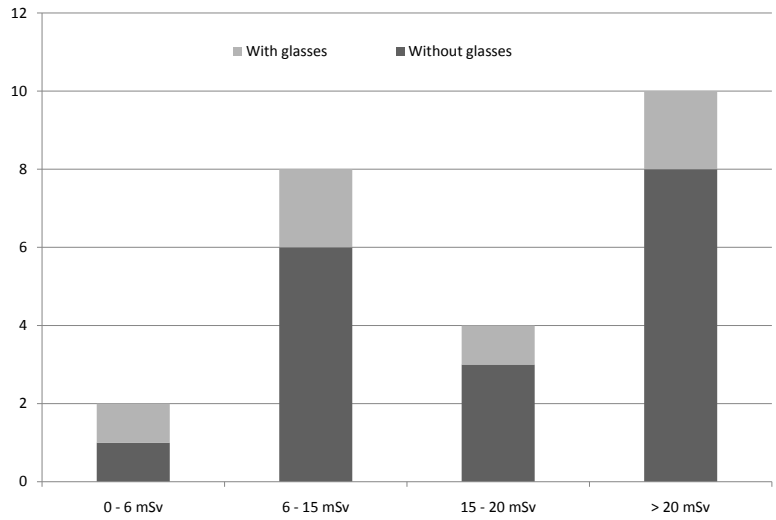

Figure 14.1: Distribution of the estimated annual eye lens dose Hp(3) (mSv) for the 24 physicians who participated in the measurement campaigns (Dark grey = physicians without lead glasses; light grey = physicians with lead glasses)

Results show that the new ICRP recommended limit of 20 mSv y^{-1} for the eye lens can be easily surpassed by physicians and only two physicians out of 24 do not exceed $3/10^{th}$ of the limit. The European Directive 2013/59 (EURATOM, 2014) states that category A workers are systematically monitored based on individual measurements performed by a dosimetry service. In the case of the eye lens this is when the eye lens equivalent dose is greater than 15 mSv. In most technical reports (IAEA, 2013; IRPA, 2017), given the uncertainty associated with the eye lens dose assessment, eye lens dose monitoring is recommended above 6 mSv per year. The use of lead glasses, even though it substantially reduces $H_p(3)$,

does not guarantee that the 20 mSv recommended annual limit would not be reached. Workload and good working practice have a great influence on annual doses. In Zett-Lobos' study (Zett-Lobos et al., 2013) the projected annual exposure of the eye lens for an interventional cardiologist wearing 0.25 mmPb equivalent glasses reached 33 mSv, despite the fact that the degree of attenuation of the dose at eye level ranged from 40% to 58%. Similar feature were found in this study. However, if monitored physicians had all wore appropriate lead glasses ($CF_{goggles} = 0.3$), the number of physicians exceeding 20 mSv would have been 1 out of 24 instead of 10 out of 24.

Further analyses have been performed in order to compare annual eye lens equivalent dose obtained with a dedicated eye lens dosemeter or using a corrected WBD measurement. Eye lens doses per procedure obtained from $H_p(0.07)_{thorax}$ measurements ($H_p(3)_{out}^{H_p(0.07)}$/N) have been calculated as $H_p(0.07)_{thorax}$/N (where N represents the number of performed procedures during the monitoring period) for each physicians multiplied by the correction factor suggested in subsection 14.3.2:

- $H_p(3)_{out}/H_p(0.07)_{thorax} = 0.8$

The annual $H_p(3)_{out,y^{-1}}^{H_p(0.07)}$ is then calculated with the usual method by multiplying $H_p(3)_{out}^{H_p(0.07)}$/N by the number of procedures performed in one year. The relative differences RD between $H_p(3)_{out,y^{-1}}$, calculated from $H_p(3)$, and $H_p(3)_{out,y^{-1}}^{H_p(0.07)}$, calculated from $H_p(0.07)$, are obtained as:

$$RD = \frac{H_p(3)_{out,y^{-1}}^{H_p(0.07)} - H_p(3)_{out,y^{-1}}}{H_p(3)_{out,y^{-1}}} \tag{14.1}$$

When protective glasses are worn $H_p(3)$ calculated from $H_p(0.07)_{chest}$ is obtained multiplying $H_p(3)_{out,y^{-1}}^{H_p(0.07)}$ by an additional $CF_{goggles}$ that takes into account the attenuation of the goggles, as proposed in section 14.4:

- $CF_{goggles} = H_p(3)_{in}/H_p(3)_{out} = 0.5$ (if protective glasses type (c) are worn)
- $CF_{goggles} = H_p(3)_{in}/H_p(3)_{out} = 0.3$ (if protective glasses type (a) and (b) are worn)

RD is calculated in this case by the formula:

$$RD = \frac{H_p(3)_{out,y^{-1}}^{H_p(0.07)} CF_{goggles} - H_p(3)_{in,y^{-1}}}{H_p(3)_{in,y^{-1}}} \tag{14.2}$$

where $H_p(3)_{in,y^{-1}}$ is the measurement of an ELD located inside the protective lens of the glasses, multiplied by the number of procedures performed in one year.

Furthermore, in last analysis, measured $H_p(3)_{in,y^{-1}}$ are compared to $H_p(3)_{out,y^{-1}}$ multiplied by the corresponding $CF_{goggles}$ for the lead glasses attenuation. The RD is calculated as:

$$RD = \frac{H_p(3)_{out,y^{-1}} CF_{goggles} - H_p(3)_{in,y^{-1}}}{H_p(3)_{in,y^{-1}}} \tag{14.3}$$

In Figure 14.2 the RDs are represented.

The difference in which we incur by calculating $H_p(3)$ applying correction factors ranges from +1% (for Pr_2 and Pr_5) to +106% (for Pr_4). The arrows indicate in which cases the difference implies that the recommended limit of 20 mSv is exceeded by the estimation through $H_p(0.07)$ or $H_p(3)_{out}$ but not by $H_p(3)$ from direct measurements (yellow arrow - false positive), and when the 20 mSv are not surpassed by the indirect estimation but they are by $H_p(3)$ measurements (red arrows - false negative). For all data considered for the estimation of annual eye lens equivalent doses, we found:

- 2 false negative out of 6 for the physicians with goggles
- 3 false negative and 2 false positive out of 17 for the physicians who did not wear goggles.

In general, the estimate is better using Equation 14.3 than Equation 14.2, but the number of false negative is the same. 7 cases out of 23 provide erroneous information as regards exceeding of the recommended limit. In Farah study (Farah et al., 2014), the ELDO approach (Farah et al., 2013) was applied to assess cumulative doses on 14 cardiologists. High uncertainties were associated to the estimate of the eye lens equivalent dose and the authors suggested that an indirect approach to quantify $H_p(3)$ should be used only to indicate which individuals are more likely to reach annual doses close to the 20 mSv. In this case, a dedicated eye lens dosemeter is required.

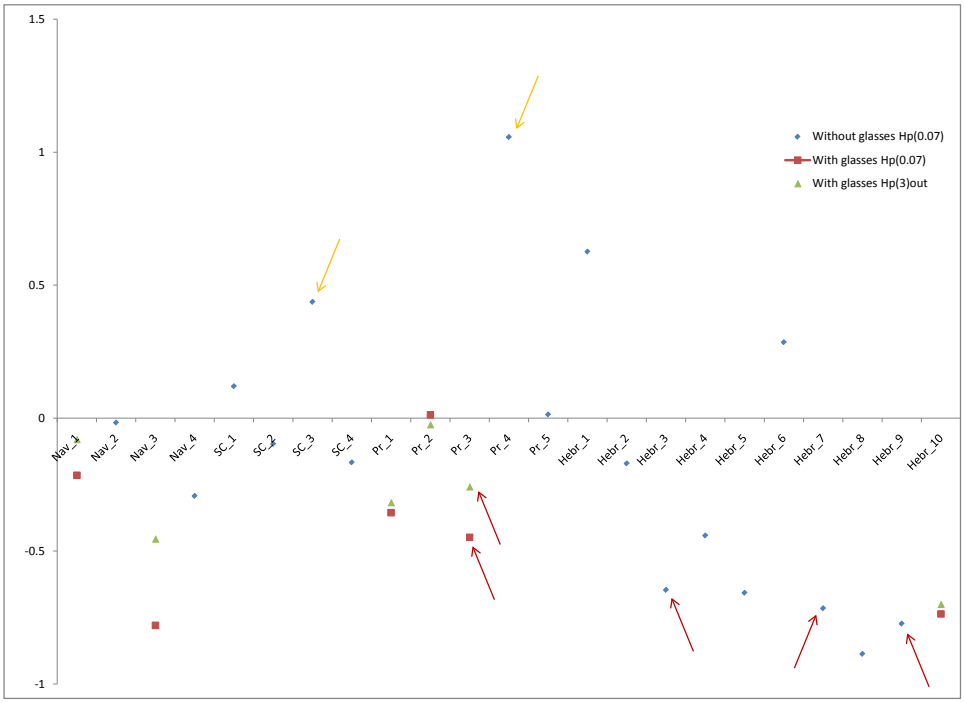

Figure 14.2: Relative differences RD between measured $H_p(3)$ and $H_p(3)$ assessed from corrected $H_p(0.07)$ and $H_p(3)_{out}$

14.7 Assessment of eye lens dose using the KAP indication in the X-ray console

A review of eye lens dose data reported in the literature shows great variability (Martin, 2009) between KAP and eye lens equivalent dose: a mean value of 0.79 was found, within the range 0.29 and 1.9, from 9 datasets of previous studies. This is in agreement with the rather large range obtained in this study. Mean and median $H_p(3)$/KAP of 1.24 and 1.11 μSv Gy^{-1}cm^{-2} are obtained respectively (sd = 73%). These ratios are in agreement with the mean $H_p(0.07)_{eye}$/KAP from the ORAMED campaign of 1.0 μSv Gy^{-1}cm^{-2} (Vanhavere et al., 2011) for CA/PTCA procedures, and with maximum value of 7.7. The highest eye dose per unit KAP was found for PM/ICD with an average ratio $H_p(0.07)_{eye}$/KAP of 2 μSv Gy^{-1}cm^{-2}. A comparison with previous published data is given in Table 14.6. In our analysis, for general assessment of eye lens equivalent dose using KAP, only physicians at the first position are considered at the Vall d'Hebron Hospital to avoid increasing the variability of the measurements (row 5, Table 14.5). The importance of separately considering first physicians from assisting physicians has been underlined by other works, as doses received by physicians at second position can vary from 30 to 100% of the dose received by the primary operator (Antic et al., 2013; Martin, 2016). In Antic et al.'s work mean $H_p(3)$/KAP of 0.94 μSv Gy^{-1}cm^{-2} was obtained by measurements on primary operators. This value is lower for operators at the second position or nurses: in this case mean $H_p(3)$/KAP is 0.33 μSv Gy^{-1}cm^{-2}. A weak but significant ($p < 0.01$) correlation is found between the eye dose and the KAP for both operators and nurses. A similar mean $H_p(3)$/KAP of 0.86 μSv Gy^{-1}cm^{-2}, within the range (0.46 - 1.25), was suggested by Bor et al. study (Bor et al., 2009), carried out on 9 cardiologists. A significantly lower $H_p(0.07)_{eye}$/KAP of 0.5 μSv Gy^{-1}cm^{-2} was obtained in Koukorava et al.'s study on two cardiologists (Koukorava et al., 2011). The eye lens was measured by passive dosemeters calibrated in terms of $H_p(0.07)$ and located on the side closest to the X-ray tube. The limited number of operators who participated in the follow-up reduces the relevance of the study. Nevertheless, this value is within the range of eye lens dose per unit DAP or KAP found in other works (Principi et al., 2015a; Bor et al., 2009). Mean value for the Vall d'Hebron Hospital of 1.89 μSv Gy^{-1}cm^{-2} highlights the fact that the use of protection is not optimised. In particular, for pediatric interventions, for the same amount of KAP, high $H_p(3)$ values are recorded, due to the proximity of the physician to the tube because of the small size of the patient and the preferred use of biplane system to the monoplane. Vano et al. (Vano et al., 2008) studied the relation between eye lens dose and patient dose for pediatric cardiologists. The eye lens dose was assessed by means of active dosemeters located at the cardiologist's eye position and three different

examination protocols were performed with newborn, infant and child phantoms. A mean value of 7 μSv Gy^{-1}cm^{-2} was obtained and a strong correlation between the two quantities was observed (R^2=0.99). The same measurement protocol was implemented in Leyton et al.'s study (Leyton et al., 2014), but for adult patients only. Eye lens dose was then obtained again by solid state dosemeters calibrated in terms of $H_p(10)$. $H_p(10)_{eye}$/KAP is considerably lower than for pediatric patients, in fact a mean value of 1.35 is obtained (R^2=0.99). Mean $H_p(0.07)_{eye}$/KAP of 0.5 μSv Gy^{-1}cm^{-2} and 0.86 μSv Gy^{-1}cm^{-2} have been suggested by Koukorava's and Bor's studies (Koukorava et al., 2011; Bor et al., 2009).

Author		Eye lens equivalent dose/KAP μSv Gy^{-1}cm^{-2}
Bor et al. (2009)	Clinical	0.86 (0.46 - 1.25)
Koukorava et al. (2011)	Clinical	0.5
Antic et al. (2013)	Clinical	1.3±0.94 (CA, 1^{st}) 0.36±0.18(CA, 2^{nd}/nurse) 0.94±0.61(All, 1^{st}) 0.33±0.26(All, 2^{nd})
This work - Vall d'Hebron 1^{st}-2^{nd}week	Clinical	3.41±0.56 (1^{st}, no shield) 1.69±0.82 (1^{st}, shield) 0.55±0.36 (2^{nd},no shield) 0.49±0.06 (2^{nd}, shield) 0.18 (nurse)
This work - All (derived from slope in Figure 12.9	Clinical	1.67 (Vall d'Hebron-1^{st} op.) 1.04 (Navarra) 0.62 (Princesa) 0.55 (San Carlos) 0.78 (All)
Vano et al. (2008)	phantom, pediatric	7
Leyton et al. (2014)	Phantom	1.35

Table 14.6: Eye lens dose per unit KAP measured by different measurement campaigns on clinical operator or phantom (as specified)

A correction factor of about 1 μSv Gy^{-1}cm^{-2} for first operator can be derived from the data of this study and the literature review, if some measurements on very few operators (Koukorava et al. (2011)) and pediatric measurements (Vano et al. (2008))are disregarded, as they are very specific cases and entail higher eye lens dose per unit KAP, as also demonstrated by this work. However, the influence of protective equipment and the position of the operator depending on the catheter access position cannot be taken into consideration by a conversion factor based on KAP values. $H_p(3)$/KAP from the present study show the fact that the relation between these two quantities depends on the use of shielding and the position of the operator. Overall, as the use of protective tools introduces large variability, the possibility of deriving eye lens dose from KAP can not be considered to be a trustworthy solution to eye lens dose monitoring in the author's opinion.

When all physicians are studied together, disregarding the hospital where they worked, mean and median $H_p(3)_{out}$/KAP values of 0.97 and 0.84 μSv Gy^{-1}cm^{-2} were obtained, respectively, within the range 0.09 – 3.94 μSv Gy^{-1}cm^{-2} (sd = 75%). When only data from physicians at the first position at the Vall d'Hebron Hospital are included (as in the case of the study of the correlation, then daily data instead of weekly data are used), mean and median $H_p(3)_{out}$/KAP of 1.24 and 1.11 μSv Gy^{-1}cm^{-2} are obtained, respectively (sd = 73%). As regards the $H_p(3)_{out}$/KAP ratio for nurses the spread of data increases (sd = 27%) and values range from 0.04 to 1.01 μSv Gy^{-1}cm^{-2}, with mean and median values of 0.46 and 0.19.

Part VI

Conclusions

Conclusions

This thesis is aimed at investigating possible solutions to introduce eye lens dose monitoring in a real clinical scenario and to improve radiation protection for medical staff in IC/IR. The study was mainly devoted to broadening the knowledge of the main issues related to eye lens dosimetry in IC/IR, i.e. calibration, measurements, MC simulation, taking into account the multi-parametric dependence of eye lens dose on several factors and its intrinsic variability. The main conclusions of this thesis are the following.

1. ***This thesis has set up an easy-to-use eye lens dosemeter (UPC-ELD) and provides the basis for its accurate calibration in terms of Hp(3) for photon radiation.***

   Calibration should be preferably performed on the 20 cm x 20 cm cylindrical phantom developed during the ORAMED European project using $H_{\mathrm{p}}(3)$ operational quantity. The UPC-ELD is shown to fulfill the IEC 62387-1 requirements for energy and angular dependence for photon radiation with a response between 0.71 and 1.67. Overall good performance is proven through its results in the EURADOS 2014 eye lens intercomparison study.
   Conversion coefficients from air kerma to equivalent dose at 3 mm depth $h_{\mathrm{p}K}(3)$ for radiation qualities RQR 2−9 and for angles of incidence from 0 to 180° are provided for the cylindrical phantom, with an uncertainty of 2% (one standard deviation). This is the same uncertainty stated in ISO 4037-3 for ISO 4037-1 qualities conversion coefficients. The set of coefficients were published in *Radiation Protection Dosimetry* journal and used in the two intercomparisons organized up to now by EURADOS for eye lens dosemeters. The study also highlights the fact that, although MC calculations are considered to be the gold standard method for this type of calculations, the interpolation method, when it is carefully chosen, provides satisfactory results.

2. ***This thesis highlights the risk of exceeding the new recommended eye lens dose limit of 20 mSv per year.***

   Measurement campaigns performed at several Spanish hospitals showed that the actual annual limit of 150 mSv for the eye lens equivalent dose was not exceeded by any of the monitored workers. However, approximately 40% of the physicians exceed the new limit of 20 mSv. The annual eye lens doses depend largely on workload and on the appropriate use of protection, but the results of this study highlight the fact that there is a need to both introduce monitoring of the eye lens in this field and also to make better use of existing protections. At one of the monitored hospitals, eye lens dose fom nurses was clearly below the new limit, whereas at another hospital, the limit could be surpassed. This observation reinforces the need to study exposure levels of all staff required to work in close proximity to X-ray sources during interventional procedures.

3. ***This thesis provides guidance and recommendations for eye lens dose monitoring.***

   The measurement campaigns at several hospitals confirm that a dosemeter measuring $H_{\mathrm{p}}(3)$ placed close to the eye is the best method for an accurate assessment of eye lens dose and it should be implemented whenever there is large workload. The correlation between the dose measured close to the eye and the dose in other parts of the body or the patient dose (KAP), demonstrates the fact that large uncertainties are associated with an eye lens dose assessment based on indirect measurements. Results of the EURADOS 2014 intercomparison showed that nowadays dosimetry services can provide users with appropriate dosemeters.
   In spite of their limitations, it is shown that eye lens indirect monitoring methodologies can be very useful in identifying the group of people who require a more specific monitoring programme. In particular, at one of the monitored hospitals, nurses would not need specific eye lens monitoring. In general, the relationship between $H_{\mathrm{p}}(3)$ and $H_{\mathrm{p}}(10)$ or $H_{\mathrm{p}}(0.07)$ measured on the chest or collar with an unprotected whole body dosemeter is more reproducible than the relationship between

$H_p(3)$ and KAP, in particular in the case of nurses. Thus, if a specific eye lens dosemeter is not used, at least an unprotected WBD should be required when participating in fluoroscopy guided procedures. The proposed correction factor derived from this study is $H_p(3)_{out}/H_p(0.07)_{thorax} = 0.8$. These recommendations are in line with the latest *IRPA guidance on implementation of eye dose monitoring and eye protection of workers* published at the beginning of 2017 (IRPA, 2017).

Eye lens monitoring when using lead glasses is a specific issue since the dosemeter should be placed underneath the protection. However, this is often very cumbersome. This thesis proposes a correction factor of 0.3 for wraparound glasses or a more conservative value of 0.5 when the design of the glasses is unknown, in order to assess the eye lens dose when using eye protection and the dosemeter is situated outside the glasses. The proposed correction factor has been based on experimental measurements and MC calculations and it is in agreement with previous works (Magee et al., 2014; Thornton et al., 2010; Rooijen et al., 2014; Moore et al., 1980) and recommendations from ISO (2015).

4. ***This thesis provides practical recommendations to reduce eye lens dose for workers exposed to X-rays in interventional cardiology and radiology.***

   Measurements on a phantom in a clinical scenario and MC calculations demonstrate that protection such as the ceiling shield and lead glasses drastically reduce eye exposure. However, as shown in the hospital campaigns, in practice the efficiency of protection is much lower. Thus, better training in the use of protection and the selection of an appropriate design for glasses are recommended to reduce the eye lens dose. To improve the use of ceiling shield and the workers' awareness of exposure, the use of electronic, direct reading dosemeters, such as the Doseaware, which were tested and satisfactorily compared with passive dosemeters in this thesis, is recommended.
   A detailed MC analysis has highlighted the influence of different parameters studied independently, such as the operator position, height and orientation with respect to the source, on eye lens exposure during an interventional procedure. To reduce eye lens exposure, placing the monitors away from the primary X-ray field is recommended. A rotation of the head of 30° or 45° away from the tube can reduce eye lens dose by approximately 50%, in particular at distances of $20cm$ and $40cm$ from the X-ray source.

The conclusion of this thesis could be used to prepare a training course for improving radiation protection of staff involved in IC/IR procedures.

Part VII

Appendices

Appendix A

Publications in peer-review journals

- S. Principi, C. Guardiola, M. A. Duch, M. Ginjaume. Air kerma to $H_{\mathrm{p}}(3)$ conversion coefficients for IEC 61267 RQR X-ray radiation qualities: Application to dose monitoring of the lens of the eye in medical diagnostics. *Radiation Protection Dosimetry*, 170(1-4):45-48, 2015.
- S. Principi, C. Delgado, M. Ginjaume, M. Beltran, J. J. Rovira, M. A. Duch. Eye Lens Dose in Interventional Cardiology. *Radiation Protection Dosimetry*, 165(1-4):289-293, 2015.
- S. Principi, M. Ginjaume, M. A. Duch, R. M. Sánchez, J. M. Fernández, E. Vanó. Influence of dosemeter position for the assessment of eye lens dose during interventional cardiology. *Radiation Protection Dosimetry*, 164(1-2):79-83, 2015.
- S. Principi, J. Farah, P. Ferrari, E. Carinou, I. Clairand, M. Ginjaume. The influence of operator position, height and body orientation on eye lens dose in interventional radiology and cardiology: Monte Carlo simulations versus realistic clinical measurements. *Physica Medica*, 32(9):1111–1117, 2016.

Appendix B

Uncertainty calculation for the personal dose equivalent assessment

The uncertainty associated to the determination of $H_{\mathrm{p}}(d)$ is calculated by applying the Guide to the expression of Uncertainty in Measurement, GUM, (ISO/IEC, 2008) to Equation 6.1:

$$H_{\mathrm{p}}(d) = (L_i f_i - < B >) N_{cal} \frac{\varepsilon_{cal}}{\varepsilon_t} \tag{B.1}$$

As decribed in chapter 10, the calibration factor N_{cal} is derived from calibration factors obtained for reference qualities. In practice, in general the energy field is not known, thus, a sigle N_{cal} value is used for each equivalent dose quantity. A mean value is used for $H_{\mathrm{p}}(0.07)$ and $H_{\mathrm{p}}(3)$, whereas for $H_{\mathrm{p}}(10)$ the calibration factor is assigned as a function of the ratio between the readings $M(10)$ and $M(0.07)$ as shown in Figure 10.1.

To facilitate the application of the GUM, Equation B.1 can be written as:

$$H_{\mathrm{p}}(d) = M_Q N_{cal}(H_{\mathrm{p}}(d)) f(Q,\alpha) f\left(\frac{\varepsilon_{cal}}{\varepsilon_t}\right) \tag{B.2}$$

Where:

- $M_Q = L_i f_i - < B >$ is the reading corrected for individual sensitivity and background. For UPC-WBD and UPC-ELD, as there are two detectors for each quantity to be measured, a mean value of the two is used [1].
- $N_{cal}(H_{\mathrm{p}}(d))$ is the calibration factor defined in chapter 10.
- $f(Q,\alpha)$ is a function which takes into account the influence of the energy (Q) and the angular response (α). It is set equal to 1 with an uncertainty associated to the variability of N_{cal} as a function of Q and α.
- $f\left(\frac{\varepsilon_{cal}}{\varepsilon_t}\right)$ is a function which takes into account the stability of the efficiency of the dosemeters between the date of calibration and the date of measurement. As mentioned in subsection 6.2.1, during our study this function is set to one with a maximum variation of $\pm 1\%$, thus with an associated relative standard uncertainty of $1/\sqrt{3}\%$ [2].

[1] In most cases, the best available estimate of a quantity that varies randomly and for which n independent observations have been obtained under the same conditions of measurement is the arithmetic mean or average of the n observations. The individual observations differ in value because of random variations in the influence quantities, or random effects. The variability of the observed values, or more specifically, their dispersion about their mean is characterized by the experimental standard deviation (s) of the observations. The number of observations n should be large enough to ensure that the mean provides a reliable estimate of the expected value of the quantity. In our case, very often measurement is performed using the reading of one or two dosemeters. In order to better estimate the associated uncertainty of the reading, the GUM recommends using the information about the variability of the quantity obtained from a well-characterized measurement under statistical control. This is, for example, in our case the set of readings obtained when the badge is irradiated in known conditions, once corrected for individual sensibility. This procedure is called to use a 'pooled experimental standard deviation', s_p. In our case s_p is derived from the experimental standard deviation of the 300 detectors when irradiated with ^{137}Cs at 3 mGy and is equal to 3.3% (k=1). If m detectors are used in one measurement the pooled uncertainty is equal to $s_p/\sqrt{m}$. In our case we compare the pooled uncertainty and the experimental standard deviation of the mean of the m measurements: $s/\sqrt{m}$. The largest value is considered as the uncertainty associated to this quantity. This approach is used for any set of TL readings, independently if they are used for calibration, background or dose measurement.

[2] According to GUM, for variables where it may be possible to estimate only bounds (upper and lower limits), it can be

B.1 Uncertainty of the calibration factor $N_{cal}(Q,H_{\mathrm{p}}(d))$

The uncertainty of the calibration factor for each reference quality $N_{cal}(Q, H_{\mathrm{p}}(d))$ (Equation 10.1) is obtained, according to GUM, as:

$$\frac{u(N_{cal}(Q, H_{\mathrm{p}}(d)))}{N_{cal}(Q, H_{\mathrm{p}}(d))} = \sqrt{\left[\frac{u(H_{\mathrm{p}}(d)_{ref})}{H_{\mathrm{p}}(d)_{ref}}\right]^2 + \left[\frac{u(M_Q)}{M_Q}\right]^2} \tag{B.3}$$

The uncertainty of the reference quantity $H_{\mathrm{p}}(d)_{ref}$ is provided by the calibration laboratory and it is equal to 2.5% (k=1).

The uncertainty of M_Q is equal to:

$$u(M_Q) = \sqrt{s^2_{L_i f_i} + s^2_{<B>}} \tag{B.4}$$

$s_{L_i f_i}$ is the standard deviation derived from the distribution of the set of 300 detectors readings corrected by the individual factor. If M_Q is calculated using n detectors, $s_{L_i f_i}/\sqrt{n}$ is the assigned uncertainty. The numerical value of $s_{L_i f_i}$ is 3.3 nC for a single detector. $s_{<B>}$ is the standard deviation associated to the background correction. It is calculated as the standard deviation of the mean of the corrected readings (corrected for individual sensitivity) of the background detectors. Equation B.3 is used to obtain the uncertainties presented in Table 10.1 and a numerical example is shown in Table B.2.

B.2 Uncertainty of $f(Q,\alpha)$

The uncertainty associated to the lack of knowledge of the radiation field $f(Q, \alpha)$ varies depending on $H_{\mathrm{p}}(d)$ and the hypothesis used to derive the value of N_{cal}.

B.2.1 Contribution of the radiation quality Q to the uncertainty u($f(Q,\alpha)$)

For $H_{\mathrm{p}}(3)$, a mean value of the calibration factors in the range of energies of interest is used. The associated standard uncertainty is estimated considering that the maximum deviation within $N_{cal,max}$ and $N_{cal,min}$ is $(N_{cal,max} - N_{cal,min})$ and that a constant probability distribution between these upper and lower bounds can be hypothesized for $N_{cal}(H_{\mathrm{p}}(3))$. Thus, a rectangular distribution can be assumed and $u(f(Q, \alpha)) = \dfrac{N_{cal,max} - N_{cal,min}}{2\sqrt{3}}$ for $H_{\mathrm{p}}(3)$ and for k=1. Numerically, this value is equal to 2.6% (k=1).

Likewise, **for $H_{\mathrm{p}}(0.07)$** the $u(f(Q, \alpha))$ is obtained assuming a rectangular distribution for $N_{cal}(H_{\mathrm{p}}(0.07))$ and it is numerically equal to 2.3%.

For $H_{\mathrm{p}}(10)$, $N_{cal}(H_{\mathrm{p}}(10))$ is derived applying the equation $N_{cal}(H_{\mathrm{p}}(10)) = 20.36 - 14.56 \cdot M(10)/M(0.07)$ obtained by a linear least squares fitting of the experimental values. The uncertainty associated to this fitting is 0.8% for k=1.

B.2.2 Contribution of the incident direction α to the uncertainty u($f(Q,\alpha)$)

The uncertainty related to the angular response is associated to the error performed when $N_{cal}(0°)$ is chosen instead of $N_{cal}(\alpha)$. The angular response for the UPC-ELD and the EYE-D is shown in Table 10.2. The deviation observed for angular deflections of 45° and 75° are combined and considered equal to the uncertainty associated to this parameter. Numerically, it is equal to 3.3% (k=1). For $H_{\mathrm{p}}(10)$ and $H_{\mathrm{p}}(0.07)$, the angular response has not been studied in the framework of this thesis. According to the personal dosimetry service of INTE-UPC it is equal to 3.3%.

The uncertainty associated to both the energy and the angular response $u(f(Q, \alpha))/f(Q, \alpha)$ is obtained combining quadratically the uncertainty of each parameter.

assumed that 'the probability that the variable lies within the interval *a(min)* to *a(max)* for all practical purposes is equal to one and the probability that the variable lies outside this interval is essentially zero'. One can only assume that it is equally probable for the variable to lie anywhere within it (a uniform or rectangular distribution is assumed). Then, the expected value of the variable is the midpoint of the interval with an associated uncertainty equal to $u = [a(max) - a(min)]/2\sqrt{3}$. Such hypothesis is considered for the stability of the batch, and also when a single calibration factor is used for any field.

B.3 Uncertainty of the calibration factor N_{cal}

The uncertainty of the calibration factor N_{cal} for each reference quality in an unknown field can be estimated as the combined uncertainty of $N_{cal}(Q, H_p(d))$ (section B.1) and the uncertainty of $f(Q, \alpha)$ (section B.2).

Equation B.5 has been used to obtain the uncertainties presented in subsection 10.1.1 for $N_{cal}(H_p(d))$ and a numerical example is shown in Table B.4.

$$\frac{u(N_{cal}(H_p(d)))}{N_{cal}(H_p(d))} = \sqrt{\left[\frac{u(N_{cal}(Q, H_p(d)))}{N_{cal}(Q, H_p(d))}\right]^2 + \left[\frac{u(f(Q,\alpha))}{f(Q,\alpha)}\right]^2} \tag{B.5}$$

B.4 Practical example of the assessment of the uncertainty associated to $H_p(d)$

A numerical example is provided to illustrate the uncertainty calibration budget. The data can change slightly for each measurement. Relative uncertainty $u(N_{cal}(Q, H_p(d)))/N_{cal}(Q, H_p(d))$ in Table B.2 has been calculated considering the experimental data shown in Table B.1. $u(f(Q,\alpha))/f(Q,\alpha)$ obtained as the combined uncertainty of the energy and angular response is shown in Table B.3. The uncertainty associated to N_{cal} is calculated in Table B.4. The assessment of the combined uncertainty associated to $H_p(d)$ is given in Table B.5. All uncertainty values are given for k=1.

The relative expanded uncertainty $U(H_p(d))/H_p(d)$ is obtained multiplying $u(H_p(d))/H_p(d)$ by a coverage factor k=2 (Table B.6).

Table B.1: Example of experimental data and associated uncertainties

Variable	Mean reading nC	N (detectors)	Standard deviation of the mean (nC)	$u(M_Q)$ (nC)	$u(M_Q)/M_Q$ (%)
Readings corresponding to an individual monitoring campaign	100	2	2.33	2.33	**2.48%**
Background Readings for an individual monitoring campaign	6	6	0.08		
Readings corresponding for energy calibration	200	6	1.69	1.69	**0.85%**
Background Readings for energy calibration	0.6	10	0.006		

Table B.2: $u(N_{cal}(Q, H_p(d)))/N_{cal}(Q, H_p(d))$

Variable	Relative uncertainty (%)
$u(H_p(d)_{ref})/H_p(d)_{ref}$	2.50%
$u(M_Q)/M_Q$ (for energy calibration)	0.85%
Combined uncertainty: $u(N_{cal}(Q,H_p(d)))/N_{cal}(Q,H_p(d))$	**2.64%**

Table B.3: u$(f(Q,\alpha))/f(Q,\alpha)$

Variable	$H_{\mathrm{p}}(3)$	$H_{\mathrm{p}}(0.07)$	$H_{\mathrm{p}}(10)$
Energy response	2.60%	2.30%	0.80%
Angular response	3.30%	3.30%	3.30%
Combined uncertainty: u$(f(Q,\alpha))/f(Q,\alpha)$	**4.20%**	**4.01%**	**3.40%**

Table B.4: u$(N_{cal}(H_{\mathrm{p}}(d)))/N_{cal}(H_{\mathrm{p}}(d))$

Variable	$H_{\mathrm{p}}(3)_{UPC-ELD}$	$H_{\mathrm{p}}(0.07)$	$H_{\mathrm{p}}(10)$
$u(N_{cal}(Q,H_{\mathrm{p}}(d)))/N_{cal}(Q,H_{\mathrm{p}}(d))$	2.64%	2.64%	2.64%
$u(f(Q,\alpha))/f(Q,\alpha)$	4.20%	4.01%	3.40%
Combined uncertainty: u$(N_{cal}(H_{\mathrm{p}}(d)))/N_{cal}(H_{\mathrm{p}}(d))$(k=1)	**5.0%**	**4.8%**	**4.3%**

Table B.5: Assessment of the combined uncertainty associated to $H_{\mathrm{p}}(d)$ (k=1)

Variable	$H_{\mathrm{p}}(3)$	$H_{\mathrm{p}}(0.07)$	$H_{\mathrm{p}}(10)$
$u(M_Q)/M_Q$	2.48%	2.48%	2.48%
$u(N_{cal}(Q,H_{\mathrm{p}}(d)))/N_{cal}(Q,H_{\mathrm{p}}(d))$	2.64%	2.64%	2.64%
$u(f(Q,\alpha))/f(Q,\alpha)$	4.20%	4.01%	3.40%
$u(f\left(\frac{\varepsilon_{cal}}{\varepsilon_t}\right))/f\left(\frac{\varepsilon_{cal}}{\varepsilon_t}\right)$	0.58%	0.58%	0.58%
Combined uncertainty: u$(H_{\mathrm{p}}(d))/H_{\mathrm{p}}(d)$ k=1	**5.6%**	**5.4%**	**5.0%**

Table B.6: Expanded uncertainty associated to $H_{\mathrm{p}}(d)$ (k=2)

Variable	$H_{\mathrm{p}}(3)$	$H_{\mathrm{p}}(0.07)$	$H_{\mathrm{p}}(10)$
Expanded uncertainty: U$(H_{\mathrm{p}}(d))/H_{\mathrm{p}}(d)$ k=2	**11%**	**11%**	**10%**

Bibliography

V. Antic, O. Ciraj-Bjelac, M. Rehani, S. Aleksandric, D. Arandjic, and M. Ostojic. Eye lens dosimetry in interventional cardiology: Results of staff dose measurements and link to patient dose levels. *Radiation Protection Dosimetry*, 154(3):276–284, 2013. ISSN 01448420. doi: 10.1093/rpd/ncs236.

R. Behrens. Air kerma to dose equivalent conversion coefficients not included in ISO 4037-3. *Radiation Protection Dosimetry*, 147(3):373–379, 2011. ISSN 01448420. doi: 10.1093/rpd/ncq459.

R. Behrens. Air kerma to $H_{\mathrm{p}}(3)$ conversion coefficients for a new cylinder phantom for photon reference radiation qualities. *Radiation Protection Dosimetry*, 151(3):450–455, 2012a. ISSN 01448420. doi: 10.1093/rpd/ncs032.

R. Behrens. On the operational quantity $H_{\mathrm{p}}(3)$ for eye lens dosimetry. *Journal of Radiological Protection*, 32(4):455–464, 2012b.

R. Behrens and G. Dietze. Monitoring the eye lens: which dose quantity is adequate? *Physics in Medicine & Biology*, 55(14):4047–4062, 2010. URL http://stacks.iop.org/0031-9155/55/i=14/a=007.

R. Behrens and O. Hupe. Influence of the phantom shape (slab, cylinder or Alderson) on the performance of an Hp(3) eye dosemeter. *Radiation Protection Dosimetry*, pages 1–9, 2015. doi: doi:10.1093/rpd/ncv366.

R. Behrens, J. Engelhardt, M. Figel, O. Hupe, M. Jordan, and R. Seifert. $H_{\mathrm{p}}(0.07)$ photon dosemeters for eye lens dosimetry: Calibration on a rod vs. a slab phantom. *Radiation Protection Dosimetry*, 148 (2):139–142, 2012. ISSN 01448420. doi: 10.1093/rpd/ncr028.

P. Bilski, J. M. Bordy, J. Daures, M. Denoziere, E. Fantuzzi, P. Ferrari, G. Gualdrini, M. Kopeć, F. Mariotti, F. Monteventi, and S. Wach. The new EYE-D dosemeter for measurements of $H_{\mathrm{p}}(3)$ for medical staff. *Radiation Measurements*, 46(11):1239–1242, 2011. ISSN 13504487. doi: 10.1016/j.radmeas.2011.04.031.

D. Bor, T. Olgar, E. Onal, A. Caglan, and T. Toklu. Assessment of radiation doses to cardiologists during interventional examinations. *Medical Physics*, 36(8):3730–3736, 2009. ISSN 0094-2405. doi: 10.1118/1.3168971. URL http://www.ncbi.nlm.nih.gov/pubmed/19746806.

J. Bordy, J. Daures, M. Denoziere, J. Gouriou, C. Itie, L. Donadile, L. Struelens, and F. Schultz. Design of a realistic radiation field for the calibration of dosimeters used in interventional radiology cardiology (Medical personnel dosimetry). ISBN 978-3-9805741-9-8. *Proceedings of the international workshop on uncertainty assessment in computational dosimetry. A comparison of approaches. ENEA - Rome*, 2007.

S. Bouffler, E. Ainsbury, P. Gilvin, and J. Harrison. Radiation-induced cataracts: the Health Protection Agency's response to the ICRP statement on tissue reactions and recommendation on the dose limit for the eye lens. *Journal of Radiological Protection*, 32(4):479–488, 2012. ISSN 0952-4746. doi: 10.1088/0952-4746/32/4/479. URL http://stacks.iop.org/0952-4746/32/i=4/a=479?key=crossref.fa649f83863c1bb412cefd511ab39339.

N. Buls, J. Pages, F. Mana, and M. Osteaux. Patient and staff exposure during endoscopic retrograde cholangiopancreatography. *British Journal of Radiology*, 75(893):435–443, 2002. ISSN 00071285. doi: 10.1259/bjr.75.893.750435.

C. Cagua and M. Ginjaume. Proyecto Final de Estudios Máster en Ingeniería Biomédica: Caracterización de un dosímetro de cristalino desarrollado en la UPC de acuerdo con la Norma Internacional IEC 62387:2012. *Univ. Barcelona, 26 junio 2016*, 2016. URL https://www.dropbox.com/sh/0bls0y92u61decr/AACSb9ZfWi9MDpn4Dft6C0wga?dl=0.

E. Carinou, M. Brodecki, J. Domienik, L. Donadille, C. Koukorava, S. Krim, D. Nikodemová, N. Ruiz-Lopez, M. Sans-Merce, L. Struelens, and F. Vanhavere. Recommendations to reduce extremity and eye lens doses in interventional radiology and cardiology. *Radiation Measurements*, 46(11): 1324–1329, 2011. ISSN 13504487. doi: 10.1016/j.radmeas.2011.05.027. URL http://dx.doi.org/10.1016/j.radmeas.2011.05.027.

E. Carinou, M. Ginjaume, U. OConnor, R. Kopec, and M. S. Merce. Status of eye lens radiation dose monitoring in European hospitals. *Journal of Radiological Protection*, 34(4):729–739, 2014. URL http://stacks.iop.org/0952-4746/34/i=4/a=729.

E. Carinou, P. Ferrari, O. C. Bjelac, M. Ginjaume, M. S. Merce, and U. O'Connor. Eye lens monitoring for interventional radiology personnel: dosemeters, calibration and practical aspects of $H_{\mathrm{p}}(3)$ monitoring. A 2015 review. *Journal of Radiological Protection*, 35(3):17–34, 2015. ISSN 0952-4746. doi: 10.1088/0952-4746/35/3/R17. URL http://stacks.iop.org/0952-4746/35/i=3/a=R17?key=crossref.d18df021009a51a352e48855c999e1b3.

Z. Cemusová, D. Ekendahl, and L. Judas. Assessment of eye lens doses in interventional radiology: A simulation in laboratory conditions. *Radiation Protection Dosimetry*, 170(1-4):256–260, 2016. ISSN 17423406. doi: 10.1093/rpd/ncv376.

S. Chiriotti, M. Ginjaume, E. Vano, R. Sanchez, J. M. Fernandez, M. A. Duch, and J. Sempau. Performance of several active personal dosemeters in interventional radiology and cardiology. *Radiation Measurements*, 46(1–4):1266–1270, 2011.

G. Chodick, N. Bekiroglu, M. Hauptmann, B. H. Alexander, D. M. Freedman, M. M. Doody, L. C. Cheung, S. L. Simon, R. M. Weinstock, A. Bouville, and A. J. Sigurdson. Risk of Cataract after Exposure to Low Doses of Ionizing Radiation: A 20-Year Prospective Cohort Study among US Radiologic Technologists. *American Journal of Epidemiology*, 168(6):620–631, 2008. doi: 10.1093/aje/kwn171. URL +http://dx.doi.org/10.1093/aje/kwn171.

L. T. J. Chylack, L. E. Peterson, A. H. Feiveson, M. L. Wear, F. Keith Manuel, W. H. Tung, D. S. Hardy, L. J. Marak, and F. A. Cucinotta. NASA Study of Cataract in Astronauts (NASCA). Report 1: Cross-Sectional Study of the Relationship of Exposure to Space Radiation and Risk of Lens Opacity. *Radiation Research*, 172(1):10–20, 2009. doi: http://dx.doi.org/10.1667/RR1580.1.

O. Ciraj-Bjelac, M. Rehani, A. Minamoto, K. Sim, H. Liew, and E. Vano. Radiation-Induced Eye Lens Changes and Risk for Cataract in Interventional Cardiology. *Cardiology*, 123(1006):168–171, 2012.

I. Clairand, M. Ginjaume, F. Vanhavere, E. Carinou, J. Daures, M. Denoziere, E. H. Silva, M. Roig, S. Principi, and L. Van Rycheghem. First eurados intercomparison exercise of eye lens dosemeters for medical applications. *Radiation Protection Dosimetry*, 170(1–4):21–26, 2016. doi: 10.1093/rpd/ncv368. URL +http://dx.doi.org/10.1093/rpd/ncv368.

P. Clerinx, N. Buls, H. Bosmans, and J. De Mey. Double-dosimetry algorithm for workers in interventional radiology. *Radiation Protection Dosimetry*, 129(1-3):321–327, 2008. ISSN 01448420. doi: 10.1093/rpd/ncn148.

J. Daures, J. Gouriou, and J. M. Bordy. Monte Carlo determination of the conversion coefficients $H_{\mathrm{p}}(3)/K_{\mathrm{a}}$ in a right cylinder phantom with 'PENELOPE' code. Comparison with 'MCNP' simulations. *Radiation Protection Dosimetry*, 144(1-4):37–42, 2011. ISSN 01448420. doi: 10.1093/rpd/ncq359.

J. Domienik, M. Brodecki, and D. Rusicka. A study of the dose distribution in the region of the eye lens and extremities for staff working in interventional cardiology. *Radiation Measurements*, 47(2):130–138, 2012. ISSN 13504487. doi: 10.1016/j.radmeas.2011.12.004. URL http://dx.doi.org/10.1016/j.radmeas.2011.12.004.

L. Donadille, E. Carinou, M. Brodecki, J. Domienik, J. Jankowski, C. Koukorava, S. Krim, D. Nikodemova, N. Ruiz-Lopez, M. Sans-Merce, L. Struelens, F. Vanhavere, and R. Zaknoune. Staff eye lens and extremity exposure in interventional cardiology: Results of the ORAMED project. *Radiation Measurements*, 46(11):1203–1209, 2011. ISSN 13504487. doi: 10.1016/j.radmeas.2011.06.034. URL http://dx.doi.org/10.1016/j.radmeas.2011.06.034.

A. Duran, E. Vano, N. K. Kleinman, D. E. Echeverri, M. C. Cabrera, and M. R. Miller. Retrospective Evaluation of Lens Injuries and Dose: Relid Study. *Journal of the American College of Cardiology*, 57(14):E1951, 2011. ISSN 07351097. doi: 10.1016/S0735-1097(11)61951-7. URL https://www.researchgate.net/publication/251594748_RETROSPECTIVE_EVALUATION_OF_LENS_INJURIES_AND_DOSE_RELID_STUDY.

E. P. Efstathopoulos, D. G. Katritsis, S. Kottou, N. Kalivas, E. Tzanalaridou, E. Giazitzoglou, S. Korovesis, and K. Faulkner. Patient and staff radiation dosimetry during cardiac electrophysiology studies and catheter ablation procedures: A comprehensive analysis. *Europace*, 8(6):443–448, 2006. ISSN 10995129. doi: 10.1093/europace/eul041.

EURATOM. *Council Directive (Euratom 2013/59) laying down basic safety standards for protection against the dangers arising from exposure to ionising radiation.* European Commission 2013. Official Journal of the European Union, 2014.

J. Farah, L. Struelens, J. Dabin, C. Koukorava, L. Donadille, S. Jacob, M. Schnelzer, A. Auvinen, F. Vanhavere, and I. Clairand. A Correlation Study of Eye Lens Dose and Personal Dose Equivalent for Interventional Cardiologists. *Radiation Protection Dosimetry*, 157(4):561–569, 2013.

J. Farah, L. Struelens, A. Auvinen, S. Jacob, C. Koukorava, M. Schnelzer, F. Vanhavere, I. Clairand, L. D. Dosime, B. Nuclear, N. S. Authority, G. Atomic, E. Commission, and R. E. Unit. Application of the ELDO Approach To Assess Cumulative Eye Lens Doses for Interventional. *Radiation Protection Dosimetry*, 164(1–2):84–88, 2014.

M. Ginjaume, X. Ortega, M. Duch, N. Jornet, and A. Snchez-Reyes. Characteristics of LiF: Mg, Cu, P for clinical applications. *Radiation Protection Dosimetry*, 85(1-4):389–391, 1999.

B. Grosswendt. Conversion Coefficients for Calibrating Individual Photon Dosemeters in Terms of Dose Equivalents Defined in an ICRU Tissue Cube and PMMA Slabs. *Radiation Protection Dosimetry*, 32 (4):219–231, 1990. doi: 10.1093/oxfordjournals.rpd.a080737. URL +http://dx.doi.org/10.1093/oxfordjournals.rpd.a080737.

G. Gualdrini, F. Mariotti, S. Wach, P. Bilski, M. Denoziere, J. Daures, J. M. Bordy, P. Ferrari, F. Monteventi, E. Fantuzzi, and F. Vanhavere. A new cylindrical phantom for eye lens dosimetry development. *Radiation Measurements*, 46(11):1231–1234, 2011. ISSN 13504487. doi: 10.1016/j.radmeas.2011.08.025. URL http://dx.doi.org/10.1016/j.radmeas.2011.08.025.

G. Gualdrini, J. M. Bordy, J. Daures, E. Fantuzzi, P. Ferrari, F. Mariotti, and F. Vanhavere. Air kerma to Hp(3) conversion coefficients for photons from 10 keV to 10 MeV, calculated in a cylindrical phantom. *Radiation Protection Dosimetry*, 154(4):517–521, 2013.

J. H. Hubbell and S. M. Seltzer. Tables of X-Ray Mass Attenuation Coefficients and Mass Energy-Absorption Coefficients 1 keV to 20 MeV for Elements Z = 1 to 92 and 48 Additional Substances of Dosimetric Interest. *Report NISTIR 5632*, 1995. URL http://www.nist.gov/pml/data/xraycoef/index.cfm.

IAEA. IAEA Tec Doc-1731. Implications for Occupational Radiation Protection of the New Dose Limit for the Lens of the Eye. (1731):48, 2013. ISSN 10114289.

IBM. Ibm spss statistics for windows, version 22.0, 2013.

ICRP. *Nonstochastic effects of irradiation. ICRP Publication 41. Ann. ICRP*, volume 14. 1984.

ICRP. *1990 Recommendations of the International Commission on Radiological Protection. ICRP Publication 60. Ann. ICRP*, volume 21. 1991.

ICRP. *Conversion Coefficients for use in Radiological Protection against External Radiation. ICRP Publication 74. Ann. ICRP*, volume 26. 1996.

ICRP. *Radiopathology of skin and eye and radiation risk. ICRP Publication 85. Ann. ICRP*, volume 30. 2000.

ICRP. *Recommendations of the International Commission on Radiological Protection. ICRP Publication 103. Ann. ICRP*, volume 37. 2007.

ICRP. *Radiological Protection in Fluoroscopically Guided Procedures outside the Imaging Department. ICRP Publication 117, Ann. ICRP*, volume 40. 2010.

ICRP. *ICRP Statement on Tissue Reactions / Early and Late Effects of Radiation in Normal Tissues and Organs Threshold Doses for Tissue Reactions in a Radiation Protection Context. ICRP Publication 118. Ann. ICRP*, volume 41. 2012.

ICRP. *Radiological protection in cardiology. ICRP Publication 120. Ann. ICRP*, volume 42. 2013.

ICRU. *Determination of Dose Equivalents from External Radiation Sources (Report 43)*. Bethesda, MD: ICRU Publications, 1988.

ICRU. *Measurement of Dose Equivalents from External Photon and Electron Radiations (Report 47)*. Bethesda, MD: ICRU Publications, 1992.

ICRU. *Conversion Coefficients for Use in Radiological Protection Against External Radiation (Report 57)*. Bethesda, MD: ICRU Publications, 1998.

IEC. *Medical Diagnostic X-Ray EquipmentRadiation Conditions for Use in the Determination of Characteristics*. International Electro Technical Commission. IEC 61267 Ed. 2.0, 2005.

IEC. *Radiation Protection Instrumentation-Passive Integrating Dosimetry Systems for Personal and Environmental Monitoring of Photon and Beta Radiation*. International Electro Technical Commission. IEC 62387, 2012.

IEC. *Protective devices against diagnostic medical X-radiation*. International Electro Technical Commission. IEC 61331, 2014.

IRPA. IRPA guidance on implementation of eye dose monitoring and eye protection of workers. (January), 2017. URL http://www.irpa.net/members/54696/{%}7B25334E5F-2E99-4D65-B3B7-CACA648AEBAB{%}7D/IRPAguidanceonimplementationofeyedosemonitoringandeyeprotectionofworkers.pdf.

ISO. *X and Gamma Reference Radiation for Calibrating Dosemeters and Dose RateMeters and for Determining Their Response as a Function of Photon EnergyPart 1: Radiation Characteristics and Production Method*. International Organization for Standardization. ISO 4037-1, 1996.

ISO. *X and Gamma Reference Radiation for Calibrating Dosemeters and Dose RateMeters and for Determining Their Response as a Function of Photon EnergyPart 3: Calibration of Area and Personal Dosemeters and the Measurement of Their Response as a Function of Energy and Angle of Incidence*. International Organization for Standardization. ISO 4037-3, 1999.

ISO. *Criteria and performance limits for the periodic evaluation of processors of personal dosemeters for X and gamma radiation*. International Organization for Standardization. ISO 14146, 2000.

ISO. *Procedures for monitoring the dose to the lens of the eye, the skin and the extremities*. International Organization for Standardization. ISO 15382, 2015.

ISO/IEC. *Guide 98-3:2008 Uncertainty of measurement Part 3: Guide to the expression of uncertainty in measurement*. (GUM:1995), 2008.

A. Junk, Z. Haskal, and B. Worgul. Cataract in interventional radiology - an occupational hazard? *Investigative Ophthalmology & Visual Science*, 45(13):388–388, 2004.

N. J. Kleiman, J. David, C. D. Elliston, K. M. Hopkins, L. B. Smilenov, D. J. Brenner, B. V. Worgul, E. J. Hall, and H. B. Lieberman. Mrad9 and atm haploinsufficiency enhance spontaneous and x-ray-induced cataractogenesis in mice. *Radiation Research*, 168(5):567–573, 2007. ISSN 00337587, 19385404. URL http://www.jstor.org/stable/4540768.

Y. Kong, L. Struelens, F. Vanhavere, C. S. Vargas, W. Schoonjans, and W. H. Zhuo. Influence of standing positions and beam projections on effective dose and eye lens dose of anaesthetists in interventional procedures. *Radiation Protection Dosimetry*, 163(2):181–187, 2014. ISSN 17423406. doi: 10.1093/rpd/ncu148.

C. Koukorava, E. Carinou, G. Simantirakis, T. G. Vrachliotis, E. Archontakis, C. Tierris, and P. Dimitriou. Doses to operators during interventional radiology procedures: Focus on eye lens and extremity dosimetry. *Radiation Protection Dosimetry*, 144(1-4):482–486, 2011. ISSN 01448420. doi: 10.1093/rpd/ncq328.

C. Koukorava, L. Farah, J. Struelens, I. Clairand, L. Donadille, F. Vanhavere, and P. Dimitriou. Efficiency of radiation protection equipment in interventional radiology: a systematic Monte Carlo study of eye lens and whole body doses. *Journal of Radiological Protection*, 34(3):509–528, 2014. URL http://stacks.iop.org/0952-4746/34/i=3/a=509.

F. Leyton, M. S. Nogueira, J. Saad, J. A. dos Santos, E. Vano, M. A. Oliveira, and C. Ubeda. Scatter radiation dose at the height of the operator's eye in interventional cardiology. *Radiation Measurements*, 71:349–354, 2014. ISSN 13504487. doi: 10.1016/j.radmeas.2014.07.015. URL http://www.scopus.com/inward/record.url?eid=2-s2.0-84905875624{&}partnerID=tZOtx3y1.

O. O. Lie, G. U. Paulsen, and Whni. Assessment of effective dose and dose to the lens of the eye for the interventional cardiologist. *Radiation Protection Dosimetry*, 132(3):313–318, 2008.

J. S. Magee, C. J. Martin, V. Sandblom, M. J. Carter, A. Almén, Å. Cederblad, P. Jonasson, and C. Lundh. Derivation and application of dose reduction factors for protective eyewear worn in interventional radiology and cardiology. *Journal of Radiological Protection*, 34(4):811–823, 2014. ISSN 0952-4746. doi: 10.1088/0952-4746/34/4/811. URL http://stacks.iop.org/0952-4746/34/i=4/a=811?key=crossref.20e77c07b0cf33128b8979b66b1bddf6.

C. J. Martin. A review of radiology staff doses and dose monitoring requirements. *Radiation Protection Dosimetry*, 136(3):140–157, 2009. ISSN 01448420. doi: 10.1093/rpd/ncp168.

C. J. Martin. Personal dosimetry for interventional operators: When and how should monitoring be done? *British Journal of Radiology*, 84(1003):639–648, 2011. ISSN 00071285. doi: 10.1259/bjr/24828606.

C. J. Martin. Eye lens dosimetry for fluoroscopically guided clinical procedures: Practical approaches to protection and dose monitoring. *Radiation Protection Dosimetry*, 169(1):286–291, 2016. ISSN 17423406. doi: 10.1093/rpd/ncv431.

MathWorks. Matlab 6.1, 2000.

S. McVey, A. Sandison, and D. Sutton. An assessment of lead eyewear in interventional radiology. *Journal of Radiological Protection*, 33(3):647–59, 2013.

W. Moore, G. Ferguson, and C. Rohrmann. Physical factors determining the utility of radiation safety glasses. *Medical Physics*, 7(1):8–12, 1980. doi: 10.1118/1.594661.

K. Neriishi, E. Nakashima, A. Minamoto, S. Fujiwara, M. Akahoshi, H. K. Mishima, T. Kitaoka, and R. E. Shore. Postoperative cataract cases among atomic bomb survivors: Radiation dose response and threshold. *Radiation Research*, 168(4):404–408, 2007. doi: http://dx.doi.org/10.1667/RR0928.1.

R. Nowotny and A. Hofer. *XCOMP5, program for calculating diagnostic x-ray spectra*. 1985.

D. B. Pelowitz. *MCNPX Users Manual, Version 2.6.0.* . Los Alamos National Laboratory Report LA-CP-05-0369, 2005.

S. Principi, C. Delgado, M. Ginjaume, M. Beltran, J. J. Rovira, and M. A. Duch. Eye Lens Dose in Interventional Cardiology. *Radiation Protection Dosimetry*, 165(1–4):289–293, 2015a.

S. Principi, M. Ginjaume, M. Duch, R. Sánchez, J. Fernández, and E. Vano. Influence of dosemeter position for the assessment of eye lens dose during interventional cardiology. *Radiation Protection Dosimetry*, 164(1-2):79–83, 2015b. ISSN 17423406 01448420. doi: 10.1093/rpd/ncu359.

S. Principi, C. Guardiola, M. A. Duch, and M. Ginjaume. Air kerma to $H_{\mathrm{p}}(3)$ conversion coefficients for IEC 61267 RQR X-ray radiation qualities: application to dose monitoring of the lens of the eye in medical diagnostics. *Radiation Protection Dosimetry*, 170(1–4):45–48, 2015c. doi: 10.1093/rpd/ncv435. URL +http://dx.doi.org/10.1093/rpd/ncv435.

PTB. PTB calibration certificate dated 2012-06-20. Calibration mark PTB60188-12, 2012.

RD783. *Real Decreto 783/2001, de 6 de julio, por el que se aprueba el Reglamento sobre proteccin sanitaria contra radiaciones ionizantes*. BOE 178, 2001.

M. M. Rehani, E. Vano, O. Ciraj-Bjelac, and N. J. Kleiman. Radiation and cataract. *Radiation Protection Dosimetry*, 147(1-2):300–304, 2011. ISSN 01448420. doi: 10.1093/rpd/ncr299.

B. D. V. Rooijen, M. W. D. Haan, and M. Das. Efficacy of Radiation Safety Glasses in Interventional Radiology. *CardioVascular and Interventional Radiology*, 37:1149–1155, 2014. doi: 10.1007/s00270-013-0766-0.

F. Salvat, J. M. Fernandez-Varea, and J. Sempau. *PENELOPE 2006: A Code System for Monte Carlo Simulation of Electron and Photon Transport*. Workshop Proceedings Barcelona, Spain, 47 July 2006, OECD 2006 NEA No. 6222, 2006.

R. M. Sanchez, E. Vano, J. M. Fernandez, M. Ginjaume, and M. A. Duch. Measurements of eye lens doses in interventional cardiology using OSL and electronic dosemeters. *Radiation Protection Dosimetry*, 162 (4):569–576, 2014. doi: 10.1093/rpd/nct368. URL +http://dx.doi.org/10.1093/rpd/nct368.

J. Sempau, A. Badal, and L. Brualla. A PENELOPE-based system for the automated Monte Carlo simulation of clinacs and voxelized geometries–application to far-from-axis fields. *Med. Phys.*, 38:5887 – 5895, 2011. Available at http://dx.doi.org/10.1118/1.3643029.

K. H. Sim, M. Rehani, N. Kleiman, O. Ciraj-Bjelac, and E. Vano. Radiation Induced Lens Opacities in the Eyes of Cath Lab Staff. *Journal of the American College of Cardiology*, 55(10):A201.E1888, 2010. ISSN 07351097. doi: 10.1016/S0735-1097(10)61889-X. URL http://linkinghub.elsevier.com/retrieve/pii/S073510971061889X.

W. Snyder, M. Ford, and G. Warner. *Estimates of absorbed fraction for monoenergetic photon sources uniformly distributed in various organs of a heterogeneous phantom.* Model Report ORNL-4979. Oak Ridge National Laboratory, Oak Ridge TN, USA, 1978.

S. Strocchi, A. Chiaravalli, I. Veronese, and R. Novario. On-field evaluation of operator lens protective devices in interventional radiology. *Radiation Protection Dosimetry*, 171(3):382–388, 2016. ISSN 17423406. doi: 10.1093/rpd/ncv412.

L. Struelens, E. Carinou, I. Clairand, L. Donadille, M. Ginjaume, C. Koukorava, S. Krim, H. Mol, M. Sans-Merce, and F. Vanhavere. Use of active personal dosemeters in interventional radiology and cardiology: Tests in hospitals ORAMED project. *Radiation Measurements*, 46(11):1258–1261, 2011. ISSN 13504487. doi: 10.1016/j.radmeas.2011.08.002. URL http://linkinghub.elsevier.com/retrieve/pii/S1350448711003854.

A. Sulieman, K. Theodorou, M. Vlychou, T. Topaltzikis, C. Roundas, I. Fezoulidis, and C. Kappas. Radiation dose optimisation and risk estimation to patients and staff during hysterosalpingography. *Radiation Protection Dosimetry*, 128(2):217–226, 2008. doi: 10.1093/rpd/ncm324. URL +http://dx.doi.org/10.1093/rpd/ncm324.

R. H. Thornton, L. T. Dauer, J. P. Altamirano, K. J. Alvarado, J. S. Germain, and S. B. Solomon. Comparing Strategies for Operator Eye Protection in the Interventional Radiology Suite. *Journal of Vascular and Interventional Radiology*, 21:1703–1707, 2010. doi: 10.1016/j.jvir.2010.07.019.

Z. Thrapnasnioti, P. Askounis, I. Datseris, R. Diamanti, M. Papathanasiou, and E. Carinou. Eye lens radiation exposure in Greek interventional cardiology personnel. *Radiation Protection Dosimetry*, pages 291–303, 2016. doi: 10.1093/rpd/ncw356.

UNSCEAR. *Summary of Low-Dose Radiation Effects on Health UNSCEAR 2010 Report. Vol. Report of the United Nations Scientific Committee on the Effects of Atomic Radiation.* 2011.

F. Vanhavere, E. Carinou, J. Domienik, L. Donadille, M. Ginjaume, G. Gualdrini, C. Koukorava, S. Krim, D. Nikodemova, N. Ruiz-Lopez, M. Sans-Merce, and L. Struelens. Measurements of eye lens doses in interventional radiology and cardiology: Final results of the ORAMED project. *Radiation Measurements*, 46(11):1243–1247, 2011. ISSN 13504487. doi: 10.1016/j.radmeas.2011.08.013.

F. Vanhavere, E. Carinou, G. Gualdrini, I. Clairand, M. Sans-Merce, M. Ginjaume, D. Nikodemova, J. Jankowski, J. M. Bordy, A. Rimpler, S. Wach, P. Martin, L. Struelens, S. Krim, C. Koukorava, P. Ferrari, F. Mariotti, E. Fantuzzi, L. Donadille, C. Itie, N. Ruiz, A. Carnicer, M. Fulop, J. Domienik, M. Brodecki, J. Daures, I. Barth, and P. Bilski. *ORAMED: Optimization of Radiation Protection of Medical Staff. Eurados report 2012-02.* European Radiation Dosimetry Group, 2012. ISBN 0471491101.

E. Vano, L. Gonzalez, J. M. Fernández, and Z. J. Haskal. Eye lens exposure to radiation in interventional suites: caution is warranted. *Radiology*, 248(3):945–953, 2008. ISSN 0033-8419. doi: 10.1148/radiol.2482071800.

E. Vano, C. Ubeda, F. Leyton, P. Miranda, and L. Gonzalez. Staff radiation doses in interventional cardiology: Correlation with patient exposure. *Pediatric Cardiology*, 30(4):409–413, 2009. ISSN 01720643. doi: 10.1007/s00246-008-9375-0.

E. Vano, N. J. Kleiman, A. Duran, M. M. Rehani, D. Echeverri, and M. Cabrera. Radiation Cataract Risk in Interventional Cardiology Personnel. *Radiation Research*, 174(4):490–495, 2010. ISSN 0033-7587. doi: 10.1667/RR2207.1. URL http://www.bioone.org/doi/10.1667/RR2207.1.

E. Vano, R. M. Sanchez, J. M. Fernandez, G. Bartal, L. Canevaro, R. Lykawka, and C. Melo. A set of patient and staff dose data for validation of Monte Carlo calculations in interventional cardiology. *Radiation protection dosimetry*, 165(1-4):235–9, 2015. ISSN 1742-3406. doi: 10.1093/rpd/ncv032. URL http://www.ncbi.nlm.nih.gov/pubmed/25802462.

B. V. Worgul, L. Smilenov, D. J. Brenner, A. Junk, W. Zhou, and E. J. Hall. Atm heterozygous mice are more sensitive to radiation-induced cataracts than are their wild-type counterparts. *Proceedings of the National Academy of Sciences of the United States of America*, 99(15):9836–9839, 2002. ISSN 0027-8424. doi: 10.1073/pnas.162349699. URL http://www.pubmedcentral.nih.gov/articlerender.fcgi?artid=125034{&}tool=pmcentrez{&}rendertype=abstract.

B. V. Worgul, Y. I. Kundiyev, N. M. Sergiyenko, P. Vitte, C. Medvedovsky, E. Bakhanova, A. K. Junk, O. Y. Kyrychenkoc, N. V. Musijachenko, and S. A. Shylo. Cataracts among Chernobyl clean-up workers: implications regarding permissible eye exposures. *Radiation Research*, 167:233–243, 2007.

C. Zett-Lobos, F. Vera-Muñoz, K. Arriola-Alvarez, O. Díaz-Ramos, J. Gamarra, C. Fernández-Palomo, L. Merello, A. D. Mora, A. Gutierrez, M. Catalán-Reyes, and S. Ramos-Avasola. [Protection against ionizing radiation by leaded glass googles during interventional cardiology]. *Revista Medica de Chile*, 141(1):63–9, 2013. ISSN 00349887. doi: 10.4067/S0034-98872013000100009. URL http://www.ncbi.nlm.nih.gov/pubmed/23732416.

List of Figures

List of Tables